1. Principles of Dye Laser Operation

Fritz P. Schäfer

With 69 Figures

Historical

Dye lasers entered the scene at a time when several hundreds of laser-active materials had already been found. Yet they were not just another addition to the already long list of lasers. They were the fulfillment of an experimenter's pipe dream that was as old as the laser itself: To have a laser that was easily tunable over a wide range of frequencies or wavelengths. Dye lasers are attractive in several other respects: Dyes can be used in the solid, liquid, or gas phases and their concentration, and hence their absorption and gain, is readily controlled. Liquid solutions of dyes are especially convenient: The active medium can be obtained in high optical quality and cooling is simply achieved by a flow system, as in gas lasers. Moreover, a liquid is self-repairing, in contrast to a solid-state active medium where damage (induced, say, by high laser intensities) is usually permanent. In principle, liquid dye lasers have output powers of the same magnitude as solid-state lasers, since the density of active species can be the same in both and the size of an organic laser is practically unlimited. Finally, the cost of the active medium, organic dyes, is negligibly small compared to that of solid-state lasers.

Early speculations about the use of organic compounds (Rautian and Sobel'mann 1961; Brock et al. 1961) produced correct expectations of the role of vibronic levels of electronically excited molecules (Broude et al. 1963), but the first experimental study that might have led to the realization of an organic laser was by Stockman et al. (1964) and Stockman (1964). Using a high-power flashlamp to excite a solution of perylene in benzene between two resonator mirrors, Stockman found an indication of a small net gain in his system. Unfortunately, he tried only the aromatic molecule perylene, which has high losses due to triplet-triplet absorption and absorption from the first excited singlet into higher excited singlet levels. Had he used some xanthene dye, like rhodamine 6G or fluorescein, we would undoubtedly have had the dye laser two years earlier. In 1966, Sorokin and Lankard (1966) at IBM's Thomas J. Watson Research Center, Yorktown Heights, were the first to obtain stimulated emission from an organic compound, namely chloro-aluminum-phthalocyanine. Strictly speaking, this dye is an organometallic compound, for its central metal atom is directly bonded to an organic ring-type molecule, somewhat resembling the compounds used in chelate lasers. In chelate lasers, however, stimulated emission originates in the central atom only, whereas in chloro-aluminum-phthalocyanine spectroscopic evidence clearly showed that the

emission originated in the organic part of the molecule. Sorokin and Lankard set out to observe the resonance Raman effect in this dye, excited by a giant-pulse ruby laser (Sorokin 1969). Instead of sharp Raman lines they found a weak diffuse band at 755.5 nm, the peak of one of the fluorescence bands. They immediately suspected this might be a sign of incipient laser action and indeed, when the dye cell was incorporated into a resonator, a powerful laser beam at 755.5 nm emerged.

At that time the author, unaware of Sorokin and Lankard's work, was studying in his laboratory, then at the University of Marburg, the saturation characteristics of saturable dyes of the cyanine series. Instead of observing the saturation of the absorption, he used the saturation of spontaneous fluorescence excited by a giant-pulse ruby laser and registered by a photocell and a Tektronix 519 oscilloscope. The dye 3,3'-diethyltricarbocyanine had been chosen as a most convenient sample. This scheme worked well at very low concentrations of 10^{-6} and 10^{-5} mole/liter, but when Volze, then a student, tried to extend these measurements to higher concentrations, he obtained signals about one thousand times stronger than expected, with instrument-limited risetime that at a first glance were suggestive of a defective cable. Very soon, however, it became clear that this was laser action, with the glass-air interface of the square, all-side-polished spectrophotometer cuvette acting as resonator mirrors with a reflectance of 4%. This was quickly checked by using a snooperscope to look at the bright spot where the infrared laser beam hit the laboratory wall. Together with Schmidt, then a graduate student, we photographed the spectra at various concentrations and also with reflective coatings added to the cuvette walls. Thus we obtained the first evidence that we had a truly tunable laser whose wavelength could be shifted over more than 60 nm by varying the concentration or the resonator mirror reflectivity. This was quickly confirmed and extended to a dozen different cyanine dyes. Among these was one that showed a relatively large solvatochromic effect and enabled us to shift the laser wavelength over 26 nm merely by changing the solvent (Schäfer et al. 1966). Stimulated emission was also reported in two other cyanine dyes by Spaeth and Bortfield at Hughes Aircraft Company (Spaeth and Bortfield 1966). These authors, intrigued by Sorokin and Lankard's publication, used cryptocyanine and a similar dye excited by a giant-pulse ruby. Since their dyes had a very low quantum yield of fluorescence, they had a high-lying threshold and observed only a certain shift of laser wavelength with cell length and concentration.

Stimulated emission from phthalocyanine compounds, cryptocyanine, and methylene blue was also reported in 1967 by Stepanov and coworkers (Stepanov et al. 1967a, b). They also reported laser emission from dyes that had a quantum efficiency of fluorescence of less than one thousandth of one percent; this, however, has not yet been confirmed by others.

A logical extension of this work was to utilize shorter pump wavelengths and other dyes in the hope of obtaining shorter laser wavelengths. This was first achieved in the author's laboratory by pumping a large number of dyes, among them several xanthene dyes, by the second harmonic of neodymium

and ruby lasers (Schäfer et al. 1967). Similar results were obtained independently in several other laboratories (Sorokin et al. 1967; McFarland 1967; Stepanov et al. 1967a, b; Kotzubanov et al. 1968a, b). Dye laser wavelengths now cover the whole visible spectrum with extensions into the near-ultraviolet and infrared.

Another important advance was made when a diffraction grating was substituted for one of the resonator mirrors to introduce wavelength-dependent feedback (Soffer and McFarland 1967). These authors obtained effective spectral narrowing from 6 to 0.06 nm and a continuous tuning range of 45 nm. Since then many different schemes have been developed for tuning the dye-laser wavelength; they will be discussed at length in the next chapter.

A natural step to follow was the development of flashlamps comparable in risetime and intensity to giant-pulse ruby lasers, to enable dye lasers to be pumped with a convenient, incoherent light source. This was initially achieved by techniques developed several years earlier for flash photolysis (Sorokin and Lankard 1967; W. Schmidt and Schäfer 1967). Soon after this, the author's team found that even normal linear xenon-filled flashlamps – and for some dyes even helical flashlamps – could be used, provided they were used in series with a spark gap and at sufficiently high voltage to result in a risetime of about 1 μs (Schäfer 1968). This is now standard practice for most single-shot or repetitively pumped dye lasers.

The common belief that continuous-wave (cw) operation of dye lasers was not feasible because of the losses associated with the accumulation of dye molecules in the metastable triplet state was corrected by Snavely and Schäfer (1969). Triplet-quenching by oxygen was found to decrease the steady-state population of the triplet state far enough to permit cw operation, at least in the dye rhodamine 6G in methanol solution, as demonstrated by using a lumped-parameter transmission line to feed a 500 μs trapezoidal voltage pulse to a flashlamp, giving a 140-μs dye-laser output. The premature termination of the dye laser pulse was also shown to be caused not by triplet accumulation but rather by thermal and acoustical schlieren effects. Our findings were later confirmed and extended by others who also used unsaturated hydrocarbons as triplet quenchers (Marling et al. 1970a and b; Pappalardo et al. 1970a).

The pump-power density requirements for a cw dye laser inferred from such measurements were so high that it seemed unlikely cw operation would be effected by pumping with the available high-power arc lamps. On the other hand, much higher pump-power densities can be obtained by focussing a high-power gas laser into a dye cuvette. The pumped region is thereby limited to about 50 μl, but the gain in the dye laser is usually very high.

Cw operation was a most important step towards the full utilization of the dye laser's potential; it was first achieved by O.G. Peterson et al. (1970) at Eastman-Kodak Research Laboratory. They used an argon-ion laser to pump a solution of rhodamine 6G in water with some detergent added. Water as solvent has the advantage of a high heat capacity, thus reducing temperature gradients, which are further minimized by the high velocity of the flow of dye solution through the focal region. The detergent both acts as triplet quencher

and prevents the formation of non-fluorescing dimers of dye molecules, which produce a high loss in pure water solutions.

This breakthrough triggered a host of investigations and developments of cw dye lasers in the following years; these will be covered in Chap. 2 of this book.

Towards the other end of the time scale, dye lasers, because of their extremely broad spectral bandwidth, are capable of producing ultrashort pulses of smaller half-width than with any other laser. The first attempts to produce ultrashort pulses with dye lasers involved pumping a dye solution with a mode-locked pulse train from a solid-state laser; the dye cuvette sat in a resonator with a round-trip time exactly equal to, or a simple submultiple of, the spacing of the pump pulses (Glenn et al. 1968; Bradley and Durrant 1968; Soffer and Linn 1968). It subsequently proved possible to eliminate the resonator and use the superradiant traveling-wave emission from a wedged dye cuvette (Mack 1969b). The pulsewidths obtained in this way were generally some 10 to 30 ps. Self-mode-locking of flashlamp-pumped dye lasers was first achieved by W. Schmidt and Schäfer (1968), using rhodamine 6G as the laser active medium and a cyanine dye as the saturable absorber. In an improved arrangement of this type a pulsewidth of only 2 ps was reached (Bradley et al. 1970a, b). Eventually, the technique was applied to cw dye lasers to give a continuous mode-locked emission with pulses of only 1.5 ps (Dienes et al. 1972). In 1974 the first optical pulses shorter than 1 ps were generated by Shank and Ippen with a passively mode-locked dye laser. With the introduction of the colliding pulse concept by Shank and coworkers in 1981, femtosecond pulses became a reality (Fork et al. 1981). Following the initial report of 90 fs optical pulses, several laboratories developed this technique, which recently led to the production of pulses as short as 27 fs (Valdmanis et al. 1985). This is not so far from the theoretically possible limit. If mode-locking over the full bandwidth of about 250 THz were possible, the pulsewidth should be of the order of 5 fs. Another important technique for the production of ultrashort pulses was developed by Bor and coworkers using distributed feedback dye lasers (Bor 1980). Recent development of high-performance amplifier stages has brought pulse powers up to gigawatts. Chapter 4 of this book is devoted to this important field of dye laser research. [A nonlinear optical method of pulse compression (Nakatsuka and Grischkowsky 1981) actually made it possible to reach a pulsewidth of 6 fs in 1987 (Fork et al. 1987). This interesting development will not be treated here, since it is beyond the scope of this book.]

If one tries to extrapolate this historical survey and discern the outline of future developments, one can immediately foresee some quantitative improvements in several features: The wavelength coverage will be extended farther into the ultraviolet and infrared, peak pulse powers and energies will increase by several orders of magnitude, and the generation of ultrashort pulses of unprecedentedly small pulsewidth using dye mixtures might become possible. A qualitative improvement will be the incoherent pumping of cw dye lasers with specially developed high-power arc lamps that will allow a much higher output power than pumping with gas lasers. This important achievement has

recently been reported by Drexhage and coworkers (Thiel et al. 1987). A most important development will concern the chemical aspect of the dye laser, namely the synthesis of special laser dyes with improved efficiency and photochemical stability (Schäfer 1983). The latter aspect will be particularly important for potential industrial applications, which at present are practically nonexistent, while applications of dye lasers in fundamental and applied research have become innumerable.

Organization of the Book

Chapter 1 by Schäfer is introductory. The chemical and spectroscopic properties of organic compounds are described, there is a tutorial presentation of the general principles of dye-laser operation, and aspects of the dye laser not treated in one of the special chapters are reviewed. Emphasis here is on an easy understanding of the physical and chemical principles involved, rather than on completeness, or historical or systematic presentation. The specialized chapters will build on this basis.

Chapter 2 by Snavely presents a review of cw dye lasers, with emphasis on the gain analysis. Special attention is given to the triplet problem.

Chapter 3 by Gerhardt describes the tremendous progress in cw dye lasers since 1973 in a brief overview. It does not cover frequency-stabilization techniques, since this subject has developed into a field that is beyond the scope of this book.

Mode-locking of dye lasers is the topic of Chapter 4 by Shank and Ippen. After an introduction covering methods of measuring ultrashort pulses, the authors discuss experimental methods applicable to mode-locking, pulsed and cw dye lasers, and for amplification of ultrashort pulses to very high powers.

The chemical and physical properties of dyes are discussed in Chapter 5 by Drexhage. A large amount of data on dyes is presented in support of the rules found by the author for the selection or synthesis of useful laser dyes. A list of laser dyes completes this chapter. Since this list covers only the laser dyes reported in the literature until 1973, the interested reader is referred to the books by Maeda (1984) and Brackmann (1986) for later data.

Finally, Chapter 6 by Snyder and Hänsch is a review of laser wavemeters, which have become indispensable tools in work with widely tunable dye lasers. This chapter replaces the chapter "Applications of Dye Lasers" by Hänsch in the earlier editions, since by now the number of such applications has become indeterminable.

The authors have tried to make the chapters as self-contained as possible, so that they can be read independently, albeit at the cost of some slight overlap.

1.1 General Properties of Organic Compounds

Organic compounds are defined as hydrocarbons and their derivatives. They can be subdivided into saturated and unsaturated compounds. The latter are

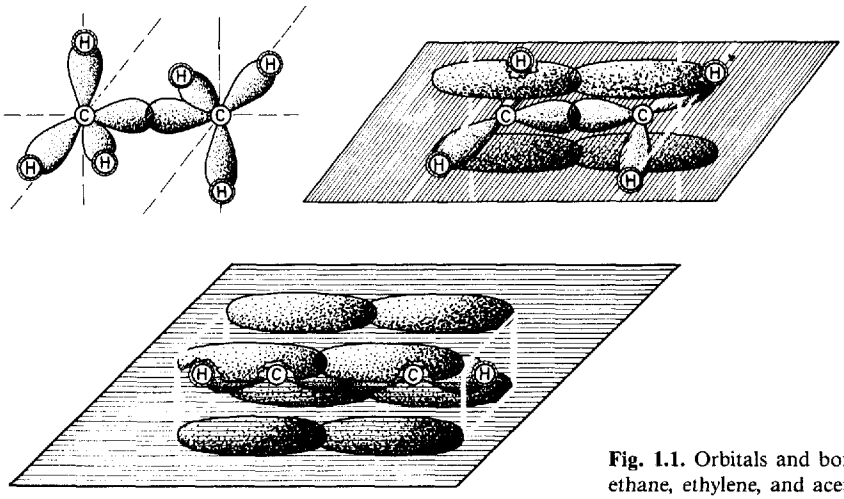

Fig. 1.1. Orbitals and bonds in ethane, ethylene, and acetylene

characterized by the fact that they contain at least one double or triple bond. These multiple bonds not only have a profound effect on chemical reactivity, they also influence spectroscopic properties. Organic compounds without double or triple bonds usually absorb at wavelengths below 160 nm, corresponding to a photon energy of 180 kcal/mole. This energy is higher than the dissociation energy of most chemical bonds, therefore photochemical decomposition is likely to occur, so such compounds are not very suitable as the active medium in lasers. In unsaturated compounds all bonds are formed by σ electrons; these are characterized by the rotational symmetry of their wave function with respect to the bond direction, i.e. the line connecting the two nuclei that are linked by the bond. Double (and triple) bonds also contain a σ bond, but in addition use π electrons for bonding. The π electrons are characterized by a wave function having a node at the nucleus and rotational symmetry along a line through the nucleus and normal to the plane subtended by the orbitals of the three σ electrons of the carbon or heteroatom (Fig. 1.1). A π bond is formed by the lateral overlap of the π-electron orbitals, which is maximal when the symmetry axes of the orbitals are parallel. Hence, in this position, bond energy is highest and the energy of the molecule minimal, thus giving a planar molecular skeleton of high rigidity. If two double bonds are separated by a single bond, as in the molecule butadiene,

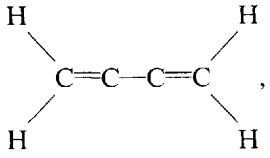

the two double bonds are called *conjugated*. Compounds with conjugated double bonds also absorb light at wavelengths above 200 nm. All dyes in the

proper sense of the word, meaning compounds having a high absorption in the visible part of the spectrum, possess several conjugated double bonds. The basic mechanism responsible for light absorption by compounds containing conjugated double bonds is the same, in whatever part of the spectrum these compounds have their longest wavelength absorption band, whether near-infrared, visible, or near-ultraviolet. We thus use the term *dye* in the wider sense as *encompassing all substances containing conjugated double bonds.* Whenever the term *dye* is used in this book, it will have this meaning.

For the remainder of this chapter we restrict our discussion of the general properties of organic compounds to dyes, since for the foreseeable future these are the only organic compounds likely to be useful laser-active media in the near-ultraviolet, visible and near infrared.

The thermal and photochemical stability of dyes is of utmost importance for laser applications. These properties, however, vary so widely with the almost infinite variety of chemical structure, that practically no general valid rules can be formulated. Thermal stability is closely related to the long-wavelength limit of absorption. A dye absorbing in the near-infrared has a low-lying excited singlet state and, even slightly lower than that, a metastable triplet state. The triplet state has two unpaired electrons and thus, chemically speaking, biradical character. There is good reason to assume that most of the dye molecules that reach this highly reactive state by thermal excitation will react with solvent molecules, dissolved oxygen, impurities, or other dye molecules to yield decomposition products. The decomposition would be of pseudofirst order with a reaction constant $k_1 = A \exp(-E_A/RT)$, where A is the Arrhenius constant and has most often a value of $10^{12}\,s^{-1}$ for reactions of this type (ranging from 10^{10} to $10^{14}\,s^{-1}$), E_A is the activation energy, R is the gas constant and T the absolute temperature. The half-life of such a dye in solution then is $t_{1/2} = \ln 2/k_1$. Assuming as a minimum practical lifetime one day, the above relations yield an activation energy of 24 kcal/mole, corresponding to a wavelength of 1.2 μm. If $A = 10^{10}\,s^{-1}$, this shifts the wavelength to 1.7 μm, and with $A = 10^{14}\,s^{-1}$ it would correspond to 1.1 μm. If we assume that a year is the minimum useful half-life of the dye (and $A = 10^{12}\,s^{-1}$), we get a wavelength of 1.0 μm.

Obviously, it becomes more and more difficult to find stable dyes having the maximum of their long-wavelength band of absorption in the infrared beyond 1.0 μm, and there is little hope of ever preparing a dye absorbing beyond 1.7 μm that will be stable in solution at room temperature. Thus, dye-laser operation at room temperature in the infrared will be restricted to wavelengths not extending far beyond 1.0 μm. This limit seems to have been reached with some new laser dyes synthesized by Drexhage and coworkers (Polland et al. 1983) which have their peak absorption wavelength at up to 1.45 μm, thus enabling dye laser action to be extended to 1.85 μm.

The short-wavelength limit of dye-laser operation, already mentioned implicitly, is given by the absorption of dyes containing only two conjugated double bonds and having their long-wavelength absorption band at wavelengths of about 220 nm. Since the fluorescence, and hence the laser emission, is always

red-shifted, dye lasers can hardly be expected to operate at wavelengths below about 250 nm. Even if we were to try to use compounds possessing only one double bond, like ethylene, absorbing at 170 nm, we could at best hope to reach 200 nm in laser emission. At this wavelength, however, photochemical decomposition already competes effectively with radiative deactivation of the molecule, since the energy of the absorbed quantum is higher than the energy of any bond in the molecule. In addition, at shorter wavelengths the probability of excited state absorption, cf. p. 29, can become higher than that of stimulated emission, thus preventing laser action. This seems to be the main reason why at present, after years of attempts to extend dye laser action further into the ultraviolet, the shortest dye laser wavelength still remains fixed at 308.5 nm (Zhang and Schäfer 1981).

Another important subdivision of dyes is into ionic and uncharged compounds. This feature mainly determines melting point, vapor pressure, and solubility in various solvents. An uncharged dye already mentioned is butadiene, $CH_2=CH-CH=CH_2$; other examples are most aromatics: anthracene, pyrene, perylene, etc. They usually have relatively low-lying melting points, relatively high vapor pressures, and good solubility in nonpolar solvents, like benzene, octane, cyclohexane, chloroform, etc. Cationic dyes include the large class of cyanine dyes, e.g. the simple cyanine dye

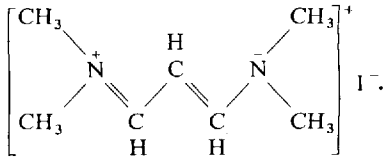

These compounds are salts, consisting of cations and anions, so they have high melting points, very low vapor pressure, good solubility in more polar solvents like alcohols, and only a slight solubility in less polar solvents. Similar statements can be made for anionic dyes, e.g. for the dye

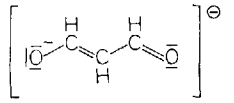

Many dyes can exist as cationic, neutral and anionic molecules depending on the pH of the solution, e.g. fluorescein:

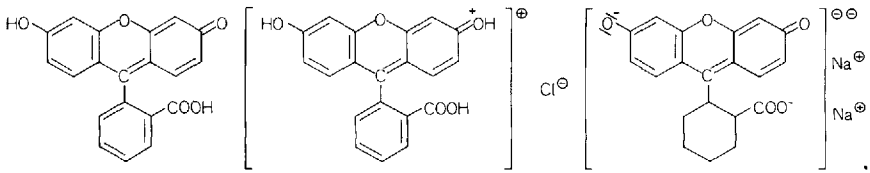

Neutral form (alcoholic solution) | Cationic form (hydrochloric acid solution) | Di-anionic form sodium hydroxyde solution

It should be stressed here that dyes are potentially useful as laser-active media in the solid, liquid and vapor phases. Since most dyes form good single crystals, it might be attractive to use them directly in this form. There are two main obstacles to their use in crystal form: The extremely high values attained by the extinction coefficient in dyes, which prevents the pump-light from exciting more than the surface layer a few microns thick; and the concentration quenching of fluorescence that usually sets in whenever the dye molecules approach each other closer than about 10 nm. Doping a suitable host crystal with a small fraction (one thousandth or less) of dye circumvents these difficulties. On the other hand, solid solutions of many different types can be used. For instance, one can dissolve a dye in the liquid monomer of a plastics material and then polymerize it; or one can dissolve it in an inorganic glass (e.g. boric acid glass) or an organic glass (e.g. sucrose glass) or some semirigid material like gelatine or polyvinylalcohol. The utilization of some of these techniques for dye lasers will be discussed later, together with the use of dyes in the liquid and vapor phases.

1.2 Light Absorption by Organic Dyes

The light absorption of dyes can be understood on a semiquantitative basis if we take a highly simplified quantum-mechanical model, such as the free-electron gas model (Kuhn 1959). This model is based on the fact that dye molecules are essentially planar, with all atoms of the conjugated chain lying in a common plane and linked by σ bonds. By comparison, the π electrons have a node in the plane of the molecule and form a charge cloud above and below this plane along the conjugated chain. The centers of the upper and lower lobes of the π-electron cloud are about one half bond length distant from the molecular plane. Hence, the electrostatic potential for any single π electron moving in the field of the rest of the molecule may be considered constant, provided all bond lengths and atoms are the same (Fig. 1.2). Assume that the conjugated chain which extends approximately one bond length to the left and right beyond the terminal atoms has length L. Then the energy E_n of the nth eigenstate of this electron is given by $E_n = h^2 n^2 / 8 m L^2$, where h is Planck's constant, m is the mass of the electron, and n is the quantum number giving the number of antinodes of the eigenfunction along the chain. According to the Pauli principle, each state can be occupied by two electrons. Thus, if we have N electrons, the lower $(1/2)N$ states are filled with two electrons each, while all higher states are empty (provided N is an even number; this is usually the case in stable molecules since only highly reactive radicals possess an unpaired electron). The absorption of one photon of energy $\Delta E = h c_0 / \lambda$ (where λ is the wavelength of the absorbed radiation and c_0 is the velocity of light) raises one electron from an occupied to an empty state. The longest wavelength absorption band then corresponds to a transition from the highest occupied to the lowest empty state with

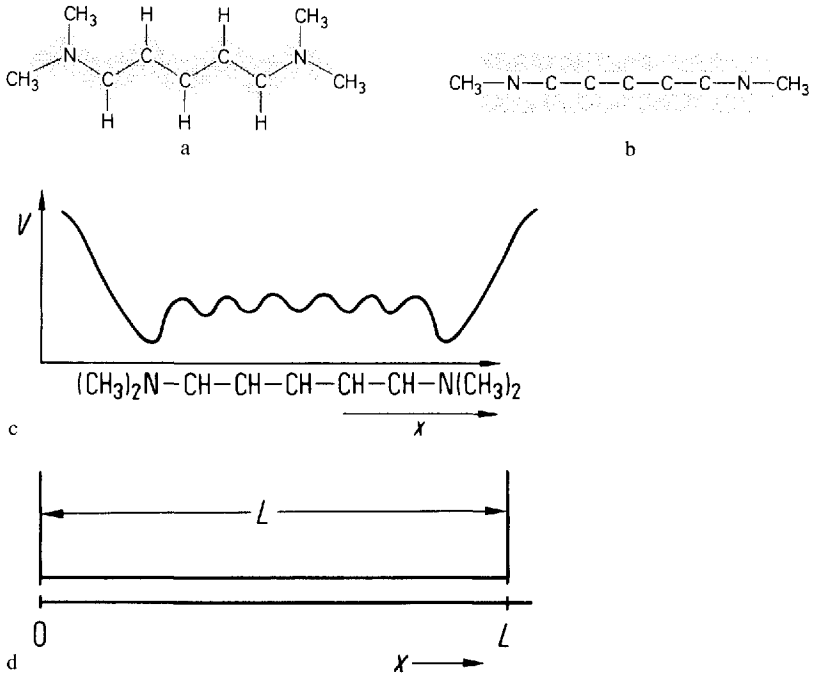

Fig. 1.2. (**a**) π-Electron cloud of a simple cyanine dye seen from above the molecular plane; (**b**) the same as seen from the side; (**c**) potential energy V of a π electron moving along the zig-zag chain of carbon atoms in the field of the rump molecule; (**d**) simplified potential energy trough; L = length of the π-electron cloud in a as measured along the zig-zag chain. (From Försterling and Kuhn 1971)

$$\Delta E_{\min} = \frac{h^2}{8mL^2}(N+1) \quad \text{or} \quad \lambda_{\max} = \frac{8mc_0}{h}\frac{L^2}{N+1} .$$

This indicates that to first approximation the position of the absorption band is determined only by the chain length and by the number of π electrons N. Good examples of this relation are the symmetrical cyanine dyes of the general formula

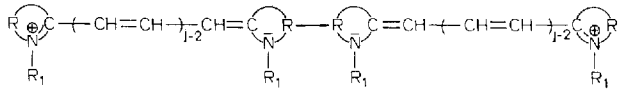

where j is the number of conjugated double bonds, R_1 a simple alkyl group like C_2H_5, and R indicates that the terminal nitrogen atoms are part of a larger group, as e.g. in the following dye (homologous series of thiacyanines):

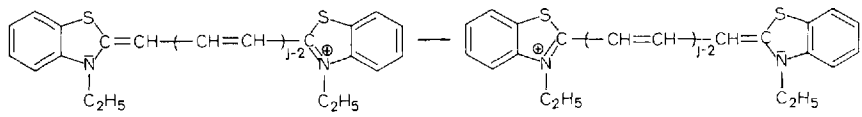

The double-headed arrow means that the two formulae are limiting structures of a resonance hybrid. The π electrons in the phenyl ring can be neglected in first approximation, or treated as a polarizable charge cloud, leading to an apparent enlargement of the chain L. In the case of the last-mentioned dye, good agreement is found between calculated and experimental absorption wavelength, when the chain length L is assumed to extend 1.3 bond lengths (instead of 1.0 bond length as above) beyond the terminal atoms. The bond length in cyanines is 1.40 Å. The good agreement between the results of this simple calculation and the experimental data for the above thiacyanines is shown by the following comparison:

Wavelength (in nm) of absorption maximum for thiacyanines

	Number of conjugated double bonds j =			
	2	3	4	5
Calculated	395	521	649	776
Experimental	422	556	652	760

Similarly good agreement can be found for all the other homologous series of symmetrical cyanines, once the value of the end length extending over the terminal N atoms is found by comparison with the experimentally observed absorption wavelength for one member of the series. Absorption wavelengths have been reported for a large number of cyanines (Miyazoe and Maeda 1970).

The following nomenclature is customarily used for cyanine dyes. If $j = 2$, then the dye is a cyanine in the narrower sense or monomethine dye, since it contains one methine group, $-CH-$, in its chain; if $j = 3$, the dye is a carbocyanine or trimethine dye; if $j = 4, \ldots, 7$, the dye is a di-, tri-, tetra-, or pentacarbocyanine or penta-, hepta-, nona- or undecamethine dye. The heterocyclic terminal groups are indicated in an abridged notation; thus "thia" stands for the benzthiazole group:

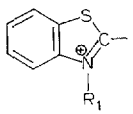

and "oxa" for the benzoxazole group

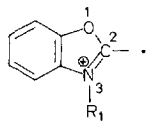

In these groups the atoms are numbered clockwise, starting from the sulfur or oxygen atom. Thus, the name of the last-mentioned thiacyanine dye is 3,3′-diethyl-thiadicarbocyanine for $j = 4$. If the terminal group is quinoline, the syllable "quinolyl" indicative of this end group is frequently omitted from the name. In this case, however, the position of linkage of the polymethine chain to the quinoline ring must be given, e.g.

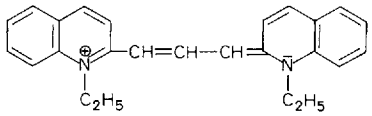

is 1,1′-diethyl-2,2′-carbocyanine (trivial name: pinacyanol), while

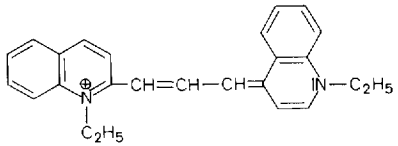

is 1,1′-diethyl-2,4′-carbocyanine (trivial name: dicyanine), and

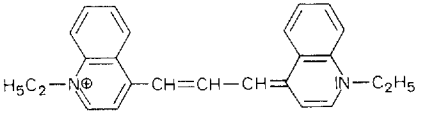

is 1,1′-diethyl-4,4′-carbocyanine (trivial name: cryptocyanine). Where there are two different end groups, these are named in alphabetical order, e.g. 3,3′-diethyl-oxa-thiacarbocyanine is

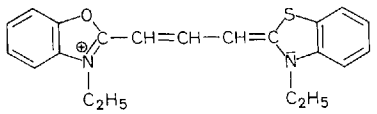

It is easy to eliminate the above assumption of identical atoms in the conjugated chains. If, for instance, one CH group is replaced by an N atom, the higher electronegativity of the nitrogen atom adds a small potential well to the constant potential; a simple perturbation treatment shows that every energy level is shifted by $\varepsilon = -B\Psi^2$, where B is a constant characteristic of the electronegativity of the heteroatom (in the case of $=N-$, $B = 3.9\times10^{-20}$ erg cm) and Ψ is the value of the normalized wave function at the heteroatom. This means that the shift of an energy level is zero if the wave function has a node at the heteroatom, and maximal if it has an antinode there. The change in absorption wavelength with heterosubstitution calculated in this way is in good agreement with the experimentally observed values. The second of the above assumptions, that of equal bond lengths along the chain, can be eliminated in a similar way. An illustrative example is offered by the polyenes of the general

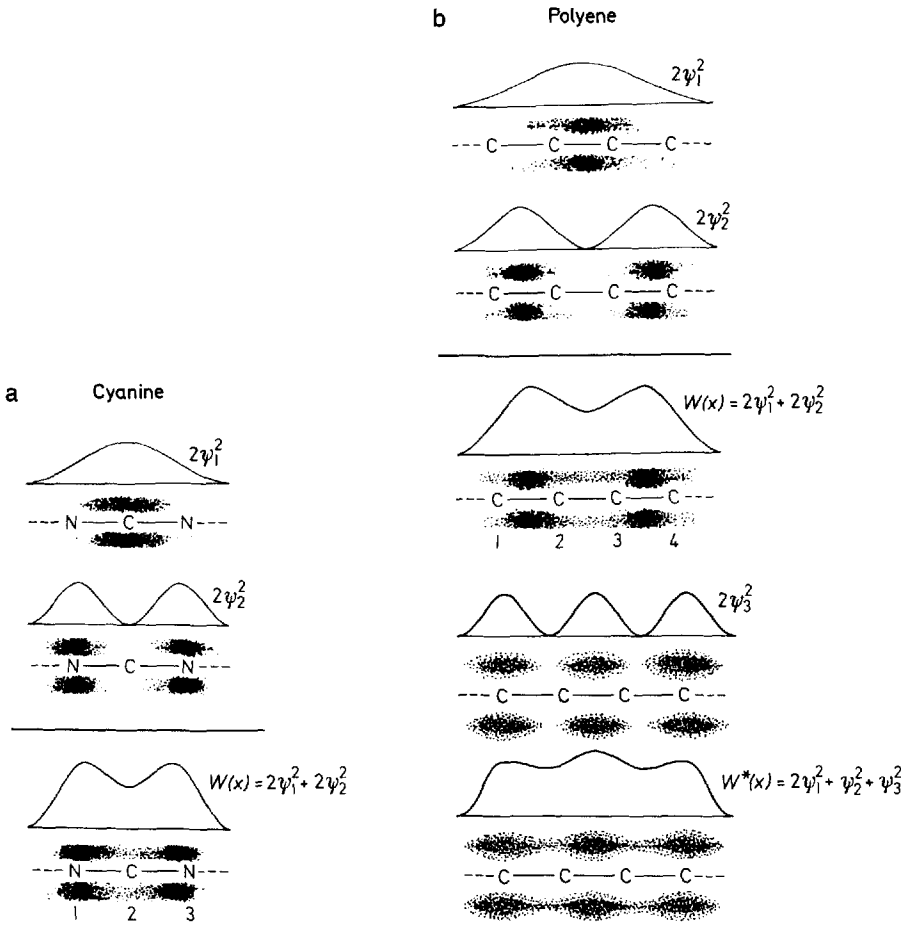

Fig. 1.3. Electron densities (proportional to the square of the wave function, ψ^2) along the conjugated chain of (**a**) a cyanine, (**b**) a polyene (butadiene). The symbols ψ_1 and ψ_2 denote the wave functions of the first and second filled π-electron molecular orbital, and ψ_3 that of the lowest orbital normally empty, which is occupied by one electron when excited. $W(x)$ is the total π-electron density for a molecule in the ground state, and $W^*(x)$ is the same for butadiene in the first excited state

formula $R-(CH=CH)_j-R$. These compounds have an even number of atoms. The total charge distribution results in localized double and single bonds (Fig. 1.3) and hence in alternating short and long bond lengths (1.35 Å and 1.47 Å, respectively). A π electron moving along the chain will therefore experience greater attraction to the neighboring atoms in the middle of a double bond than in the middle of a single bond. This fact may be represented by a periodic perturbing potential with minima at the center of the double bonds and maxima at the center of the single bonds (Fig. 1.4). Assuming a sinusoidal potential with an amplitude of 2.4 eV gives good agreement between the

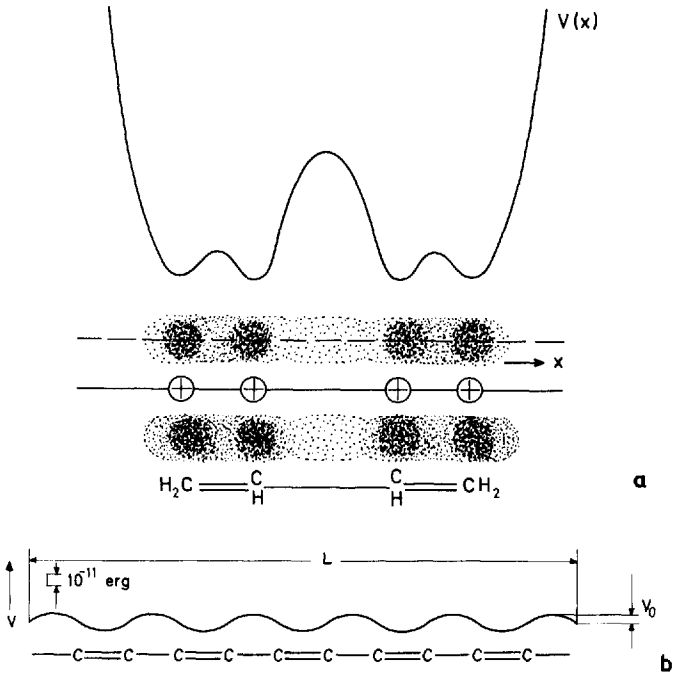

Fig. 1.4. (a) Potential energy $V(x)$ of a π electron moving along the carbon atom chain in the field of the rump molecule of butadiene; (b) simplified potential energy trough of a long polyene molecule with perturbing sinusoidal potential of amplitude $V_0 = 2.4$ eV. The energy difference between highest filled and lowest empty orbital is given by $\Delta E = (h^2/8mL^2)(2j+1)+0.83(1-1/2j) \times V_0$, where j is the number of conjugated double bonds. (From Kuhn 1959)

calculated and experimental values of the absorption wavelengths. The relation between chain length and absorption wavelength is found to be very different in the cyanines and the polyenes. In symmetrical cyanines the absorption wavelength is shifted by a constant amount of roughly 100 nm on going from one member of a series to the next higher which has one more double bond. In polyenes this shift decreases with increasing number of double bonds. A similar treatment can be applied to unsymmetrical cyanines in which the difference in electronegativity of the different end groups gives a similar polyene-type perturbation. The perturbation is less pronounced when the difference in electronegativity of the end groups is less.

Many dyes containing a branched chain of conjugated double bonds can, in a first approximation, be classified either as symmetrical cyanine-like or polyene-like substances, or as intermediate cases. For example, Michler's hydrol blue

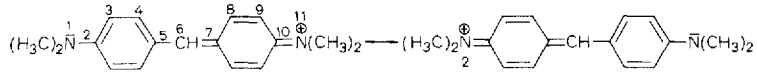

absorbs at practically the same wavelength as the symmetrical cyanine

$$(H_3C)_2\bar{N}\text{-}(CH{=}CH)_4\text{-}CH{=}\overset{\oplus}{N}(CH_3)_2$$

$$\leftrightarrow (H_3C)_2\overset{\oplus}{N}{=}CH\text{-}(CH{=}CH)_4\text{-}\bar{N}(CH_3)_2.$$

Hence it seems justified to treat it like a cyanine by neglecting the lower branches in the formula of Michler's hydrol blue. If, however, additional branching is introduced by connecting positions 4 and 8 through a $\left(\begin{array}{c}=N-\\ \quad|\\ \quad CH_3\end{array}\right)$ bridge, this gives acridine orange

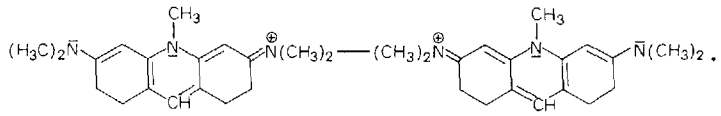

The absorption wavelength is shifted from 603 nm to 491 nm. It indicates that in this case branching cannot be neglected even in a first approximation.

With an O atom as bridging group instead of the $N-CH_3$ group, the xanthylium dye pyronine G with an absorption wavelength of 550 nm is obtained:

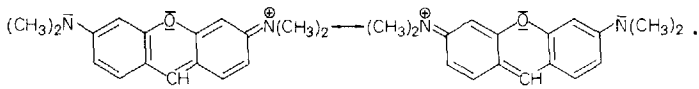

For a detailed treatment of molecules containing such a branched free-electron gas, the reader is referred to the literature (Kuhn 1959).

Another important class of dyes in which the branching of the conjugated chain can be neglected to first approximation, are the phthalocyanines and similar large-ring molecules. In first approximation the benzene rings are separated resonance systems, leaving the 16-membered ring indicated in Fig. 1.5 by heavy lines. Now there are 18π electrons on a ring of circumference $L = 16l$. In the lowest state ($n = 0$) the eigenfunction has no nodes, for $n \neq 0$ there are two degenerate eigenfunctions for every n, corresponding to the sine and cosine in the constant-potential approximation. A large perturbation is, however, introduced by the nitrogen atoms, which remove the degeneracy. This effect is most pronounced for $n = 4$, since one eigenfunction then has its nodes at the N atoms, the other its antinodes. The lowest unfilled levels are again degenerate because of equal perturbation energy. The absorption wavelengths for the two transitions from $n = 4$ to $n = 5$ are then readily calculated (with the above value for B): $\lambda_1 = 690$ nm and $\lambda_2 = 340$ nm (Fig. 1.5). The experimental values are 674 nm and 345 nm.

The free-electron model, even in its simplest form, gives very satisfactory agreement between calculated and experimental values of the absorption wavelength for large dye molecules. Nevertheless, its one-electron functions are not sufficient for a quantitative description of light absorption by small molecules of high symmetry, like benzene, naphthalene and similar molecules,

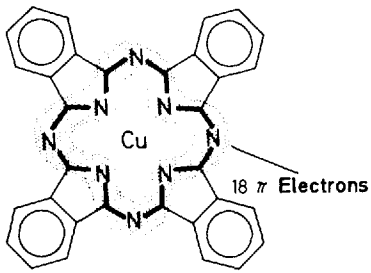

a Cu-Phtalocyanin

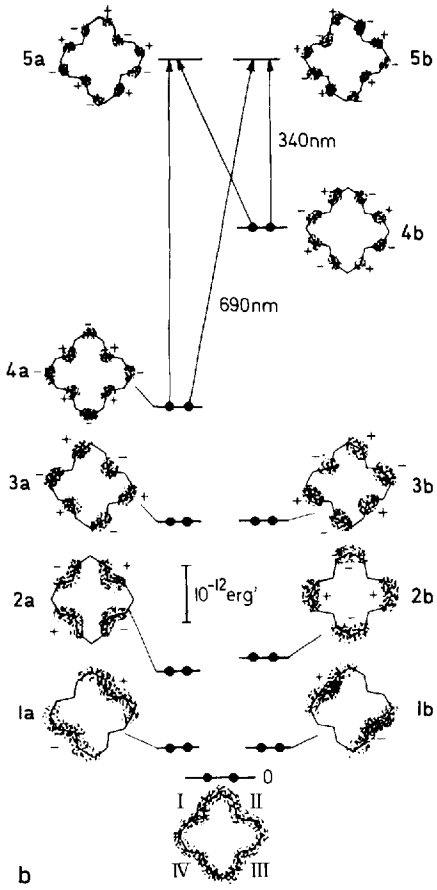

Fig. 1.5a, b. Formula, eigenstates, and eigenfunctions of Cu-phthalocyanine. (From Kuhn 1959)

since here the repulsion between the π electrons plays an important role. For the inclusion of electron correlations into the free electron model, the reader is referred to Försterling et al. (1966).

The oscillator strength of the absorption bands can also be calculated easily by the free-electron model. Transition moments X and Y along and normal to the long molecular axis are connected with the oscillator strength f of the absorption band by

$$f = 2\,\frac{8m_0\pi^2}{3h^2}\,\Delta E(X^2+Y^2)\ ,$$

and can be calculated using the electron gas wave functions ψ_a and ψ_b of the eigenstates between which the transition occurs:

$$X = \int\limits_{\text{molecule}} \psi_a x \psi_b dx\ , \qquad Y = \int\limits_{\text{molecule}} \psi_a y \psi_b dy\ .$$

The relative strengths of the x and y components also yield the orientation of the transition moment in the molecule. One finds good agreement on comparing the f values obtained from the absorption spectrum of the dye using the relation

$$f = 4.32 \times 10^{-9} \int_{\substack{\text{absorption} \\ \text{band}}} \varepsilon(\tilde{\nu}) d\tilde{\nu} \ ,$$

where ε is the numerical value of the molar decadic extinction coefficient measured in liter/(cm mole), and $\tilde{\nu}$ is the numerical value of the wave number measured in cm^{-1}.

A peculiarity of the spectra of organic dyes as opposed to atomic and ionic spectra is the width of the absorption bands, which usually covers several tens of nanometers. This is immediately comprehensible when one recalls that a typical dye molecule may possess fifty or more atoms, giving rise to about 150 normal vibrations of the molecular skeleton. These vibrations, together with their overtones, densely cover the spectrum between a few wave numbers and $3000\,\text{cm}^{-1}$. Many of these vibrations are closely coupled to the electronic transitions by the change in electron densities over the bonds constituting the conjugated chain. After the electronic excitation has occurred, there is a change in bond length due to the change in electron density. If, e.g. in Fig. 1.3, the bond length connecting atoms 1 and 2 is r (typically 1.35 Å) and this bond is lengthened in the excited molecule, the new equilibrium distance being r^*, atoms 1 and 2 will start to oscillate, classically speaking, around this new position with an amplitude $r^* - r$ (typically 0.02 Å) after the electronic transition has occurred. A molecular skeletal vibration is excited in this way. The new equilibrium total π electron density $W^*(x)$ for the excited state is given in Fig. 1.3c demonstrating the large increase in π electron density over the bond connecting atoms 2 and 3. Quantum-mechanically this means that transitions have occurred from the electronic and vibrational ground state S_0 of the molecule

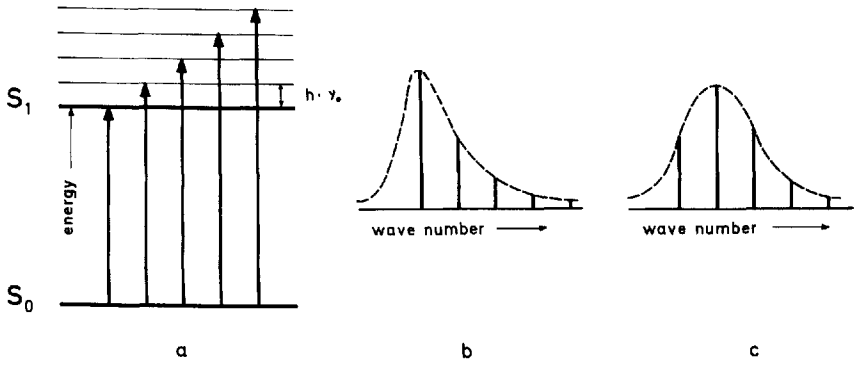

Fig. 1.6. (**a**) Electronic and vibronic energy levels of a dye molecule; S_0: ground state, S_1: excited state, and absorptive transitions from S_0 to S_1; (**b**) and (**c**) two possible forms of concomitant spectra

to an electronically and vibrationally excited state S_1, as depicted in Fig. 1.6. This results in spectra like Fig. 1.6b or c, depending on how many of the vibrational sublevels, spaced at $h\nu_0$ $(v+1/2)$, with $v = 0, 1, 2, 3 \ldots$, are reached and what the transition moments to these sublevels are.

In the general case of a large dye molecule, many normal vibrations of differing frequencies are coupled to the electronic transition. Furthermore, collisional and electrostatic perturbations, caused by the surrounding solvent molecules, broaden the individual lines of such vibrational series as that given in Fig. 1.6. As a further complication, every vibronic sublevel of every electronic state, including the ground state, has superimposed on it a ladder of rotationally excited sublevels. These are extremely broadened because of the frequent collisions with solvent molecules which hinder the rotational movement so that there is a quasicontinuum of states superimposed on every electronic level. The population of these levels in contact with thermalized solvent molecules is determined by a Boltzmann distribution. After an electronic transition, which, as described above, leads to a nonequilibrium state (Franck-Condon state) the approach to thermal equilibrium is very fast in liquid solutions at room temperature. The reason is that a large molecule experiences at least 10^{12} collisions/s with solvent molecules, so that equilibrium is reached in a time of the order of one picosecond. Thus the absorption is practically continuous all over the absorption band. The same is true for the fluorescence emission corresponding to the transition from the electronically excited state of the molecule to the ground state. This results in a mirror image of the absorption band displaced towards lower wave numbers by reflection at the wave number of the purely electronic transition. This condition exists, since the emissive transitions start from the vibrational ground state of the first excited electronic state S_1 and end in vibrationally excited sublevels of the electronic ground state. The resulting typical form of the absorption and fluorescence spectra of an organic dye is given in Fig. 1.7.

Further complications of dye spectra arise from temperature and concentration dependence and acid–base equilibria with the solvent. If the temperature of a dye solution is increased, higher vibrational levels of the ground state are populated according to a Boltzmann distribution and more and more transitions occur from these to higher sublevels of the first excited singlet state. Consequently, the absorption spectrum becomes broader and the superposition of so many levels blurs most of the vibrational fine structure of the band, while cooling of the solution usually reduces the spectral width and enhances any vibrational features that may be present. Thus, spectra of solid solutions of dyes in EPA, a mixture of 5 parts ethyl ether, 5 parts isopentane, and 5 parts ethanol that forms a clear organic glass when cooled down to 77 K, are often used for comparison with calculated spectra because of their well-resolved vibrational structure. Further cooling below the glass point, when the free movement of solvent molecules or parts thereof is inhibited, usually brings about no further sharpening of the spectral features (Fig. 1.8). The many possible different configurations of the solvated molecule in the cage of solvent molecules cannot be attained when the temperature is lowered because the ac-

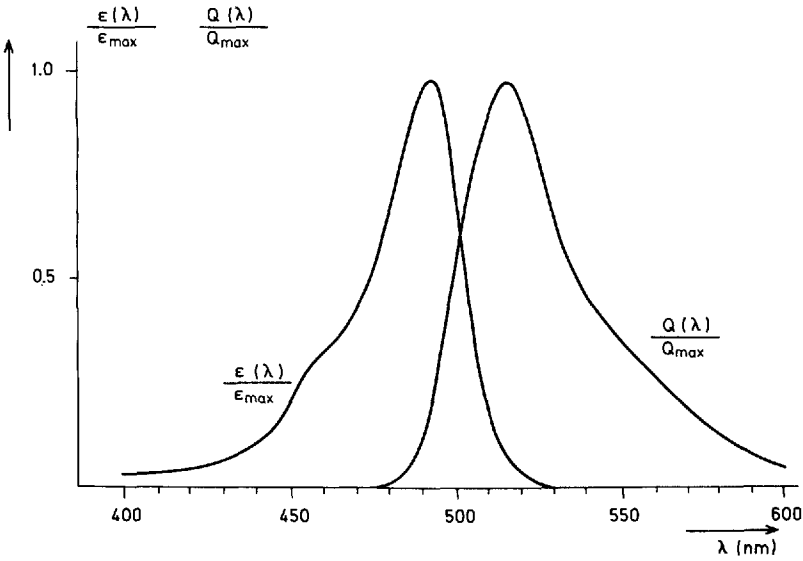

Fig. 1.7. Absorption spectrum, $\varepsilon(\lambda)/\varepsilon_{max}$, and fluorescence spectrum, $Q(\lambda)/Q_{max}$, of a typical dye molecule (fluorescein-Na in water)

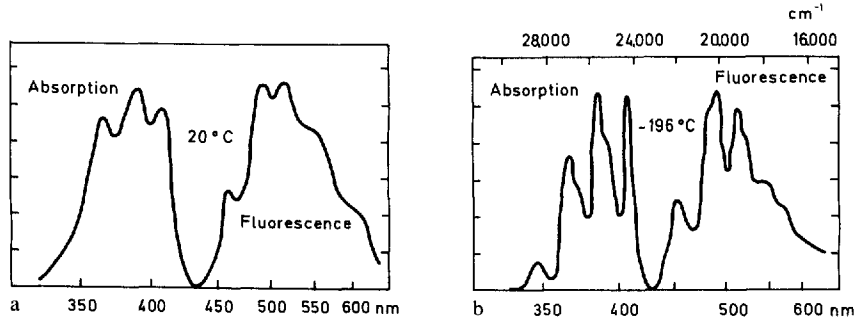

Fig. 1.8. Absorption and fluorescence spectra of diphenyloctatetraene in xylene. **(a)** at 20 °C, **(b)** at −196 °C. (From Hausser et al. 1935)

tivation energy required to reach the new equilibrium positions is too high. A very special case is the Shpolski effect (Shpolski 1962): This refers to the appearance of very sharp, line-like spectra (often termed quasi-line spectra in the Russian literature) of about one cm^{-1} width instead of the usual diffuse band spectra of dye molecules (most often aromatics) in a matrix of *n*-paraffins at low temperature (usually below 20 K). Evidently this is because there are only a few different possibilities of solvation of the molecule in that matrix, and each of the different sites causes a series of spectral lines in absorption as well as in emission. Analyzing these series gives the energy difference of the different sites, usually a few hundred cm^{-1} (Fig. 1.9). The Shpolski effect has

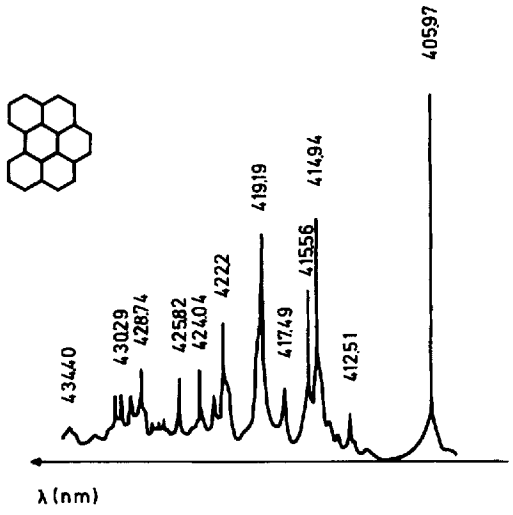

Fig. 1.9. Fluorescence spectrum of 1,12-benzoperylene in n-hexane at 77 K (Shpolski effect). (From Personov and Solochmov 1967)

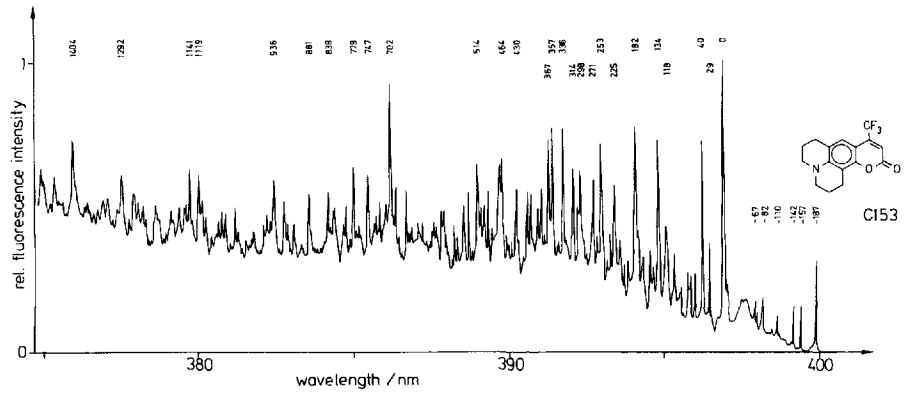

Fig. 1.10. Excitation spectrum of jet-cooled laser dye C153 with "rigidized" amino group. (From Ernsting et al. 1982)

also been called the optical analog of the Mössbauer effect (Rebane and Khizhnyakov 1963), since here also the recoil of the interacting photons seems to be taken up by the matrix as a whole.

The highest resolution absorption and fluorescence spectra of laser dyes can be obtained using the relatively new tool of cold beam spectroscopy. For this purpose a stream of noble gas is passed over a heated sample of the dye and then expanded through a small orifice into a vacuum. The adiabatic expansion cools the molecules quickly down to a few degrees Kelvin after a flight over a few millimeters. The density of the isolated cool molecules is then still very high (up to $10^{14}\,cm^{-3}$), so that absorption and fluorescence spectra can easily be obtained. An example of such a spectrum is shown in Fig. 1.10.

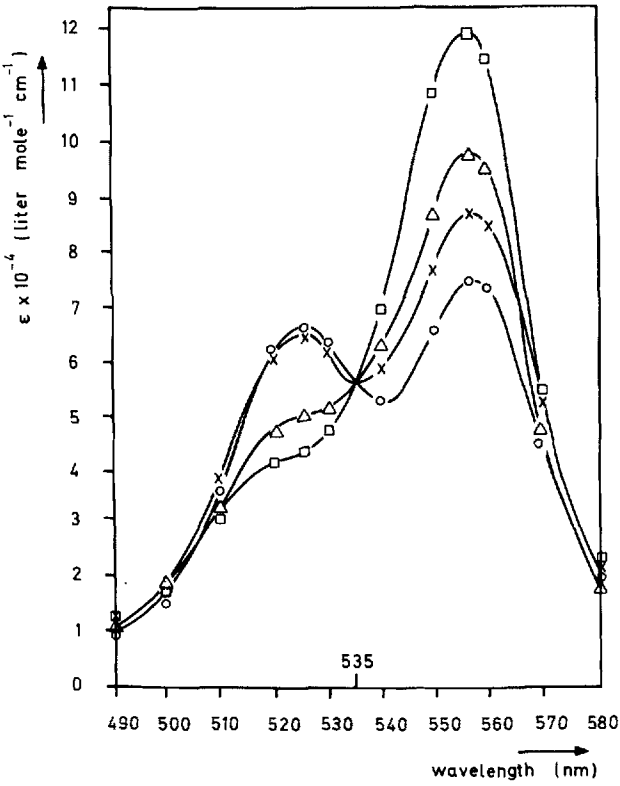

Fig. 1.11. Absorption spectra of aqueous solutions of rhodamine B at 22 °C, (○) 1.5×10^{-3} M, (×) 7.6×10^{-4} M, (△) 1.5×10^{-4} M, (□) 3.0×10^{-6} M. (From Selwyn and Steinfeld 1972)

The concentration dependence of dye spectra is most pronounced in solutions where the solvent consists of small, highly polar molecules, notably water. Dispersion forces between the large dye molecules tend to bring the dye molecules together in a position with the planes of the molecules parallel, where the interaction energy usually is highest. This is counteracted by the repulsive Coulomb forces if the dye molecules are charged. In solvents of high dielectric constants this repulsion is lowered and the monomer–dimer equilibrium is far to the side of the dimer. The equilibrium constant of the dimerization process monomer + monomer $\rightleftharpoons$ dimer is $K = [\text{dimer}]/[\text{monomer}]^2$ and can easily be obtained from spectra of differently concentrated dye solutions (Fig. 1.11). Usually the polymerization process stops at this stage, as evidenced by at least one isosbestic point (535 nm in Fig. 1.11). However, in some cases reversible polymerization occurs to a degree of polymerization of up to 1 million dye molecules (Scheibe 1941; Bücher and Kuhn 1970). In this case, a very sharp, high-intensity absorption and emission line becomes prominent in the spectra. The spectral differences between monomer and dimer, or even polymer, dye molecules can easily be understood at least qualitatively (Förster 1951). Figure 1.12 shows schematically the two main electronic energy levels of two distant dye molecules, and the splitting of the degenerate levels

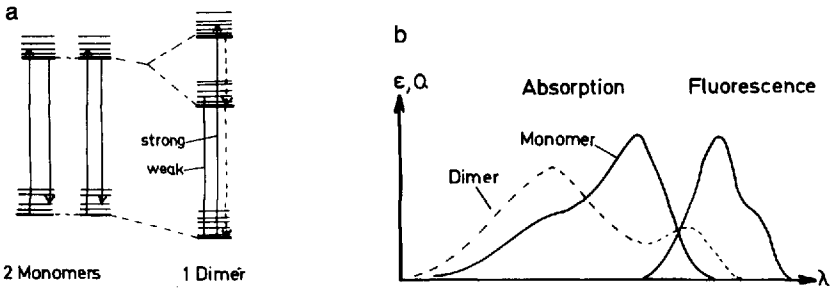

Fig. 1.12. (**a**) Energy levels of two monomers and the dimer molecule formed by them; (**b**) resulting spectra

if they come close enough to each other to experience interaction energy and the concomitant formation of a dimer. Now two transitions are possible, and these in general possess different transition moments depending on the wave functions of the dimer. Most often the long-wavelength transition has a practically vanishing transition moment, so that only one absorption band of the dimer is observed, lying to the short-wavelength side of the monomer band. This has an important consequence for the fluorescence of such dimers. Since the upper level from which the fluorescence starts is always the lowest-lying excited electronic level, and since a small transition moment is coupled to a long lifetime of the excited state, these dimers would show a very slow decay of their fluorescence. This, however, makes them susceptible to competing quenching processes, which in liquid solution are generally diffusion-controlled and hence very fast processes. Consequently, in most of these cases the fluorescence of the dimers is completely quenched and cannot be observed.

This is the reason why dimers constitute an absorptive loss of pump power in dye lasers and must be avoided by all means. There are several ways in which this may be done. One is to use a less polar solvent, like alcohol or chloroform. There are very few dyes which show dimerization in alcohol at the highest concentrations and at low temperatures. Another possibility is to add a detergent to the aqueous dye solution, which then forms micelles that contain one dye molecule each (Förster and Selinger 1964). This method is of prime importance for cw dye lasers and is discussed in Chap. 5, on laser dyes.

Acid–base equilibria have already been mentioned above for the case of fluorescein. Very often these equilibria are less obvious. For example, the dye 3,6-bis-dimethylaminoacridine can be protonated at the central nitrogen atom and then exhibits an absorption band shifted to longer wavelengths by about 55 nm (J. Ferguson and Mau 1972b), as shown in Fig. 1.13. Several other cases of acid–base equilibria of laser dyes will be discussed in detail in Chap. 5.

In addition to above-mentioned transitions between σ orbitals ($\sigma \rightarrow \sigma^*$ transitions) and the extensively discussed transitions between π orbitals ($\pi \rightarrow \pi^*$ transitions), we should also mention the transitions from the orbital of a lone-electron pair (so-called n orbitals), e.g. in a keto group, C=O, to a π orbital. Since the n orbitals have either spherical or rotational symmetry, with the sym-

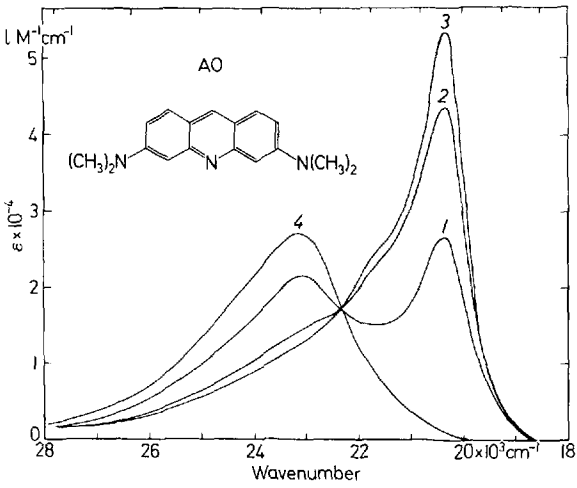

Fig. 1.13. Absorption spectra of 3,6-bis-dimethylamino-acridine (AO) in ethanol, (*1*) 3×10^{-5} M, (*2*) 2% water added, (*3*) bubbled with CO_2 gas, (*4*) anhydrous potassium carbonate added. (From J. Ferguson and Mau 1972b)

metry axis lying in the molecular plane, the overlap with π orbitals, and hence the transition moments, is very small. Correspondingly, the molar decadic extinction coefficient ε (as defined by Beer's law, $I = I_0 \cdot 10^{-\varepsilon c d}$, where I and I_0 are the transmitted and incident light intensity, c is the concentration in mole/liter of the absorbing species, and d is the thickness of the absorbing layer in cm) of absorption bands caused by $n\rightarrow\pi^*$ transitions usually ranges from 1 to 10^3 l/(mole cm), while $\pi\rightarrow\pi^*$ transitions exhibit values of ε lying between 10^3 and 10^6 l/(mole cm).

The free-electron model can also provide a simple explanation for another important property of the energy levels of organic dyes, namely the position of the triplet levels relative to the singlet levels. In the ground state of the dye molecule, which in the free-electron model is the state with the $(1/2)N$ lowest levels filled, the spins of two electrons occupying the same level are necessarily antiparallel, resulting in zero spin. However, there is also the possibility of a parallel arrangement of the spins if one of the electrons is raised to a higher level. The resulting spin $S = 1$ can place itself either parallel, antiparallel or orthogonal with respect to an external magnetic field. The parallel arrangement of the spins of the two most energetic electrons thus gives a triplet state of the same energy as the singlet state with zero spin within the framework of one-electron functions. The Dirac formulation of the Pauli exclusion principle states the total wave function, including the spin function, must be antisymmetric with respect to the exchange of any two electrons. In the two-electron case considered this means that the following four antisymmetrical product wave functions can be used. Here spin $+1/2$ is described by the spin function α, spin $-1/2$ by the spin function β:

$$\psi_s = \{\psi_m(1)\psi_n(2) + \psi_n(1)\psi_m(2)\}\{\alpha(1)\beta(2) - \alpha(2)\beta(1)\} ,$$

$$\psi_{T,+1} = \{\psi_m(1)\psi_n(2) - \psi_n(1)\psi_m(2)\}\{\alpha(1)\alpha(2)\} ,$$

$$\psi_{T,0} = \{\psi_m(1)\psi_n(2) - \psi_n(1)\psi_m(2)\}\{\alpha(1)\beta(2) + \alpha(2)\beta(1)\} ,$$

$$\psi_{T,-1} = \{\psi_m(1)\psi_n(2) - \psi_n(1)\psi_m(2)\}\{\beta(1)\beta(2)\} ,$$

where ψ_s is the singlet, $\psi_{T,+1}$, $\psi_{T,-1}$, $\psi_{T,0}$ are the three triplet wave functions, and the argument 1 or 2 refers to electron no. 1 or no. 2. Because of the symmetry of the spin factor, the spatial factor of these functions is symmetric for the singlet wave function and antisymmetric for the triplet wave functions. These spatial factors of one-dimensional two-electron functions can be interpreted in terms of two-dimensional one-electron functions

$$\psi_{m,n}(s_1, s_2) + \psi_{n,m}(s_1, s_2)$$

for the singlet case and

$$\psi_{m,n}(s_1, s_2) - \psi_{n,m}(s_1, s_2)$$

for the triplet case.

In a crude approximation, one can think of electron 1 as travelling in the upper lobe of the electron cloud along the molecular chain, its coordinate being s_1, and electron 2 in the lower lobe, its coordinate being s_2, as depicted for three relative positions in the right half of Fig. 1.14a. In the left half of this figure these three positions A, B, C are plotted in a plane determined by s_1 and s_2 as cartesian coordinates.

For every configuration of the two electrons we can give the repulsion energy of the two electrons

$$V = \frac{e_0^2}{Dr} = \frac{e_0^2}{D[(s_1 - s_2)^2 + d^2]^{1/2}} ,$$

where r is the distance between the two electrons, $d = 0.12$ nm is the distance between the centers of the upper and lower lobes, and D denotes the dielectric constant in which the two electrons are imbedded.

The potential energy profile has a crest along the symmetry axis $s_1 = s_2$ (Fig. 1.14b). Since the spatial factor of the singlet function is symmetric with respect to this axis, it must have antinodes there. By contrast, the antisymmetric spatial factor of the triplet wave functions has a nodal line along $s_1 = s_2$. Consequently, the mean potential energy of the electrons in the singlet state with quantum numbers n, m is higher than those in the triplet state with the same quantum numbers. This crude model gives the most important result that *for every excited singlet state there exists a triplet state of somewhat lower energy.* In addition the numerical calculation usually yields a value of the energy difference between corresponding singlet and triplet states that is correct within a factor of two or three.

Direct observation of absorptive transitions from the singlet ground state into triplet states is very difficult since the transitions are spin-forbidden and

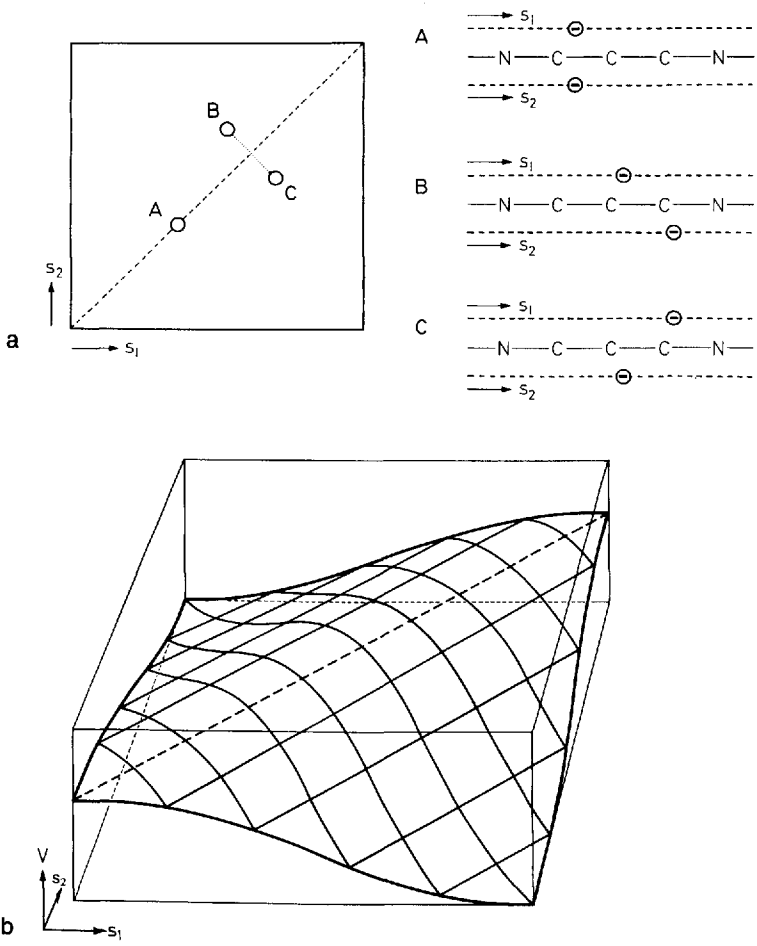

Fig. 1.14. (**a**) Three configurations of a two-electron system. The three points A, B, C in the cartesian coordinate system on the left belong to the three two-electron configurations pictured on the right. (**b**) Potential energy $V(s_1, s_2)$ of the two-electron system. (From Kuhn 1955)

the corresponding extinction coefficient at least a factor of 10^6 lower than that in spin-allowed $\pi \rightarrow \pi^*$ transitions.

Proceeding finally from the two-electron wave function to the N-electron wave function, the following picture of the eigenstates of the dye molecule is obtained (Fig. 1.15). There is a ladder of singlet states $S_i (i = 1, 2, 3, \ldots)$ containing also the ground state G. Somewhat displaced towards lower energies there is the ladder of triplet states $T_i (i = 1, 2, 3, \ldots)$. The longest wavelength absorption is from G to S_1, the next absorption band from G to S_2, etc. By contrast the absorption from G to T_i is spin-forbidden. The absorptions $G-S_1$, $G-S_2$, etc., will usually have differing transition moments. The fate of a molecule after it has undergone an absorptive transition and finds itself in an excited state S_1 or S_2 is discussed in the next section.

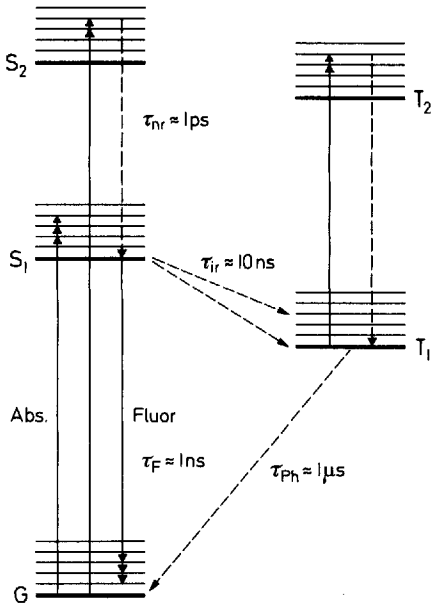

Fig. 1.15. Eigenstates of a typical dye molecule with radiative (*solid lines*) and nonradiative (*broken lines*) transitions

Recently a first example of dye laser emission of a radical was recorded (Ishizaka and Kotani 1985). The transient radical H_2N–⟨⟩–S was photochemically produced by irradiation of a liquid solution of H_2N–⟨⟩–S–S–⟨⟩–NH_2 by a XeCl laser and excited by the absorption of one or more additional photons of XeCl laser radiation. In this case of radicals with an odd number of π electrons, we have doublet and quartet instead of singlet and triplet states. Since the ground state is a doublet, and the quartet states, being doubly excited, lie higher than the corresponding doublet states, there is no intersystem crossing and consequently no quartet–quartet absorption with concomitant losses in dye laser operation.

1.3 Deactivation Pathways for Excited Molecules

There are very many processes by which an excited molecule can return directly or indirectly to the ground state. Some of these are schematically depicted in Fig. 1.15. It is the relative importance of these which mainly determines how useful a dye will prove in dye lasers. The one process that is directly used in dye lasers is the radiative transition from the first excited singlet state S_1 to the ground state G. If this emission, termed "fluorescence", occurs spontaneously, its radiative lifetime τ_{rf} is connected with the Einstein coefficient for spon-

taneous emission A and the oscillator strength f of the pertinent absorption band by

$$A \equiv 1/\tau_{rf} = (8\pi^2\mu^2 e_0^2/m_0 c_0)\tilde{\nu}^2 f \ ,$$

where μ is the refractive index of the solution, e_0 is the charge and m_0 is the mass of the electron, c_0 is the velocity of light, and $\tilde{\nu}$ denotes the wave number of the center of the absorption band. This relation is valid if the half-width of the emission band is small and its position is not shifted significantly from that of the absorption band. Since the f values of the transition are near unity in most dyes, the radiative lifetime τ_{rf} is typically of the order of a few nanoseconds. Generally, however, the fluorescence spectrum is broad and shows considerable Stokes shift. In this case the radiative lifetime can be computed with the aid of the following relation (Strickler and Berg 1962):

$$\frac{1}{\tau_{rf}} = 2.88\times 10^{-9}\mu^2 \frac{\int F(\tilde{\nu})d\tilde{\nu}}{\int \tilde{\nu}^{-3}F(\tilde{\nu})d\tilde{\nu}} \int_{\substack{\text{longest}\\ \text{wavelength}\\ \text{absorption band}}} \frac{\varepsilon(\tilde{\nu})d\tilde{\nu}}{\tilde{\nu}}$$

where $F(\tilde{\nu}) = dQ/d\tilde{\nu}$ is the fluorescence spectrum (in quanta Q per wave number) and $\varepsilon(\tilde{\nu})$ is the molar decadic extinction coefficient. There also exists the possibility that the energy hypersurface of the excited state will approach closely enough to the ground state for the molecule to tunnel through the barrier between them. It is then found in a very highly excited vibronic level of the ground state. This process is generally termed "internal conversion" and its rate constant is k_{SG}. There is very little theoretical knowledge about this and other related radiationless processes (Robinson and Frosch 1963; Nitzan and Jortner 1973a, b; E. J. Heller and Brown 1983; Kommandeur 1983). Experimental results (which range over several orders of magnitude of k_{SG}) will be discussed in detail in Chap. 5.

The difficult problem of the measurement of picosecond vibrational relaxation times of dye molecules in liquid solution in the ground and excited singlet states has been solved with different methods (Malley and Mourou 1974; Mourou and Malley 1974; Magde and Windsor 1974a; Ricard and Ducuing 1974; Ricard et al. 1972; Lin and Dienes 1973a; Mourou 1975; Laubereau et al. 1975; Ricard and Ducuing 1975; Shilov et al. 1976; Penzkofer and Falkenstein 1976; Penzkofer et al. 1976; Shank et al. 1977). Especially noteworthy is the measurement of vibrational relaxation times in a large dye molecule (coumarin 6) in the vapor phase under collisionless conditions, which showed that even in this case vibrational relaxation times are still only a few picoseconds (Maier et al. 1977) or even less (Erskine et al. 1984; A. J. Taylor et al. 1984; Rosker et al. 1986; Ackerman et al. 1982; Rentzepis and Bondybey 1984). A direct measurement of the intermolecular energy transfer between dye and solvent molecules is reported by Seilmeier et al. (1984).

The internal conversion between S_2 (and higher excited states) and S_1 is usually extremely fast, taking place in less than 10^{-11} s. This is the reason why

fluorescence quantum spectra of dyes generally do not depend on the excitation wavelength. The only known exception to these general rules was for a long time the aromatic molecule azulene and ist derivatives. The fluorescence of this molecule is directly from S_2 to the ground state, while internal conversion from S_1 to the ground state is so fast that no fluorescence originating in S_1 can be detected except with very high peak power laser pulses (Birks 1972). Recently several other examples of a weak fluorescence from S_2 to the ground state have been discovered (Steer and Ramamurthy 1988).

The radiationless transition from an excited singlet state to a triplet state can be induced by internal perturbations (spin-orbit coupling, substituents containing nuclei with high atomic number) as well as by external perturbations (paramagnetic collision partners, like O_2 molecules in the solution or solvent molecules containing nuclei of high atomic number). These radiationless transitions are usually termed "intersystem crossing" and have the rate constant k_{ST}.

If some fluorescence quenching agent Q is present in a solution or gas mixture in a known concentration [Q], its contribution to the radiationless deactivation can be separated and expressed by a rate constant $k'_{SG} = k_Q[Q]$. Since for most quenchers quenching occurs at every encounter with an excited dye molecule, k_Q equals the diffusion-controlled bimolecular rate constant, given by $k_Q = 8RT/2000\eta$, where R is the gas constant, T the absolute temperature and η the viscosity of the solvent (Osborne and Porter 1965).

The quantum yield of fluorescence, ϕ_f, is then defined as the ratio of radiative and nonradiative transition rates

$$\phi_f = \frac{1/\tau_{rf}}{1/\tau_{rf} + k_{ST} + k_{SG} + k_Q[Q]} .$$

The denominator is the reciprocal of the observed fluorescence lifetime τ_f. The quantum yield of fluorescence can thus be calculated from the measured fluorescence lifetime τ_f and the radiative lifetime τ_{rf}, obtained through the absorption spectrum: $\phi_f = \tau_f/\tau_{rf}$. This method usually gives good results, whereas the direct experimental measurement of absolute quantum yields is very difficult (see Chap. 5).

The radiative transition from $T_1 \rightarrow G$ is termed "phosphorescence". In principle, one should be able to estimate the radiative lifetime τ_{rp} of the phosphorescence on the basis of the $G \rightarrow T_1$ absorption. Since this transition is normally completely obscured by absorption due to impurities, the phosphorescence radiative lifetime can be obtained from the quantum yield of phosphorescence, ϕ_p, and the observed phosphorescence lifetime τ_p, as for fluorescence: $\tau_p = \phi_p \tau_{rp}$. As expected for spin-forbidden transitions, it is extremely long, ranging from milliseconds to many seconds for molecules with small spin-orbit coupling. Consequently, even relatively slow quenching processes can lead to radiationless deactivation in liquid solution. Hence the observed τ_p is generally very low in liquid solution, becoming appreciable only at low temperatures, e.g. 77 K in solid solutions. (A similar comment can be

made regarding the long-lived emission resulting from the above-mentioned $\pi^* \leftarrow n$ transitions, which are usually very weak, if any fluorescence is observed at all.) Note that ϕ_p is the true quantum yield of phosphorescence. It is defined as the ratio of the phosphorescence rate to the total rate of radiative and radiationless deactivation

$$\phi_p = \frac{1/\tau_{rp}}{1/\tau_{rp} + k_{TG} + k_Q[Q]} .$$

For comparison, one often quotes the apparent quantum yield of phosphorescence ϕ_p^+, which relates the rate of phosphorescence emission to the rate of light absorption. The relation between the two is $\phi_p^+ = \phi_p \phi_T$. Here ϕ_T is the triplet formation efficiency, i.e. the ratio of the intersystem crossing rate k_{ST} to the total rate of deactivation of the fluorescent level:

$$\phi_T = \frac{k_{ST}}{1/\tau_{rf} + k_{ST} + k_{SG} + k_Q \cdot [Q]} .$$

Usually no measurable phosphorescence can be observed in liquid solutions. Here τ_p, which is identical with the triplet lifetime τ_T, is often determined by flash spectroscopy from the vanishing of the triplet–triplet absorption bands. Assuming the value of the radiative lifetime at elevated temperatures is the same as at low temperatures, the quantum yield ϕ_p in liquid solutions can be obtained. To give a typical example, for the eosin-di-anion in methanol (7×10^{-5} mole/l) the phosphorescence lifetime at room temperature is $\tau_p = 1.5$ ms, the apparent quantum yield of phosphorescence $\phi_p^+ = 3.9 \times 10^{-3}$, the triplet quantum yield $\phi_T = 0.45$, hence the radiative lifetime $\tau_{rp} = 0.2$ s (Parker and Hatchard 1961).

The lowest singlet and triplet states can also be deactivated by a long-range radiationless energy transfer to some other dye molecule. For this to happen, the absorption band of the latter, "acceptor" molecule must overlap the fluorescence or phosphorescence band of the former, "sensitizer" molecule. The so-called critical distance, at which the quantum yield is reduced by a factor of two, can reach values of 10 nm for the case of singlet–singlet energy transfer. For details of these and some other processes resulting in "delayed fluorescence", which is less important in the present context, the reader is referred to Parker (1968).

Other deactivation pathways for the excited molecule include reversible and irreversible photochemical reactions, e.g. protolytic reactions, cis-trans-isomerizations, dimerizations, ring-opening reactions and many others. Some of these which are of major importance in dye lasers are discussed in Chap. 5.

The absorptive transitions of excited molecules into higher excited states can constitute a loss mechanism for the pump as well as the dye-laser radiation. It thus is of utmost importance for dye-laser operation.

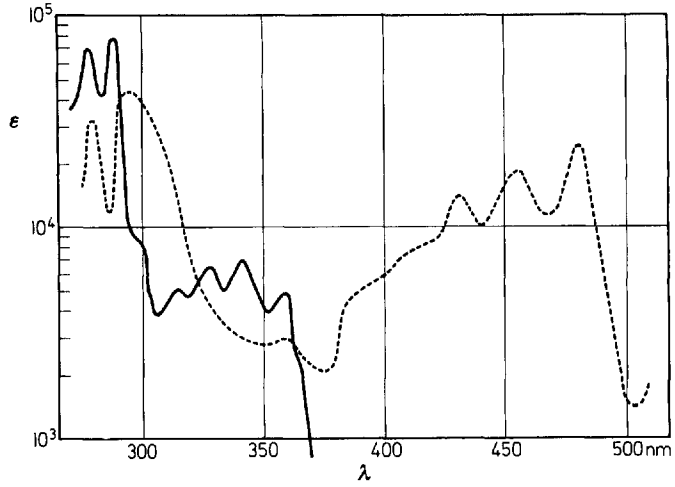

Fig. 1.16. Triplet–triplet absorption spectrum (*broken line*) of 1,2-benzanthracene in hexane (*solid line*: absorption spectrum from ground to excited states). (From Labhart 1964)

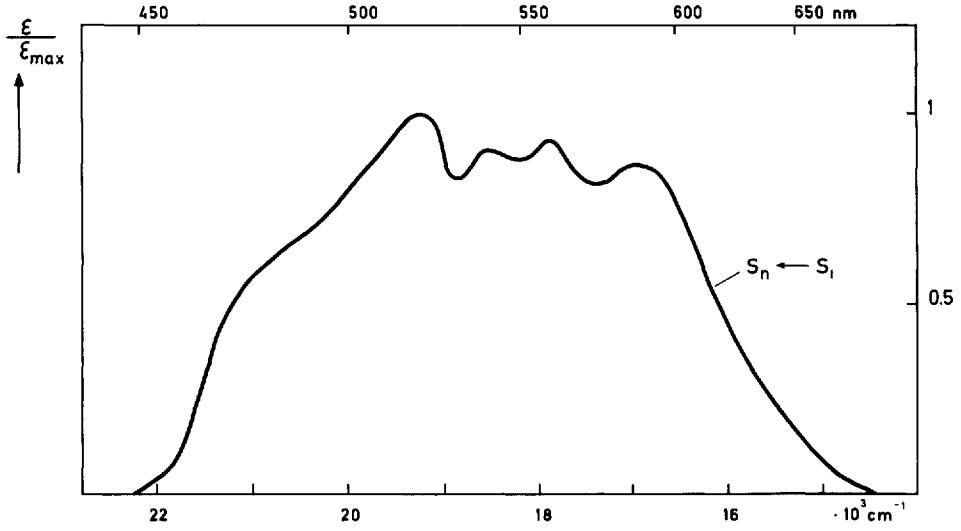

Fig. 1.17. $S_1 \rightarrow S_n$-absorption spectrum of 1,2-benzanthracene in ethanol. (From Müller and Sommer 1969)

Triplet–triplet absorption is measured by flash photolysis as well as by photostationary methods (Porter and Windsor 1958; Labhart 1964; Zanker and Miethke 1957b). An example of dye spectra thus obtained is given in Fig. 1.16. It is much more difficult to measure the absorption from the short-lived excited singlet state and has only become possible through the use of laser spectroscopy methods (Novak and Windsor 1967; Müller 1968; Bonneau et al.

1968). So far spectra for only about 20 molecules have been recorded (Birks 1970). An example is given in Fig. 1.17.

1.4 Laser-Pumped Dye Lasers

1.4.1 Oscillation Condition

From the foregoing discussion of the spectroscopic properties of dyes one might come to the conclusion that there are two possible ways, at least in principle, of using an organic solution as the active medium in a laser: One might utilize either the fluorescence or the phosphorescence emission. At first sight the long lifetime of the triplet state makes phosphorescence look more attractive. On the other hand, due to the strongly forbidden transition, a very high concentration of the active species is required to obtain an amplification factor large enough to overcome the inevitable cavity losses. In fact, for many dyes this concentration would be higher than the solubility of the dyes in any solvent. A further unfavorable property of these systems is that there will almost certainly be losses due to triplet–triplet absorption. It must be remembered that triplet–triplet absorption bands are generally very broad and diffuse and the probability they will overlap the phosphorescence band is high. Because of these difficulties no laser using the phosphorescence of a dye has yet been reported [a preliminary report (Morantz et al. 1962 and Morantz 1963) was evidently in error]. The possibility cannot be excluded, however, that further study of phosphorescence and triplet–triplet absorption in molecules of different types of chemical constitution might eventually lead to a triplet dye laser operating, for example, at the temperature of liquid nitrogen. On the other hand, the probability for this seems low at present and these systems will not be considered here. For a more detailed discussion of phosphorescent systems the reader is referred to Lempicki and Samelson (1966).

If the fluorescence band of a dye solution is utilized in a dye laser, the allowed transition from the lowest vibronic level of the first excited singlet state to some higher vibronic level of the ground state will give a high amplification factor even at low dye concentrations. The main complication in these systems is the existence of the lower-lying triplet states. The intersystem crossing rate to the lowest triplet state is high enough in most molecules to reduce the quantum yield of fluorescence to values substantially below unity. This has a twofold consequence: Firstly, it reduces the population of the excited singlet state, and hence the amplification factor; and secondly, it enhances the triplet–triplet absorption losses by increasing the population of the lowest triplet state. Assume a light-flux density which slowly rises to a level P [quanta s^{-1} cm^{-2}], a total molecular absorbing cross-section σ[cm^2][1], a quantum yield ϕ_T of

[1] The absorption cross-section σ can be determined from the molar decadic extinction coefficient ε by $\sigma = 0.385 \times 10^{-20} \varepsilon$. Here σ is given in cm^2, if ε is measured in liter/(mole cm).

triplet formation, a triplet lifetime τ_T, populations of the triplet and ground state of n_T and n_0 [cm^{-3}], respectively, and, neglecting the small population of the excited singlet state, a total concentration of dye molecules of $n = n_0 + n_T$. A steady state is reached when the rate of triplet formation equals the rate of deactivation:

$$P\sigma n_0 \phi_T = n_T/\tau_T \ . \tag{1.1}$$

Thus, the fraction of molecules in the triplet state is given by

$$n_T/n = P\sigma\phi_T\tau_T/(1+P\sigma\phi_T\tau_T) \ . \tag{1.2}$$

Assuming some typical values for a dye, $\sigma = 10^{-16}\,cm^2$, $\phi_T = 0.1$ (corresponding to a 90% quantum yield of fluorescence), and $\tau_T = 10^{-4}\,s$, the power to maintain half of the molecules in the triplet state is $P_{1/2} = 10^{21}$ quanta $s^{-1}\,cm^{-2}$, or an irradiation of only 1/2 kW cm^{-2} in the visible part of the spectrum. This is much less than the threshold pump power calculated below. Hence a slowly rising pump light pulse would transfer most of the molecules to the triplet state and deplete the ground state correspondingly. On the other hand, the population of the triplet level can be held arbitrarily small, if the pumping light flux density rises fast enough, i.e. if it reaches threshold in a time t_r which is small compared to the reciprocal of the intersystem crossing rate $t_r \ll 1/k_{ST}$. Here t_r is the risetime of the pump light power, during which it rises from zero to the threshold level. For a typical value of $k_{ST} = 10^7\,s^{-1}$, the risetime should be less than 100 ns. This is easily achieved, for example with a giant-pulse laser as pump light source, since giant pulses usually have risetimes of 5–20 ns. In such laser-pumped dye-laser systems one may neglect all triplet effects in a first approximation.

We thus can restrict our discussion to the singlet states. Molecules that take part in dye-laser operation have to fulfill the following cycle (Fig. 1.18): Absorption of pump radiation at $\tilde{\nu}_p$ and with cross-section σ_p lifts the molecule from the ground state with population n_0 into a higher vibronic level of the first (or second) excited singlet state S_1 (or S_2) with a population n_1' (or n_2'). Since the radiationless deactivation to the lowest level of S_1 is so fast (see Sect. 1.3), the steady-state population n_1' is negligibly small, provided the temperature is not so high that this vibronic level is already thermally populated by the Boltzmann distribution of the molecules in S_1. At room temperature, $kT = 200\,cm^{-1}$, so that this is not the case. Stimulated emission then occurs from the lowest vibronic level of S_1 to higher vibronic levels of G. Again the population n_0' of this vibronic level is negligible since the molecules quickly relax to the lowest vibronic levels of G.

It is easy then to write down the oscillation condition for a dye laser (Schäfer 1968; Schäfer et al. 1968). In its simplest form a dye laser consists of a cuvette of length L [cm] with dye solution of concentration n [cm^{-3}] and of two parallel end windows carrying a reflective layer each of reflectivity R for the laser resonator. With n_1 molecules/cm^3 excited to the first singlet state, the

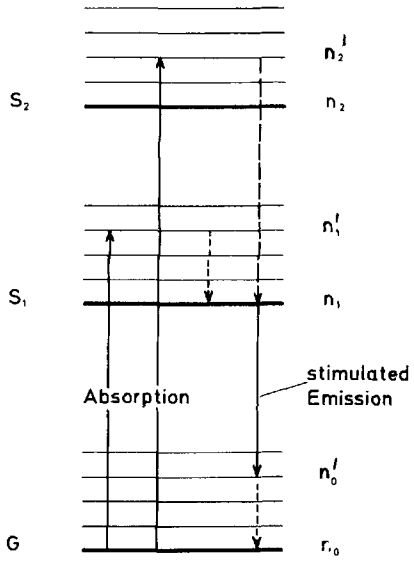

Fig. 1.18. Pump cycle of dye molecules

dye laser will start oscillating at a wave number $\tilde{\nu}$, if the overall gain is equal to or greater than one:

$$\exp\left[-\sigma_a(\tilde{\nu})n_0 L\right] R \exp\left[+\sigma_f(\tilde{\nu})n_1 L\right] \geqq 1 \ . \tag{1.3}$$

Here $\sigma_a(\tilde{\nu})$ and $\sigma_f(\tilde{\nu})$ are the cross-sections for absorption and stimulated fluorescence at $\tilde{\nu}$, respectively, and n_0 is the population of the ground state. The first exponential term gives the attenuation due to reabsorption of the fluorescence by the long-wavelength tail of the absorption band. The attenuation becomes the more important, the greater the overlap between the absorption and fluorescence bands. The cross-section for stimulated fluorescence is related to the Einstein coefficient B

$$\sigma_f(\tilde{\nu}) = g(\tilde{\nu})Bh\tilde{\nu}/c_0 \int\limits_{\substack{\text{fluorescence}\\ \text{band}}} g(\tilde{\nu})d\tilde{\nu} = 1 \ . \tag{1.4}$$

Substituting the Einstein coefficient A for spontaneous emission according to

$$B = \frac{1}{8\pi\tilde{\nu}^2} A \frac{1}{h\tilde{\nu}} \tag{1.5}$$

and realizing that $g(\tilde{\nu})A\phi_f = Q(\tilde{\nu})$, the number of fluorescence quanta per wave number interval, one obtains

$$\sigma_f(\tilde{\nu}) = \frac{1}{8\pi c_0 \tilde{\nu}^2} \frac{Q(\tilde{\nu})}{\phi_f} \ . \tag{1.6}$$

Since the fluorescence band usually is a mirror image of the absorption band, the maximum values of the cross-sections in absorption and emission are found to be equal:

$$\sigma_{f,\max} = \sigma_{a,\max} \cdot \tag{1.7}$$

Taking the logarithm of (1.3) and rearranging it leads to a form of the oscillation condition which makes it easier to discuss the influence of the various parameters:

$$\frac{S/n + \sigma_a(\tilde{\nu})}{\sigma_f(\tilde{\nu}) + \sigma_a(\tilde{\nu})} \leqq \gamma(\tilde{\nu}) \ , \tag{1.8}$$

where $S = (1/L) \ln (1/R)$ and $\gamma(\tilde{\nu}) = n_1/n$.

The constant S on the left-hand side of (1.8) only contains parameters of the resonator, i.e. the active length L, and reflectivity R. Other types of losses, like scattering, diffraction, etc., may be accounted for by an effective reflectivity, R_{eff}. The value $\gamma(\tilde{\nu})$ is the minimum fraction of the molecules that must be raised to the first singlet state to reach the threshold of oscillation. One may then calculate the function $\gamma(\tilde{\nu})$ from the absorption and fluorescence spectra for any concentration n of the dye and value S of the cavity. In this way one finds the frequency for the minimum of this function. This frequency can also be obtained by differentiating (1.8) and setting $d\gamma(\tilde{\nu})/d\tilde{\nu} = 0$. This yields

$$\frac{\sigma_a'(\tilde{\nu})}{\sigma_f'(\tilde{\nu}) + \sigma_a'(\tilde{\nu})} (\sigma_f(\tilde{\nu}) + \sigma_a(\tilde{\nu})) = \frac{S}{n} \tag{1.9}$$

(prime means differentiation with respect to $\tilde{\nu}$) from which the start-oscillation frequency can be obtained.

Figure 1.19 represents a plot of the laser wavelength λ (i.e. the wavelength at which the minimum of $\gamma(\tilde{\nu})$ occurs) versus the concentration with S a fixed parameter. Similarly, Fig. 1.20 shows the laser wavelength versus the active length L of the cuvette with dye solution, with the concentration of the dye as a parameter. Both figures apply to the dye 3,3'-diethylthiatricarbocyanine (DTTC). These diagrams demonstrate the wide tunability range of dye lasers

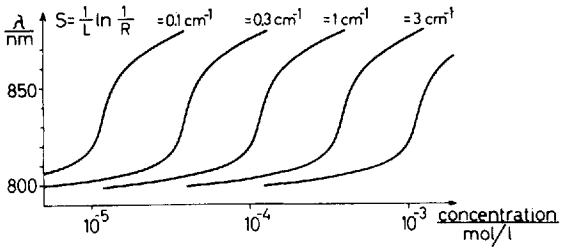

Fig. 1.19. Plot of calculated laser wavelength vs concentration of the laser dye 3,3'-diethylthiatricarbocyanine bromide, with S as a parameter. (From Schäfer 1968)

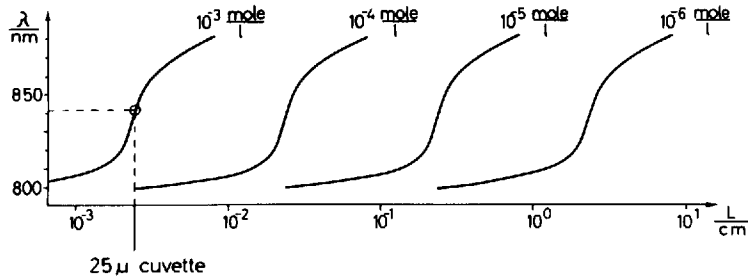

Fig. 1.20. Plot of calculated laser wavelength vs active length of the laser cuvette, with the concentration of the solution of the dye 3,3'-diethylthiatricarbocyanine bromide as a parameter. (From Schäfer 1968)

which can be induced by changing the concentration of the dye solution, or length, or Q of the resonating cavity. They also show the high gain which permits the use of extremely small active lengths.

The absorbed power density W necessary to maintain a fraction γ of the molecular concentration n in the excited state is

$$W = \gamma n h c_0 \tilde{\nu}_p / \tau_f \ , \tag{1.10}$$

and the power flux, assuming the incident radiation is completely absorbed in the dye sample,

$$P = W/n\sigma = \gamma h c_0 \tilde{\nu}_p / \tau_f \sigma \ , \tag{1.11}$$

where $\tilde{\nu}_p$ is the wave number of the absorbed pump radiation. If the radiation is not completely absorbed, the relation between the incident power W_{in} and the absorbed power is $W = W_{in}[1 - \exp(-\sigma_p n_0 L)]$. Since in most cases $n \approx n_0$, this reduces for optically thin samples to $W = W_{in}\sigma_p n L$. The threshold incident power flux, P_{in}, then is

$$P_{in} = \gamma h c_0 \tilde{\nu}_p / \tau_f \sigma_p \ .$$

In the above derivation of the oscillation condition and concentration dependence of the laser wavelength, broad-band reflectors have been assumed. The extension to the case of wavelength-selective reflectors and/or dispersive elements in the cavity is straightforward and will not be treated here.

1.4.2 Practical Pumping Arrangements

A simple structure for a dye-solution laser was used in many of the early investigations. It is still useful for exploratory studies of new dyes. It consists of a square spectrophotometer cuvette filled with the dye solution (Fig. 1.21) which is excited by the beam from a suitable laser. As shown in the figure, the resonator is formed by the two glass-air interfaces of the polished sides of the

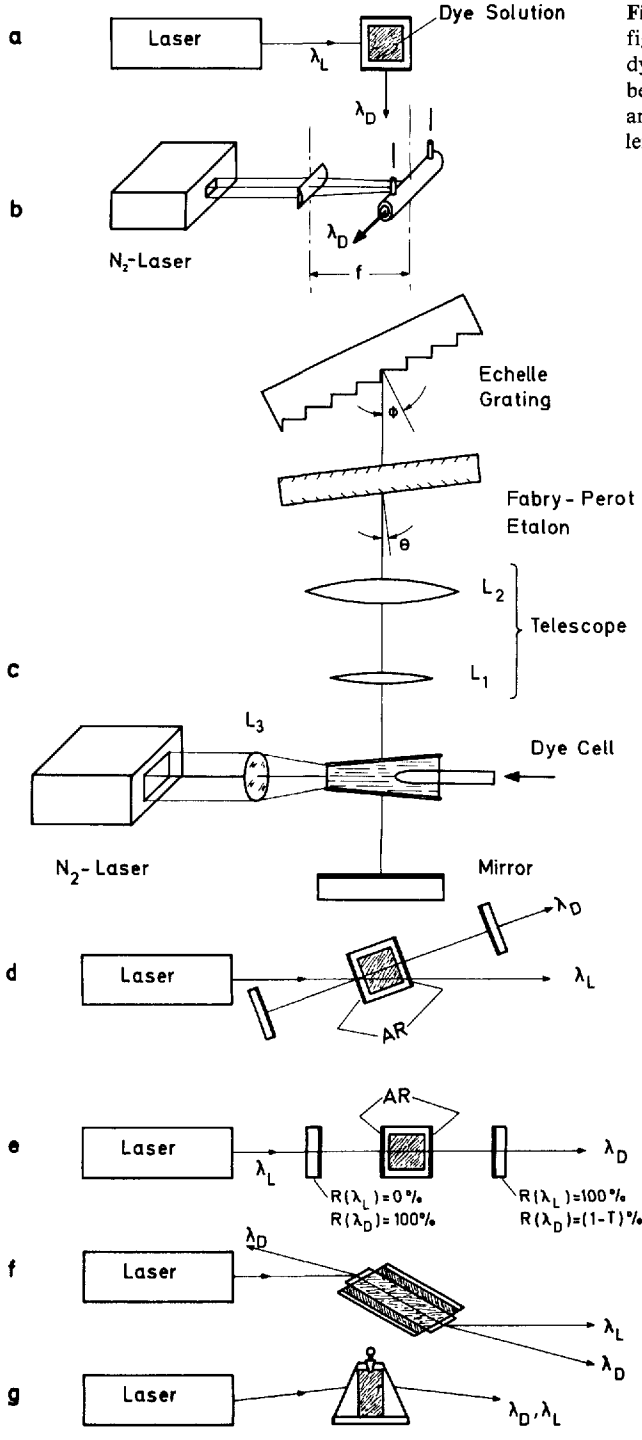

Fig. 1.21a–g. Resonator configurations for laser-pumped dye lasers. (λ_L pumping-laser beam, λ_D dye-laser beam, AR antireflection coating, f focal length of cylindrical lens

cuvette (heavy lines in Fig. 1.21 a) and the exciting laser and dye-laser beams are at right angles. Reflective coatings on the windows consisting of suitable metallic or multiple dielectric layers enhance the Q of the resonator. It is also possible to use antireflective coatings or Brewster windows at the cuvette and separate resonator mirrors. In the transverse pumping arrangement (Fig. 1.21 a) the population inversion in the dye solution is nonuniform along the exciting laser beam, since the exciting beam is attenuated in the solution. Consequently, at a higher concentration, the threshold might only be reached in a thin layer directly behind the entrance window of the exciting beam. This gives rise to large diffraction losses and beam divergence angles. If the concentration is not too high, say, less than 10^{-4} molar, the measured threshold pump power in such an arrangement can be used to test the value calculated from the oscillation condition. Using (1.8) and (1.11), known spectral data, and the observed spontaneous decay time of fluorescence $\tau_f = 2$ ns, one computes a threshold pump power flux of $P = 1.2\times10^5$ W/cm^2 for the exciting giant pulse ruby laser and a 10^{-4} molar solution of 3,3'-diethylthiatricarbocyanine bromide in methanol in a 1 cm square spectrophotometric cuvette. The experimental value is 3.0×10^5 W/cm^2, while the calculated and observed values for a 10^{-3} molar solution are 1.2×10^4 W/cm^2 and 1.2×10^5 W/cm^2, respectively (Volze 1969). The higher value of the observed threshold for the 10^{-4} molar solution is easily accounted for by neglection of triplet losses. The risetime of the exciting pulse was 8 ns in these experiments, while the spontaneous lifetime of the dye is 2 ns. An estimate of the quantum yield of fluorescence gives $\phi_f = 0.4$. Hence, an appreciable fraction of the molecules has already been converted to the triplet state at threshold. The larger discrepancy between calculated and observed values for the 10^{-3} molar solution can be traced to the high diffraction losses. In this experiment the exciting laser beam is attenuated to 1/e of incident intensity in a depth of only 85 μm. A similar transverse arrangement is often used for nitrogen laser-pumped dye lasers (Fig. 1.21 b). Here the emission of a nitrogen laser is focused by a cylindrical lens into a line that coincides with the axis of a quartz capillary of inside diameter $d \approx 1$ mm. The transmitted pump radiation is reflected by an aluminum coating at the back surface of the capillary tube. If the beam divergence of the nitrogen laser is α and the length of the cylindrical lens f, then the width of the focal line is $H = f\alpha$ and is best so chosen that H is about one fourth of the inside diameter of the tube. The dye concentration c is then adjusted so that the absorption $A = 2\varepsilon c d \approx 1$. The endfaces of the tube can either be normal to the axis and act directly as resonator mirrors, or set at the Brewster angle for use with external mirrors.

Another arrangement developed early for the pumping of dye lasers with a nitrogen laser is shown in Fig. 1.21 c (Hänsch 1972). The dye cell is 10 mm long and is made of 12-mm diameter Pyrex tubing. Antireflection-coated quartz windows are sealed to the ends of the cell under a wedge angle of about 10 degrees to avoid internal cavity effects. The dye solution is transversely circulated by means of a small centrifugal pump at a flow speed of about 1 m/s in the active region. The nitrogen laser emission is focused by a spherical lens

of 135 mm focal length into a line of about 0.15 mm width at the inner cell wall. To provide a near-circular active cross-section, the dye concentration is adjusted so that the penetration of the pump light is also of the order of 0.15 mm. A plane outcoupling mirror is mounted at one end of the optical cavity at a distance of 50 mm. Because of the large ratio of this distance to the diameter of the active region, the latter acts as an active pinhole and the emerging beam is essentially diffraction-limited and has a beam divergence (at 600 nm emission wavelength) of 2.4 mrad. The other end of the cavity contains an inverted telescope, consisting of two lenses L_1 and L_2 of focal lengths $f_1 = 8.5$ mm and $f_2 = 185$ mm (antireflection-coated multielement systems corrected for spherical aberration and coma within $\lambda/8$) and a separation between cell and lens L_1 of 75 mm. The lenses are used slightly off-axis to avoid back reflection and etalon effects. The initial waist size of 0.08 mm is thus enlarged to 4 mm and the beam divergence is reduced to 0.05 mrad. This is especially important if a diffraction grating in Littrow mounting is to be used instead of a second mirror. In this case, if the beam were unexpanded, it would eventually burn the grating and the spectral resolution would be very low.

A better configuration for laser-pumped dye lasers is the longitudinal arrangement (Sorokin et al. 1966b) of Fig. 1.21e. In this arrangement the exciting laser beam passes through one of the resonator mirrors of the dye laser. For best effect this is coated by a dielectric multilayer mirror with a very low reflection coefficient at the exciting-laser wavelength and a high one at the dye-laser wavelength. Concentration and depth of the solution should be adjusted so that the excitation power is very nearly uniform over the whole volume of the cuvette. This results in a much lower beam divergence. Typical values of 3–5 mrad were reported. It is often more convenient to orient the exciting-laser beam a few degrees to the normal of the mirror for spatial separation of the exciting-laser and the dye-laser beams. If the dimension of the cuvette is much smaller than the cavity length, the exciting-laser beam may pass by the side of the laser mirror (Fig. 1.21d). This eliminates the requirement for a special mirror system that must withstand the full power of the exciting laser.

Another advantage of the longitudinal pumping arrangement is the possibility of using an extremely small depth of dye solution. Volze (1969) described a dye laser consisting of two mirrors in direct contact with the dye solution and kept apart by spacers ranging from 100 μm down to 5 μm. The mirrors had 80% transmission at the exciting ruby-laser wavelength, and a constant 98% reflection over the range of the dye-laser emission. Using a 10^{-3} molar solution of 3,3′-diethylthiatricarbocyanine bromide (or other anion), the observed threshold for a 5 μm spacer is 350 kW/cm^2, while the computed value is 120 kW/cm^2. This is about the same error factor as in the above transverse pumped case with the 10^{-4} molar solution. Here, too, the error should be due mainly to neglect of the triplet losses. The operation of a dye laser of only 5 μm width demonstrates the extremely high gain in the dye solution. This experiment indicates an amplification factor of 1.02 per 5 μm which implies a gain of $G = 170$ dB/cm.

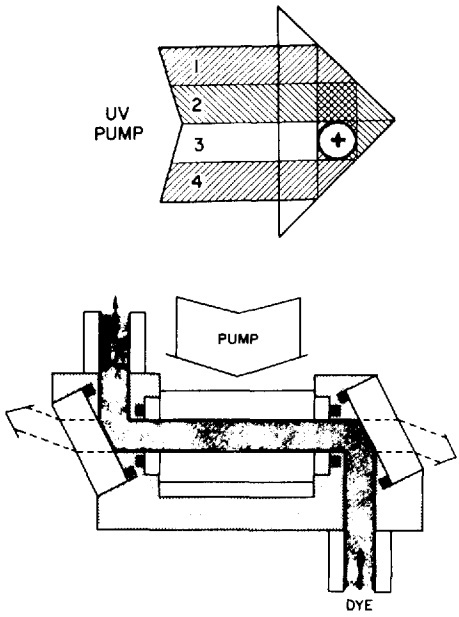

Fig. 1.22. Cross-sections through a Bethune-type cell. (From Bethune 1981)

An ingenious improvement of transversal pumping was reported by Bethune (1981). It takes advantage of a dye cell in the form of a roof-top prism with a longitudinal bore, as shown in Fig. 1.22. If a pump beam enters the hypotenuse face normally, the four partial beams 1–4, indicated by different hatching in the figure, illuminate the bore from four sides, thus creating a more uniform illumination of the dye solution in the bore than can be obtained with the normal transverse pumping using only a cylindrical lens. A quantitative treatment shows that this solution is still not completely satisfactory, since the pump intensity of each partial beam decreases towards the center by the absorption in the dye solution, resulting in a minimum of the intensity distribution near the axis, thus creating a ring-shaped inversion for any value of absorption coefficient that gives reasonable pump-light absorption.

An improvement circumventing the described disadvantage was described by Schäfer (1986). It makes use of a 45° glass cone with an axial bore, as shown in cross-section in Fig. 1.23. A pump beam entering normal to the cone base is totally reflected at the conical surface and impinges normally on the bore containing the dye solution. Since now the pump radiation is focused on the axis, one can easily calculate that the intensity has a maximum on the axis and perfect rotational symmetry is obtained.

Superradiant dye lasers can be pumped either by a normal giant-pulse laser or by ultrashort pulses. In the first case (Fig. 1.21 f), the exciting-laser pulse passes through a cuvette of small optical length compared to the length of the exciting pulse.

Typically, the solution is contained in a 5-cm Brewster cuvette with quartz tubing and windows (Volze 1969). The solvent DMSO has the same refractive

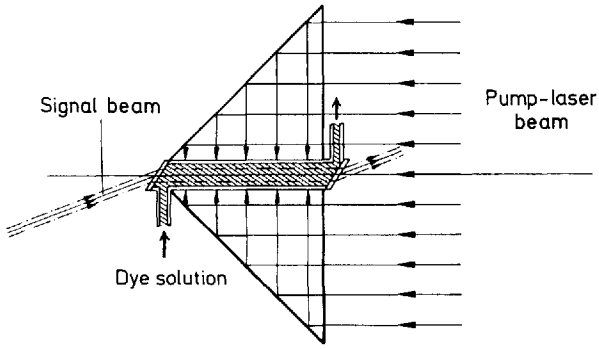

Fig. 1.23. Cross-section through an axicon dye cell. (Adapted from Schäfer 1986)

index ($n = 1.48$) as the cuvette walls. The cuvette tubing is surrounded by a cylinder containing a suitable dye solution in a solvent of higher refractive index so that fluorescence light incident on the cuvette walls is absorbed. This eliminates the unwanted closed-feedback path. Near the peak of the exciting-laser pulse the spatial distribution of pump light in the cuvette is nearly stationary. With this assumption, the amplification can be computed for spontaneously emitted fluorescence quanta that originate at one window and travel along the optical axis towards the other window. As expected, in this model the superradiant dye-laser intensities are almost equal in both forward and backward directions, and the beam divergence is determined by the aspect ratio of the cuvette. A plot of the superradiant versus the exciting intensity for this configuration with a 3×10^{-5} molar solution of DTTC is shown in Fig. 1.24.

For traveling-wave excitation of a superradiant dye laser, the solution is contained in a wedged (10°) cell typically 2 cm in depth (Mack 1969). A methanol solution of DTTC or some similar dye is pumped by a ruby-laser pulse of a few ps half-width and 5 GW peak power. This results in an almost complete inversion of the dye solution at the position of the exciting pulse with correspondingly high gain. For a pulsewidth of 5 ps, corresponding to an inverted region of 2 mm, spontaneously emitted fluorescence quanta passing through this region would experience a maximum gain of 50 dB in a 10^{-4} molar solution of DTTC. It is assumed that no saturation effects occur and that the relaxation time from the initial Franck-Condon state to the upper laser level is negligible compared to the duration of the exciting pulse. Since the vibrational relaxation time of dyes in solution is generally of the order of a few ps, and since saturation certainly must occur as the exciting pulse travels through the cuvette, the actual gain is less than the above value. The traveling-wave nature of the superradiant dye-laser emission may be verified by measuring the forward to backward ratio of the dye-laser emission. It turned out to be 100 to 1 in this experiment, and the beam divergence was 15 mrad.

The polarization of the dye laser beam in the longitudinal and transverse arrangements is determined mainly by the polarization of the exciting laser beam, the relative orientation of the transition moments in the dye molecule for the pumping and laser transitions, and the rotational diffusion–relaxation

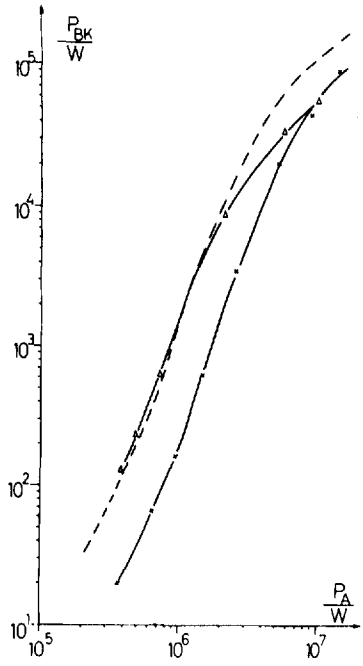

Fig. 1.24. Superradiant power P_{BK} from a Brewster angle cuvette vs pumping laser power P_A for a 3×10^{-5} M solution of 3,3'-diethylthiacarbocyanine bromide. (Triangles: emission in backward direction; crosses: emission in forward direction. The broken line gives the theoretical expectation). (From Volze 1969)

time. The latter is determined by solvent viscosity, temperature and molecular size. The direction of the transition moments of the fluorescence and the long-wavelength absorption is identical, since the same electronic transition is involved in both processes. For rotational diffusion–relaxation times which are long compared to the exciting pulse, the following table gives the theoretically expected relative orientation of the pumping and dye-laser polarization. In two cases one obtains a depolarized dye-laser beam. There the emissive transition moments of the excited molecules are directed along the resonator axis. Hence, the molecules must first rotate before they can radiate along the resonator axis. Since this rotation is effected by diffusion, the resulting angular orientation distribution is essentially isotropic and the laser output is depolarized. The same is true when the rotational diffusion-relaxation time is short compared to the pumping pulse. A special case is that of large, ring-type molecules like the phthalocyanines. These have two degenerate transitions with orthogonal transition moments in the plane of the ring. The polarization of dye lasers with these compounds is given in brackets in the following table. Very few such possibilities have been experimentally investigated and verified (Sorokin et al. 1967; Sevchenko et al. 1968a, b; McFarland 1967). In addition, the polarization of dye laser beams can, of course, be manipulated in obvious ways by introducing into the resonator polarizing elements like Brewster windows.

The above techniques employ cells for the containment of liquid dye solutions, but even simpler arrangements are possible with solid solutions of dyes or dye crystals. Various dyes have been incorporated in polymethylmethacry-

Relative orientation of pumping and dye-laser polarizations	Relative orientation of transition moments in absorption and emission	
	∥ to each other	⊥ to each other
Longitudinal pumping	∥ (depol.)	⊥ (depol.)
Transverse pumping, pump laser polar. ⊥ to P	∥ (depol.)	⊥ (⊥)
Transverse pumping, pump laser polar. ∥ to P	depol. (⊥)	depol. (depol.)

P = plane containing exciting and dye-laser beams. Data in brackets refer to large, ring-type molecules, e.g. phthalocyanines.

late and other plastics (Soffer and McFarland 1967). If two parallel faces of such a sample are optically polished, the Fresnel reflection of the air-plastics interface can be utilized as the air-glass reflection in the spectrophotometer cuvette of Fig. 1.21a. A number of dyes have been dissolved in gelatin. The molten gelatin was poured onto a glass slide in a layer a few microns thick. After hardening, this thin film could be stripped off the glass slide. It showed strong superradiant emission when the emission of a nitrogen laser was focused on it with a cylindrical lens (Hänsch et al. 1971a).

Free jets of flowing dye solutions have completely replaced the easily damaged dye cells for cw dye lasers. Since they are not often used with pulsed dye lasers, they will be described in Chap. 3.

Organic single crystals, e.g. fluorene crystals containing 2×10^{-3} anthracene, which grow and cleave well, can also be pumped by a nitrogen laser, using the two cleaved faces of the laser crystal itself as the optical resonator (Karl 1972). In the case of the fluorene crystal containing anthracene as laser dye, the crystals had a thickness of 0.3–0.7 mm and absorbed the pump light almost completely. Laser emission was found at 408 nm.

The vapor pressure of many nonionic laser dyes is quite high at relatively low temperatures. For example, the dye POPOP (1,4-di-[2-phenyloxazolyl]benzene) has a vapor pressure of 20 Torr at a temperature of 410 °C, corresponding to a concentration of 4×10^{-4} mole/l, similar to the concentrations used in dye solution lasers. Using exactly these conditions and a 2-cm cell with 20% reflectivity coatings at 400 nm, the first purely vapor-phase dye laser emission was observed when the power of the pumping nitrogen laser was raised above 1 MW (Steyer and Schäfer 1974a). An intermediate case between vapor phase and solution is obtained when high pressures (usually some tens of atmospheres) of solvent vapor, e.g. isopentane or ether, are used, which enhances the volatility and thermal stability of the dye molecules (Borisevich et al. 1973). Using polar solvents above the critical point, one could even expect vapor-phase dye laser emission from ionic dyes, which, however, has not yet been attempted. A fairly recent review of vapor-phase dye lasers (Stoilov 1984) lists 57 suitable laser dyes, some of which have shown efficiencies of up to 42%.

Pump lasers used so far with one or the other of the above arrangements include neodymium (1.06 μm) and its harmonics (532 nm, 354 nm, and 266 nm), ruby (694 nm) and its harmonic (347 nm), nitrogen (337 nm), excimer lasers (XeCl, 308 nm; KrF, 248 nm; XeF, 351 nm, etc.), copper-vapor lasers (510 and 578 nm), xenon-ion lasers (multiline from 430 to 596 nm), and other dye lasers.

If the repetition rate of the pump pulses is increased above about one shot per minute, the heat generated via radiationless transitions in the dye molecules and energy transfer to the solvent can cause schlieren in the cuvette, which reduce the dye-laser output. It is thus advisable to use a flow system so that the cuvette contains fresh solution for every shot. Obviously, this is also the way to deal with problems of photochemical instability.

1.4.3 Time Behavior and Spectra

Most often the pump pulse is of approximately Gaussian shape and its full width at half maximum power is less than the reciprocal of the intersystem-crossing rate constant k_{ST}. Thus, we can expect the following time behavior, neglecting finer detail for the moment. Shortly after the pump pulse reaches threshold level, dye-laser emission starts. The dye-laser output power closely follows the pump power till it drops below threshold, when dye-laser emission stops. The dye-laser pulse shape should thus closely resemble that of the part of the pump pulse above the threshold level. This behavior was indeed observed by Schäfer et al. (1966) pumping transversely a methanol solution of the dye DTTC in a square spectrophotometer cuvette of 1×1 cm dimensions, polished on all sides. Figure 1.25 shows oscillograms of this pump and dye-laser pulse at different peak pump power levels. From an evaluation of these oscillograms the input–output plot shown in Fig. 1.26 is obtained. It clearly shows how the dye fluorescence intercepted by the photocell is increased by several orders of magnitude from the spontaneous level, while the pump power is increased slightly above threshold. When the threshold is reached at the foot of the pump pulse, so that pump and dye-laser pulse forms are practically identical, the expected linear relationship between input and output obtains. The efficiency in this case was found to be 10%.

A more detailed treatment of the time behavior of the laser-pumped dye laser was given by Sorokin et al. (1967) who solved the rate equations for the excited state population in the dye and the photons in the cavity

$$dN_1/dt = W(t) - (N_1/N_t)(Q/t_c) - N_1/\tau_f$$

$$dQ/dt = (Q/t_c)(N_1/N_t - 1) \ .$$

The quantities appearing in these equations are as follows: N_1 is the excited-state population, N_t is the threshold inversion, Q is the number of quanta in the cavity, t_c is the resonator lifetime, τ_f is the fluorescence lifetime, and $W(t)$ denotes the pumping pulse which was assumed to have a Gaussian distribution with half-width at half-power points equal to T_1, i.e.

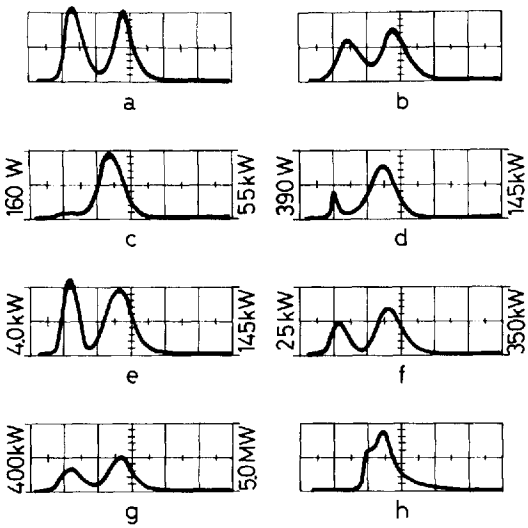

Fig. 1.25a–h. Oscillograms of fluorescence, dye-laser and pumping-laser pulses. (Sweep speed: 10 ns/division for (**a–g**), and 2 ns/div. for (**h**). (**a**) Pumping pulse and delayed reference pulse, (**b**) spontaneous fluorescence of a 10^{-5} M solution of the dye 3,3'-diethylthiatricarbocyanine bromide in methanol and delayed reference pulse, (**c–g**) dye-laser pulse from a 10^{-3} M solution of the dye and delayed reference pulse. The power corresponding to two major scale divisions is annotated to the right of each oscillogram for the pumping ruby laser pulse, to the left for the dye-laser pulse. (**h**) Dye-laser pulse just above threshold. (From Schäfer et al. 1966)

$$W(t) = W_{\max} \exp\left[-(t\sqrt{\ln 2}/T_1)^2\right]$$

and normalized to $\int_{-\infty}^{+\infty} W(t)dt = N_{\text{pump}}$, the total number of pumping photons. Digital computer solutions were obtained for a large number of parameter combinations, many of which agreed well with the experimentally observed time behavior even in such details as risetime and initial overshoot of the dye-laser pulse. A sample computer solution and an oscillogram of the dye-laser output for one set of parameters are reproduced from this work in Fig. 1.27.

For many applications it is advantageous to have a simple method for obtaining dye laser pulses that are much shorter than the pump laser pulses. This was first achieved by Lin and Shank (1975) using the method of pulse shortening by resonator transients, which had been developed earlier for solid-state lasers (Roess 1966). Pumping a 1-cm dye cell with a grating in Littrow mounting as the rear reflector and one cell window as the front reflector just above threshold with a 10-ns nitrogen laser pulse, they obtained 600-ps pulses with rhodamine 6G and 900-ps pulses with 7-dimethylamino-4-methylcoumarin. Further description of this technique can be found in (Lin 1975a and 1975b). By reducing the cavity lifetime using cells of only 10–500 μm width and pumping longitudinally with harmonics of a mode-locked Nd laser, pulses as short as 2 ps could be achieved (Fan and Gustafson 1976; Cox et al. 1982). Many different designs of ultrashort cavity dye lasers have been published since then

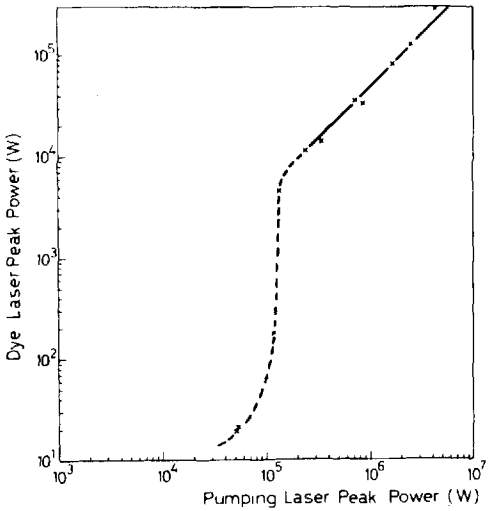

Fig. 1.26. Dye-laser peak power vs pumping laser peak power for a 10^{-3} M solution of 3,3′-diethylthiatricarbocyanine bromide in methanol. (From Schäfer et al. 1966)

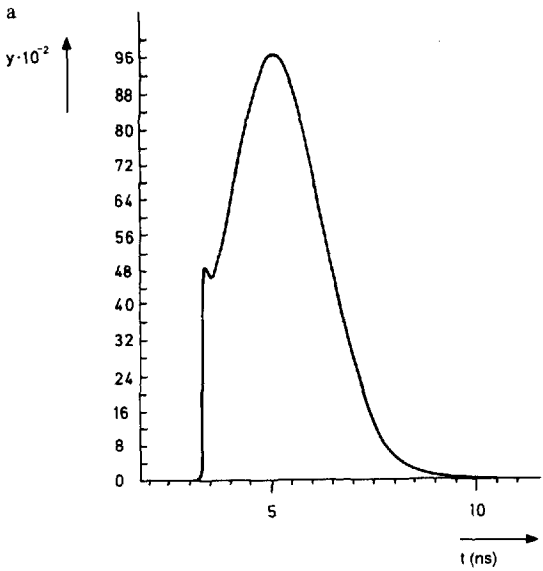

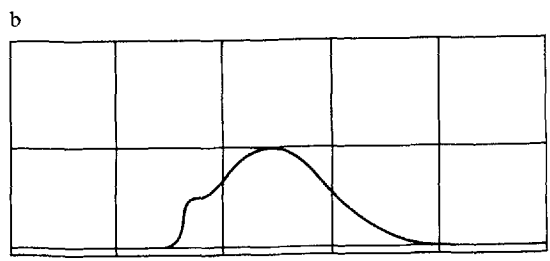

Fig. 1.27a, b. Comparison of a computer solution of the rate equations and an actual oscillogram. **(a)** Computer solution for $N_{pump}/N_t = 350$, $\tau/t_c = 3.0$, $T_1/t_c = 6.0$, $y = Q/(t\,W_{max})$; **(b)** oscillogram of a chloro-aluminum-phthalocyanine laser. (Mirror spacing: 5 cm, mirror reflectivities: 80% and 98%, sweep speed: 20 ns/division) (From Sorokin et al. 1967)

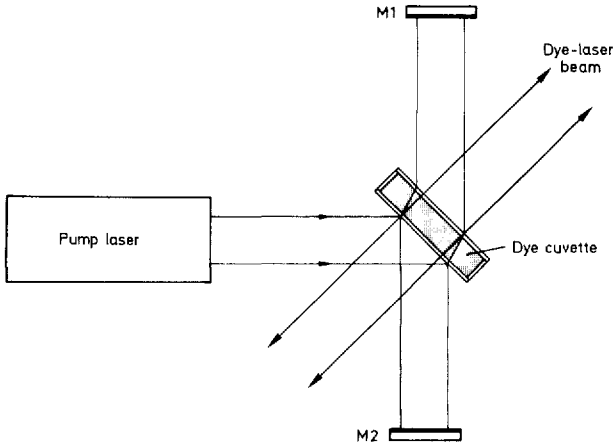

Fig. 1.28. Scheme for producing short dye laser pulses using two crossed resonators with a common dye cell. (Adapted from Eranian et al. 1973)

(Aussenegg and Leitner 1980; Yao 1982; Scott et al. 1984; Chiu et al. 1984; Ishida et al. 1985; Yamada et al. 1986; S.C. Hsu and Kwok 1986).

Another method of producing short dye laser pulses in a simple way makes use of two resonators with one dye cell as the common active medium, as shown in Fig. 1.28 (Eranian et al. 1973). While the short resonator is made up of the Fresnel reflections from the 2 mm dye cell, the long resonator consists of two mirrors of maximum reflectivity. Even though the threshold of the short resonator is high because of its low feedback, it reaches threshold first due to its short round-trip time. Its emission is, of course, normal to the cell windows. After the long resonator has reached threshold, the inversion in the dye solution drops to the critical inversion determined by the high Q of the long resonator. Since this inversion is much lower than the threshold inversion needed for the short resonator with its low Q, the dye laser emission from the short resonator is stopped. In this way a pump pulse of 20 ns produced a dye laser pulse of only 2 ns.

Similar arrangements of quenched dye lasers were described by Andreoni et al. (1975) and Braverman (1975). While both methods, resonator transients and quenching, produced dye laser pulses that were shorter than the pump pulse by a factor of about 10, the combination of both methods increased this pulse shortening factor to over 100 (Schäfer et al. 1983). This technique, called by the authors the method of quenched resonator transients, allows strong pumping of the dye cell with a steeply rising pump pulse, so that a first resonator transient of very short duration is produced, which would normally be followed by a damped transient oscillation. This is prevented, however, by careful adjustment of the length of the long resonator, which quenches the dye laser emission right after the end of the first resonator transient. Dye laser pulses of down to 100 ps were easily produced with excimer laser pump pulses of 20 ns duration. The dye laser pulsewidth could even be decreased to less

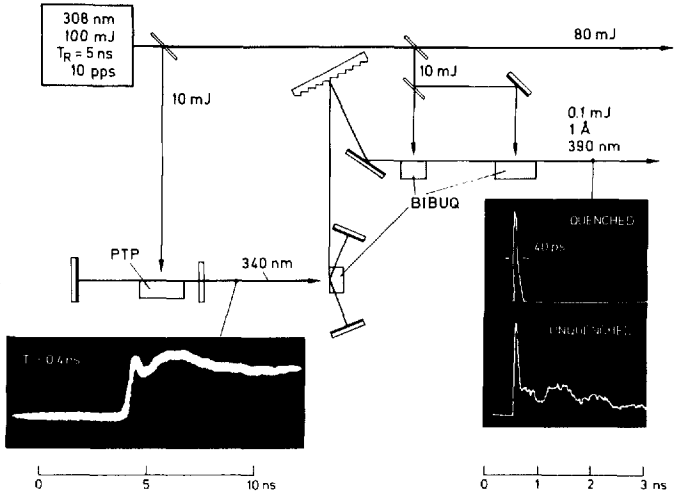

Fig. 1.29. Dye laser system to produce ultrashort pulses with long excimer laser pulse pumping. (From Bor and Rácz 1985)

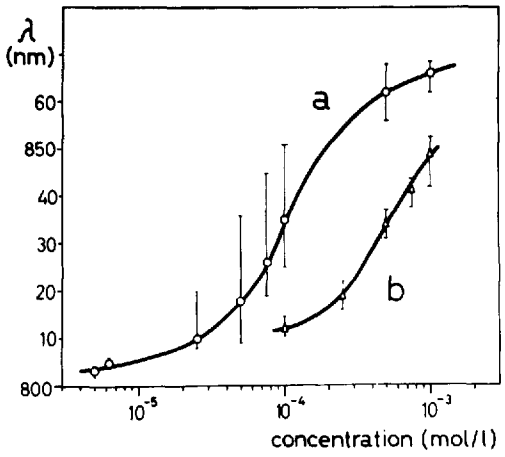

Fig. 1.30. Wavelength shift of the dye laser with concentration of a solution of 3,3'-diethylthiatricarbocyanine bromide in methanol, curve a for a silvered and curve b for an unsilvered cuvette. The circles and triangles give the wavelengths of the intensity maxima, the bars show the bandwidth of the laser emission. (From Schäfer et al. 1966)

than 30 ps by sharpening the front of the pump pulse by first pumping a standard broadband dye laser with the excimer laser in order to produce a steeply rising dye laser pulse which then pumped the quenched resonator transient arrangement, as shown in Fig. 1.29. A theoretical treatment of this method and a further experimental refinement was reported recently by Simon et al. (1986).

As explained above, it is not difficult to calculate the oscillation wavelength of a laser-pumped dye laser near threshold. Figure 1.30 gives the observed dye-laser wavelength as a function of DTTC dye concentration for a low and a high value of cavity Q (Schäfer et al. 1966). These curves show satisfactory agreement with the computed curves of Fig. 1.19. The time-integrated spectral width

of the dye-laser emission is indicated in Fig. 1.30 by bars. The width is measured with a constant pump power of 5 MW. It is seen to be rather broad in the middle of the concentration range for the high Q curve. This is due to the simultaneous and/or consecutive excitation of many longitudinal and transverse modes, which is also manifested by the increase in beam divergence. Several authors (Farmer et al. 1968; Bass and Steinfeld 1968; Gibbs and Kellog 1968; Vrehen 1971) have studied the wavelength sweep of the dye-laser emission. The results obtained are not easy to interpret. Frequently, there is a sweep from short to long wavelength of up to 6 nm, in other cases the sweep direction is reversed towards short wavelengths after reaching a maximum wavelength. Probably part of this sweep can be traced to triplet–triplet absorption, which should increase with time as the population density grows in the triplet level. Another part might be attributable to thermally induced phase gratings and similar disturbances of the optical quality of the resonator. Still another contributing factor might be the relatively slow rotational diffusion of large dye molecules in solvents like DMSO or glycerol. Inhomogeneous broadening of the ground state, on the other hand, although suggested as an explanation (Bass and Steinfeld 1968), may be excluded on this time scale as a reason for the observed sweep. This explanation assumes that vibrational excitation of the ground state of the dye molecule has a lifetime of at least a few ns in the solution but, in fact, it is deactivated in a few ps through collisions with the solvent molecules.

The dependence of the laser wavelength on the resonator Q, i.e. mainly on cell length and mirror reflectivities, can also be deduced from the start oscillation condition as described in Sect. 1.4.1. The variation with Q was first noted by Schäfer et al. (1966) when they put silver reflectors on the faces of the dye cell. This is shown in Fig. 1.30. The dependence on the cell length was experimentally observed by Farmer et al. (1969).

The temperature dependence of the dye-laser wavelength can be similarly explained. Schappert et al. (1968) found that the laser emission of DTTC in ethanol shifted towards shorter wavelengths with decreasing temperature. This is caused by the narrowing of the fluorescence and the absorption band with decreasing temperature, which results in higher gain and fewer reabsorption losses near the fluorescence peak. The solvent has a most important influence on the wavelength and efficiency of the dye-laser emission.

The first observation of large shifts of the dye-laser emission with changing solvents is reproduced in the following table for a 10^{-4} molar solution of the dye 1,1′-diethyl-γ-nitro-4,4′-dicarbocyanine tetrafluoroborate (Schäfer et al. 1966):

Solvent	Laser wavelength (in nm)	Solvent	Laser wavelength (in nm)
Methanol	796	Dimethylformamide	815
Ethanol	805	Pyridine	821
Acetone	814	Benzonitrile	822

In this case the nitro group, as a highly polar substituent in the middle of the polymethine chain, interacts with the dipoles of the solvent to shift the energy levels of the dye. This type of solvent shift is especially large for dyes whose dipole moments differ appreciably in the ground and excited states. The transition from ground to excited state by light absorption is fast compared with the dipolar relaxation of the solvent molecules. Hence the dye molecule finds itself in a nonequilibrium Franck-Condon state following light absorption, and it relaxes to an excited equilibrium state within about 10^{-13} to 10^{-11} s. Similarly, the return to the equilibrium ground state is also via a Franck-Condon state, followed by dipolar relaxation:

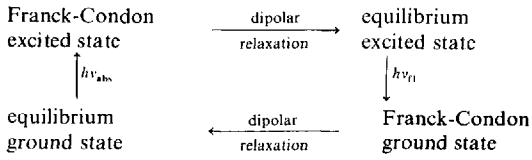

Consider the typical example of *p*-dimethylaminonitrostilbene. It has a dipole moment of 7.6 debye in the ground state and 32 debye in the excited state (Lippert 1957). Therefore, it is clear that in a polar solvent like methanol the equilibrium excited state is lowered even more strongly than the equilibrium ground state by dipole–dipole interaction. In the present case, for example, the absorption maximum occurs at 431 nm and the fluorescence maximum at 757 nm in i-butanol, while the corresponding values for cyclohexane are 415 nm and 498 nm, respectively. Similar shifts are found in laser emission.

Gronau et al. (1972) report laser emission for the similar case of the dye 2-amino-7-nitrofluorene dissolved in 1,2-dichlorobenzene.

Another property of the solvent that can have an important influence on the dye-laser emission is the acidity of the solvent relative to that of the dye. As already mentioned in Sect. 1.2, many dyes show fluorescence as cations, neutral molecules, and anions. Correspondingly, the dye laser emission of such molecules usually changes with the pH of the solution, since generally the different ionization states of the molecule fluoresce at different wavelengths. (A more detailed discussion is to be found in Chap. 5.)

An important subdivision of these dyes is that of molecules, whose acidity in the excited state is considerably different from that in the ground state due to changes of the π-electron distribution with excitation. This might cause the molecule to lase or take up a proton from the solvent. After return to the ground state, the reverse action occurs, leaving the original molecule in the ground state. Schematically the reaction is

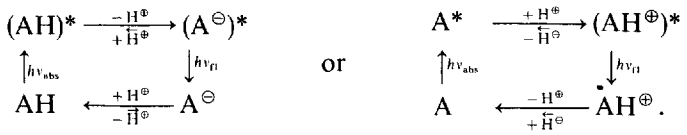

A well-known example is acetylaminopyrenetrisulfonate, which loses a proton from the amino group to form the tetra-anion in the excited state (Weller 1958).

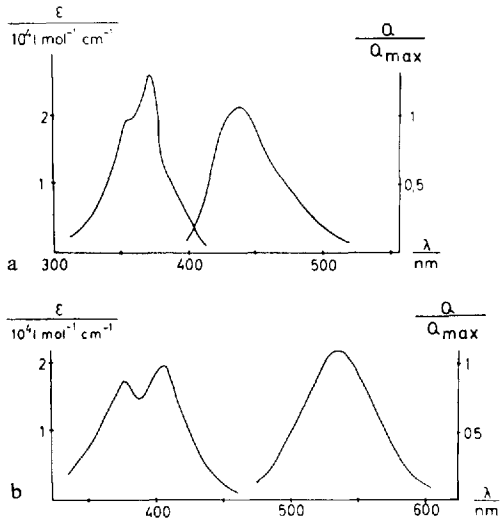

Fig. 1.31. Absorption and fluorescence spectra of acetylaminopyrene-trisulfonate, **(a)** neutral solution, **(b)** alkaline solution (1 N NaOH)

Absorption and fluorescence spectra of the neutral molecule, recorded in slightly acid solution, and of the tetra-anion, recorded in alkaline solution, are reproduced in Fig. 1.31. Many examples of this type can be found among the numerous known fluorescence indicators which show a change in fluorescence wavelength and/or intensity with a change of pH of the solution. While the first example of a dye laser utilizing such a protolytic reaction in the excited state (Schäfer 1968) was the above-mentioned acetylaminopyrenetrisulfonate pumped by a flashlamp, the first example used in a nitrogen-laser pumped dye laser and showing an especially large shift of the emission wavelength with pH was given by Shank et al. (1970a, b) and Dienes et al. (1970). They used two coumarins which can form a protonated excited form that fluoresces at longer wavelengths. The chemistry of these dyes is discussed in detail in Chap. 5. By judicious adjustment of the acidity of an ethanol/water mixture, neutral and protonated forms of these dyes could be made to lase. The tuning extended over 176 nm (from 391 to 567 nm). The term "exciplex", which these authors use for the excited protonated form, should be reserved for cases where an excited complex is formed with another solute molecule, not merely with a proton.

Donor-acceptor charge-transfer complex formation between a dye and a solvent molecule can occur in the ground state as well as in the excited state. The latter case is especially interesting, since the ground state of the complex can have a repulsion energy of a few kcal, while in the excited state the enthalpy of formation is comparable to that of a weak to moderately strong chemical bond (Knibbe et al. 1968). Thus the complex is stable in the excited state only and cannot be detected in the absorption spectrum. The rate of complex formation is limited by the diffusion of the two constituents. It is thus proportional to the product of the concentrations and strongly depends on the viscosity of the solution.

$$\begin{array}{ccc} A^* + D \rightleftharpoons (A^{\ominus} D^{\oplus})^* & & \\ \uparrow h\nu_{abs} & \downarrow h\nu_{fl} & \\ A + D \rightleftharpoons (A^{\ominus} D^{\oplus}) \longrightarrow A^{\ominus} + D^{\oplus} \longrightarrow \text{reaction products.} & & \end{array}$$

If the excited complex $(A^{\ominus} D^{\oplus})^*$ is nonfluorescing, the addition of D to A results merely in quenching of the fluorescence of A. This is generally believed to be a possible mechanism of the so-called dynamic quenching of fluorescence. On the other hand, if the excited complex is fluorescent, a new fluorescence band appears, while the original fluorescence disappears with increasing concentration of D, which might be one of the constituents of a solvent mixture. An example of this behavior is the complex formed from dimethylaniline and anthracene in the excited state (Knibbe et al. 1968). While this principle has not yet been utilized in laser-pumped lasers, a methanol solution of a pyrylium dye in a flashlamp-pumped laser showed a significant lowering of the threshold and displacement of the laser wavelength by 10 nm to the red on addition of a small quantity of dimethylaniline, evidently as a result of the formation of a charge-transfer complex in the excited state.

Assuming complete absorption of the pump radiation for a specific dye (and a constant temperature), the energy conversion efficiency is strongly dependent on the solvent. This is evidenced by the results of Sorokin et al. (1967) given in the following table of conversion efficiencies of an end-pumped DTTC laser with the concentration adjusted to absorb 70% of the ruby-laser pump radiation.

Solvent	Conversion efficiency, %
Methyl alcohol	9.0
Acetone	7.0
Ethyl alcohol	6.5
1-propanol	11.5
Ethylene glycol	14.0
DMF	15.5
Glycerin	15.5
Butyl alcohol	9.0
DMSO	25.0

Similar tabulations of conversion efficiencies for excimer-laser pumping of various dyes in a number of solvents are reported in the literature (V.S. Antonov and Hohla 1963; Cassard et al. 1981). In general, for dye lasers pumped not too high above threshold, the conversion efficiencies are roughly proportional to the corresponding quantum yields of spontaneous fluorescence. For higher pump intensities, however, the influence of excited state absorption on the pump light and on the dye-laser emission becomes more pronounced. These effects have been studied in detail (Speiser and Shakkour 1985).

We have already seen that the deactivation pathway provided by intersystem crossing can be neglected for sufficiently short pump pulses, resulting in correspondingly higher conversion efficiencies. Using picosecond pump pulses, it has recently become possible to neglect even the very fast internal conversion processes. This was done in a travelling-wave pumping arrangement described at the end of Chap. 4. In such an arrangement, molecules that have just been transferred to the first excited singlet state by the absorption of a pump-light photon are immediately brought back down to the ground state by stimulated emission at a rate much faster than the competing deactivating radiationless processes.

In this way it was possible to achieve conversion quantum efficiencies of 10%–20%, even using dyes with fluorescence quantum yields of only 5×10^{-4} (Polland et al. 1983). A demonstration experiment for easy visual observation of this effect is described by Szatmári and Schäfer (1984).

1.5 Flashlamp-Pumped Dye Lasers

1.5.1 Triplet Influence

In the case of flashlamp-pumped lasers, triplet effects become important because of the long risetime or duration of the pump light pulse. Figure 1.32 shows the time dependence of the population density n_1 in the excited singlet state (Schmidt and Schäfer 1967). The solid curve applies to a slowly rising, and the broken curve to a fast rising pump light pulse. Both are computed for two different values of the quantum yield of fluorescence ϕ_f. It is assumed that there is no direct radiationless internal conversion between the first excited singlet and the ground state, so that a fraction $\varrho = 1-\phi_f$ of excited molecules in the singlet state make an intersystem crossing to the triplet state. It is further assumed that the triplet state has a very long lifetime compared to the singlet state. It is seen that there is a maximum in the excited singlet state population

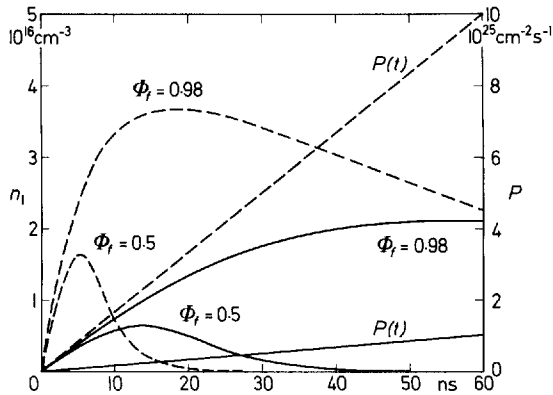

Fig. 1.32. Analog computer solutions of the population of the first excited singlet state n_1, for different pump powers $P(t)$ and quantum efficiencies of fluorescence, ϕ_f. (From Schmidt and Schäfer 1967)

density n_1, which is reached while the pump light intensity is still rising. This maximum is higher for a faster rise of the pump light and also for a higher quantum yield of fluorescence. Despite the continuing rise of the pump light intensity, n_1 falls to a low value after passing the maximum since the ground state becomes depleted and virtually all of the molecules accumulate in the triplet state. It should be pointed out that this behavior was computed for the spontaneous fluorescence of an optically thin layer of dye solution whose intensity is proportional to n_1. Obviously, this type of behavior would remain practically unaltered when stimulated emission is taken into account. Thus a dye laser may be pumped above threshold by a fast-rising light source. On the other hand, the necessary population density in the excited singlet state may not be achieved with a slowly rising light source, even if the asymptotic pump level is the same for both situations. In any case, the laser emission would be extinguished after some time. Even more important than this depletion of the ground state, however, are additional losses due to molecules accumulated in the triplet state. These give rise to triplet–triplet absorption spectra, as described in Sect. 1.3, which very often extend into the region of fluorescence emission. Therefore they can lead to losses that often are higher than the gain of the laser and eventually prevent laser emission.

Experimental evidence of the premature stopping of laser action due to triplet losses can be found in almost any flashlamp-pumped dye laser. A very convincing demonstration of the importance of triplet–triplet absorption in flashlamp-pumped dye lasers is given by Schäfer et al. (1978). They compare the output energies and pulse forms of a mixture of the laser dyes p-terphenyl and dimethyl-POPOP with those of a bifluorophoric dye, which was synthesized by linking the chromophores of these two dyes by a saturated hydrocarbon chain, which in this example was a single CH_2 group. In addition to the pump-light photons absorbed by the longer-wavelength-absorbing dimethyl-POPOP moiety in the bifluorophoric dye, those absorbed by the p-terphenyl moiety give rise to a very efficient intramolecular radiationless energy transfer to the dimethyl-POPOP moiety in less than 1 ps (B. Kopainsky et al. 1978) so that the output energy is increased in comparison to a dye solution of dimethyl-POPOP. In a mixture of equal concentrations (10^{-4} molar each) of the two dyes, however, the great intermolecular distances reduce the energy transfer from the p-terphenyl to the dimethyl-POPOP molecules to a negligible fraction. This has the important consequence that most of the p-terphenyl molecules can accumulate in the triplet state during the long pump pulse duration and prevent lasing of the dimethyl-POPOP by their triplet–triplet absorption, which is known to be strong at the laser wavelength of dimethyl-POPOP. Only at very high pumping is a weak output in a short pulse observed. These facts are clearly seen in the input–output curves of Fig. 1.33 and the oscillograms of the pulse forms given in Fig. 1.34.

It must be stressed that in the bifluorophoric dye just described, the triplet–triplet absorption of the shorter-wavelength-absorbing (donor) chromophore is eliminated by fast intramolecular singlet-singlet energy transfer, whereas the triplet–triplet absorption of the longer-wavelength-absorbing (acceptor)

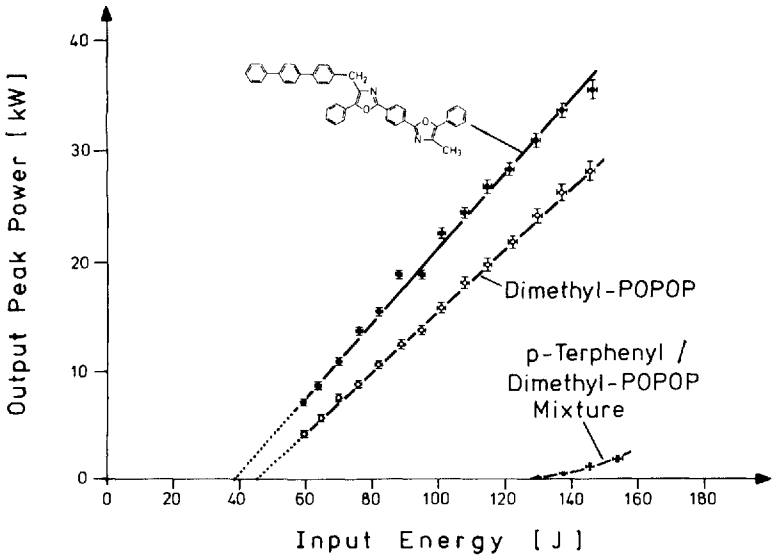

Fig. 1.33. Input–output curves of a flashlamp-pumped dye laser for a dye with intramolecular energy transfer, for dimethyl-POPOP, and for a dye mixture. (From Schäfer et al. 1978)

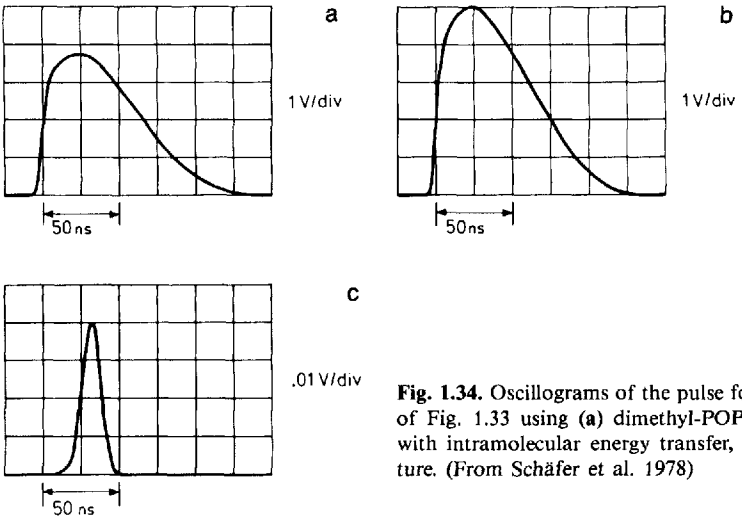

Fig. 1.34. Oscillograms of the pulse forms of the laser of Fig. 1.33 using **(a)** dimethyl-POPOP, **(b)** the dye with intramolecular energy transfer, **(c)** the dye mixture. (From Schäfer et al. 1978)

chromophore is still effective and is the reason for the relatively low overall efficiency of this laser dye and its relatively short (compared to the pump) pulse duration. In a later part of this chapter possibilities of external as well as internal quenching of the deleterious triplet state will be described.

Several authors have treated the kinetics of dye-laser emission by a set of coupled rate equations including terms to account for triplet–triplet absorp-

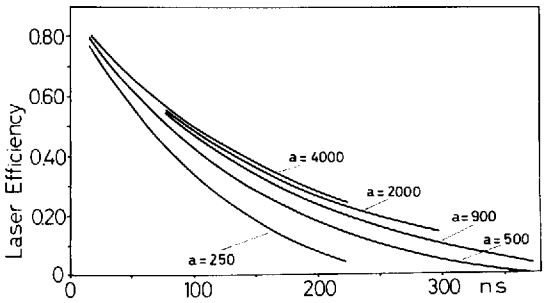

Fig. 1.35. Dye-laser efficiency vs half-width of pumping pulse at constant pulse energy (parameter a). (From Sorokin et al. 1968)

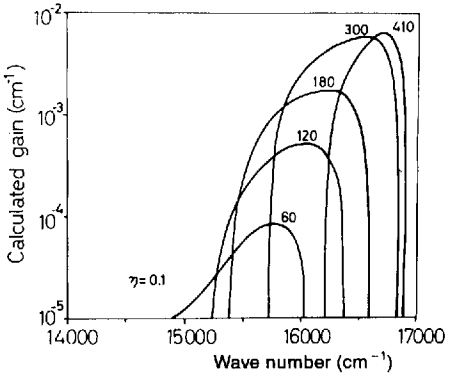

Fig. 1.36. Gain vs wavelength calculated for a rhodamine B laser with time (in ns) after initiation of the pump pulse as a parameter. (From M. J. Weber and Bass)

tion losses. Since the triplet losses are time-dependent, they affect the efficiency as well as the emission wavelength of the dye laser. Figure 1.35 gives the dye laser efficiency as a function of the excitation pulsewidth (Sorokin et al. 1968). The parameter a is the ratio of the total number of photons in the excitation pulse to the number of photons at threshold. The figure applies to the case $\phi_f = 0.88$ and $\sigma_a = 10\sigma_T$ and $\tau_T = \infty$, where σ_T is the cross-section for the triplet–triplet absorption band. Figure 1.36 is a plot of gain vs wavelength calculated for a rhodamine B laser with time (in ns) after initiation of the flashlamp pulse as a parameter (M. J. Weber and Bass 1969). The results of such calculations apply only to the specific light pulse form considered. It it therefore worthwhile to have an expression connecting population densities in the ground, lowest excited singlet, and triplet states with the laser wavelength and cavity parameters.

The following simple modification of the oscillation condition of Sect. 1.4.1 takes into accout triplet–triplet absorption losses, characterized by a cross-section σ_T. Let $\alpha = n_0/n$ be the normalized ground-state population density, and $\beta = n_T/n$ the triplet-state population density. Then the oscillation condition, its derivative with respect to wave number, and the balance of population densities give the following three equations for α, β, γ (the prime denotes differentiation with respect to wave number):

$$-\sigma_a\alpha-\sigma_T\beta+\sigma_f\gamma=S/n\ , \tag{1.12a}$$

$$-\sigma'_a\alpha-\sigma'_T\beta+\sigma'_f\gamma=0\ , \tag{1.12b}$$

$$\alpha+\beta+\gamma=1\ . \tag{1.12c}$$

From these equations and the observed wavelength, the population densities in the ground, excited singlet, and triplet states can be obtained. As an example of this procedure the case of rhodamine 6G in a cw laser will be discussed in detail in Chap. 2. The ratio β/γ, obtained from the above relations, and the time t_0 to reach threshold can be used for an estimate of k_{ST}, if one assumes $t_0 \ll \tau_T$ and a linearly rising pump light source. Then we have $d\gamma/dt$ = constant and $d\beta/dt = k_{ST}\beta$, which yields after integration $\beta/\gamma = \frac{1}{2}k_{ST}t_0$. On the other hand, the observed t_0 can give an upper limit for σ_T at the laser wavelength for known k_{ST}, since laser emission can only be achieved for $\gamma\sigma_f > \beta\sigma_T$, yielding $\sigma_T < 2\sigma_f/t_0k_{ST}$ (Sorokin et al. 1968).

For pulses that are long compared with τ_T or for continuous operation, a steady state must be reached. Then the triplet production rate $k_{ST}\gamma$ equals the deactivation rate β/τ_T, so that the ratio $\beta/\gamma = k_{ST}\tau_T$. Setting this value equal to that obtained above from the observed laser wavelength, an estimate of τ_T can be obtained.

To obviate the need for a rapidly rising pump light intensity in dye lasers and to achieve cw emission, one must reduce the triplet population density to a sufficiently low level by reducing τ_T. One way of achieving this is by adding to the dye solution suitable molecules that enhance the intersystem-crossing rate $k_{TG} = 1/\tau_T$ from the triplet to the ground state by the effects described in Sect. 1.3. The improvement in dye-laser performance possible with this method was shown by Keller (1970), who solved the complete rate equations of Sorokin et al. (1968) after adding a term n_T/τ_T for the deactivation of the triplet state to the equation for the triplet-state population density.

A molecule that has long been known to quench triplets is O_2. At the same time, however, it also increases k_{ST} and thus also quenches the fluorescence of a dye. The relative importance of triplet and fluorescence quenching then determines whether or not oxygen will improve dye-laser performance. This is shown in Fig. 1.37, which gives the output from a long-pulse rhodamine 6G laser as a function of the partial pressure of oxygen in the atmosphere in contact with the dye solution in the reservoir (Schäfer and Ringwelski 1973). While the output first rises steeply with increasing oxygen content, it levels off after about 20% oxygen content, showing that the positive effect of the reduction in triplet lifetime is offset by the detrimental effect of fluorescence quenching. This can be understood quantitatively, if one assumes that the laser output is proportional to the ratio γ/β. In the presence of an oxygen concentration $[O_2]$ the triplet production rate is $(k_{ST}+k_{QS}[O_2])n_1$ and is set equal to the deactivation rate $(k_{TG}+k_{QT}[O_2])n_T$, where k_{QS} and k_{QT} are the quenching constants for the singlet and triplet states, respectively. This yields $\gamma/\beta = (k_{TG}+k_{QT}[O_2])/(k_{ST}+k_{QS}[O_2])$. Using $k_{ST} = 2\times10^7\ s^{-1}$, $k_{QS} =$

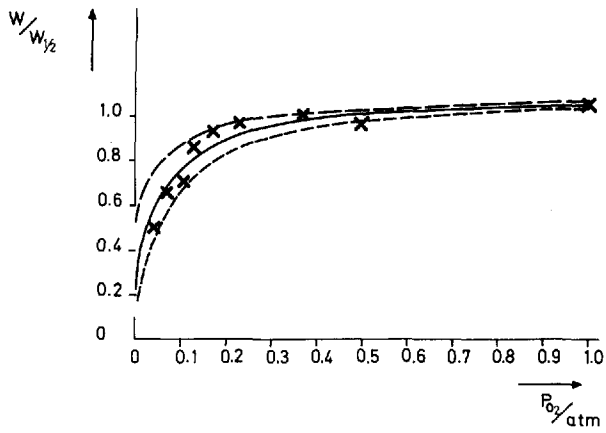

Fig. 1.37. Normalized laser output $W/W_{1/2}$ vs oxygen partial pressure P_2 in the gas mixture over a solution of rhodamine 6G. (*Crosses*: measurements; *solid line*: theoretical result for $k_{TG} = 5\times10^5\,s^{-1}$; *upper dashed curve*: same, but for $k_{TG} = 10^6\,s^{-1}$; *lower dashed curve*: same for $k_{TG} = 10^4\,s^{-1}$). (From Schäfer and Ringwelski 1973)

$3\times10^{10}\,s^{-1}\,l\,mole^{-1}$, and $k_{QT} = 3.3\times10^9\,s^{-1}\,l\,mole^{-1}$, we find good agreement with the experimental results for $k_{TG} = 5\times10^5\,s^{-1}$. The triplet lifetime of rhodamine 6G in carefully deaerated methanol solutions at room temperature is thus $\tau_T = 2\,\mu s$, while the effective triplet lifetime with 20% oxygen content in the atmosphere above the dye is $\tau_{Teff} = 1/(k_{TG}+k_{QT}[O_2])$ or 140 ns. Marling et al. (1970a) measured the effect of molecular oxygen at different partial pressures on the dye laser emission of a number of dyes. They found several dyes where the fluorescence quenching of oxygen was much stronger than its triplet quenching effect, e.g. the dye brilliant sulphaflavine, whose laser emission was extinguished when the argon atmosphere in the reservoir was replaced by one atmosphere of oxygen.

It is thus seen to be more appropriate not to use a paramagnetic gas like oxygen, which enhances both k_{ST} and k_{TG}, but rather to apply energy transfer from the dye triplet so some additive molecule with a lower-lying triplet that can act as acceptor molecule. Triplet–triplet energy transfer was shown by Terenin and Ermolaev (1956) to occur effectively with unsaturated hydrocarbons. This scheme was used by Pappalardo et al. (1970b), who used cyclooctatetraene as acceptor molecule and obtained a dye-laser output pulse from rhodamine 6G as long as 500 μs, demonstrating that the triplet lifetime had been reduced by the quenching action of cyclooctatetraene below the steady-state value necessary for cw-laser operation. This compound is still the most effective triplet quencher known for rhodamine 6G, although a number of others have been tested and several quite effective ones found (Marling et al. 1970b), e.g. N-aminohomopiperidine, 1,3-cyclooctadiene, and the nitrite ion, NO_2^-.

It must be stressed that this energy transfer occurs in such a way that energy as well as spin is exchanged between dye and acceptor molecule, leaving the

acceptor in the triplet state, according to $^3D + {}^1A \rightarrow {}^1D + {}^3A$. Marling et al. (1970b) has pointed out that there is also a possibility of quenching a dye triplet by collision with a quencher molecule in the triplet state through the process of triplet–triplet annihilation, which leaves the dye in the excited singlet state and the quencher molecule in the ground state: $^3D + {}^3A \rightarrow {}^1D^* + {}^1A$ with subsequent fluorescence emission or radiationless deactivation of the excited singlet state. In this case, the quencher molecules must first be excited to the first excited singlet state and pass by intersystem crossing to the triplet state, before they can become effective. The first excited singlet state of quencher molecules must always lie higher than that of the dye, to that no pump radiation useful for pumping the dye is absorbed and no fluorescence quenching energy transfer can occur from the first excited singlet state of the dye so that of the quencher molecule. This means that, for efficient quencher molecule triplet production, the pump light source must have a high proportion of ultraviolet light output. Usually this means at the same time a higher photodegradation rate for the dye, which also absorbs part of the ultraviolet pump light. Because of these disadvantages and its generally lower effectiveness, this indirect method of triplet quenching seems less attractive. The distinction between direct and indirect triplet quenching can, however, clarify the results of other experimental investigations (Strome and Tuccio 1971; Smolskaya and Rubinov 1971).

Whilst the above methods of triplet quenching rely on intermolecular processes, intramolecular triplet quenching proved to be most efficient, albeit more difficult to implement. Here again two chromophores are chemically linked by a short saturated hydrocarbon chain to form a bifluorophoric laser dye, as described above (p. 53). But now one of the chromophores acts as a

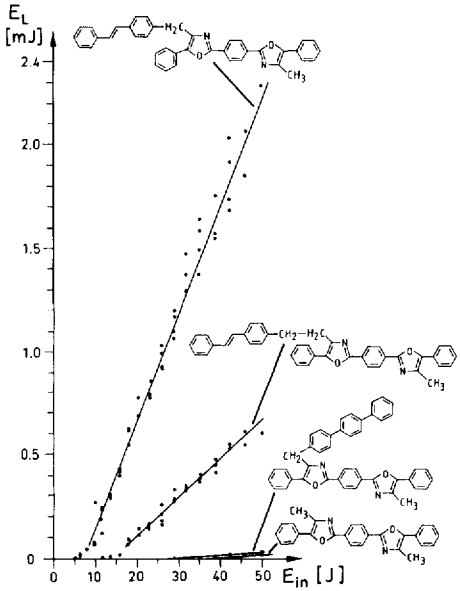

Fig. 1.38. Comparison of input–output curves for different dyes with intramolecular energy transfer with that of dimethyl-POPOP. (From Liphardt et al. 1981)

triplet quencher for the lasing chromophore. The best example is again dimethyl-POPOP as the lasing chromophore, but now linked to *trans*-stilbene, which acts as triplet quencher, since its T_1 state is lower than the T_1 state of dimethyl-POPOP (Liphardt et al. 1981). At the same time, *trans*-stilbene absorbs at a shorter wavelength than dimethyl-POPOP and its fluorescence band has a good overlap with the absorption band of dimethyl-POPOP. This means, *trans*-stilbene plays the double role of donor for singlet–singlet energy transfer to dimethyl-POPOP and acceptor for triplet–triplet energy transfer from it. The triplet lifetime of the dimethyl-POPOP moiety of this molecule was found to be only 7 ± 3 ns when it was linked to the quenching moiety via one CH_2 group, which rose to 70 ± 10 ns for a link using $-CH_2-CH_2-$ (Schäfer et al. 1982). Consequently, the output energy of this new bifluorophoric dye with intramolecular triplet quenching is many times higher than that of dimethyl-POPOP or even the corresponding bifluorophoric dye with p-terphenyl, as shown in Fig. 1.38. Actually, using the same flashlamp-pumped dye laser at 50 J electrical input energy, the outputs of the new bifluorophoric dye with one methylene group as a link and the dye using two methylene groups as a link are respectively 110 and 30 times higher than the output energy of dimethyl-POPOP (Liphardt et al. 1981).

These bifluorophoric dyes with intramolecular triplet-triplet energy transfer are a lucid example of the power of preparative organic chemistry for solving long-standing problems in dye laser technology.

1.5.2 Practical Pumping Arrangements

Flashlamp-pumped dye laser heads consist in principle of the dye cuvette, the flashlamp and a pump light reflector or diffuser. The latter serves to concentrate the pump light emitted from the extended, uncollimated, broadband source, the flashlamp, onto the absorbing dye solution in the cuvette. The reflector can be of the imaging type, e.g. an elliptical cylinder whose focal lines determine the position of linear lamp and cuvette, or it can be of the close-coupling type, which is especially advisable where there are several flashlamps surrounding the cuvette. Instead of a specular reflector, a diffusely reflecting layer of MgO or $BaSO_4$ behind a glass tube surrounding flashlamp and cuvette is often used. The design of the pump cavity is thus similar to that of solid-state lasers, except that for dye lasers it is even more important to prevent nonuniform heating of the solution in order to avoid thermally induced schlieren. Furthermore, it is advisable to use some means of filtering out photochemically active wavelengths which might decompose the dye molecules. It it often sufficient to use an absorbing glass tubing for the cuvette, otherwise a double-walled cuvette or a filter solution surrounding the flashlamp can be used (Jethwa et al. 1982; Calkins et al. 1982).

For maximum utilization of the pumplight output the length of the cuvette will generally be about the same as that of the flashlamp. This in turn makes a flow system almost mandatory, because in a long cuvette even small thermal gradients can severely degrade the resonator characteristics. The dye flow in

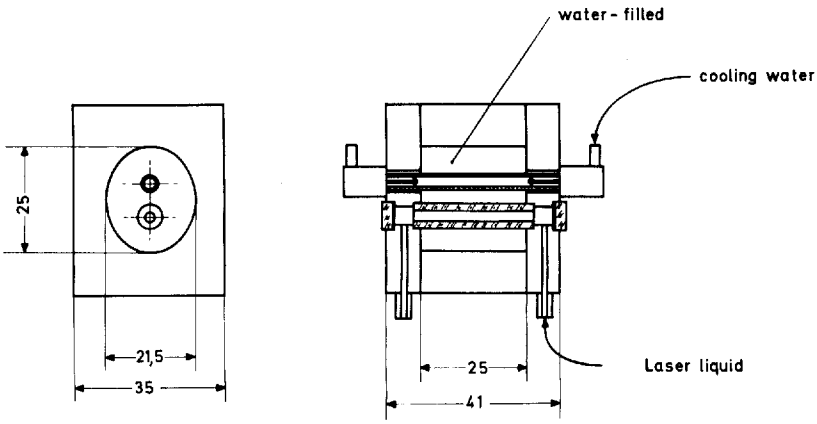

Fig. 1.39. Cross-sections of small dye-laser head for 100 Hz pulse repetition frequency (dimensions in mm). (From W. Schmidt 1970)

the cuvette may be longitudinal or transverse. In either case the flow should be high enough to be in the turbulent regime. This rapidly mixes the liquid and hence reduces thermal gradients due to nonuniform pump-light absorption in the cuvette. Both flow orientations are used in high-repetition-rate dye lasers (Boiteux and De Witte 1970; W. Schmidt 1970). If the cuvettes are not of all-glass construction, windows are generally pressed against the cuvette end and sealed by O rings. These O rings, and the hoses connecting the cuvette with the circulating pump and the reservoir, can be of silicone rubber for use with methanol or ethanol solvents. Commercial O rings, and even clear plastic hoses, usually give off absorbing or quenching filler material and hence should not be used. For other solvents, like dimethylformamide or dimethylsulfoxide, Teflon coatings are required on O rings and hoses. A similar choice is required with the circulating pump and the reservoir for the dye solution. Magnetically coupled centrifugal or toothed wheel pumps made of Teflon or stainless steel are well suited for this application, whereas membrane pumps give less reproducible results because of the pulsation in the flow rate. The metal end pieces carrying the nipples for the inflow and outflow of the dye solution, situated between the cuvette made of glass tubing and the windows, are also best made of stainless steel and should contain as little unpumped length of dye solution as possible so as to reduce the reabsorption of the dye-laser beam. As an example, the cross-sections of a small dye-laser head for 100 Hz pulse-repetition frequency and several watts average output power are given in Fig. 1.39. A great variety of flashlamps have been used in dye lasers. The simplest possibility is the use of commercial xenon flashlamps as in the laser head of Fig. 1.40. The risetime of linear and helical flashlamps can be reduced and the output power increased by the introduction of a spark gap in series with the lamp; this allows the lamp to be operated at a voltage that is much higher than the self-firing voltage. The excess voltage applied to the lamp ensures a rapid build-up of the plasma and a much higher peak power in the lamp. In this ar-

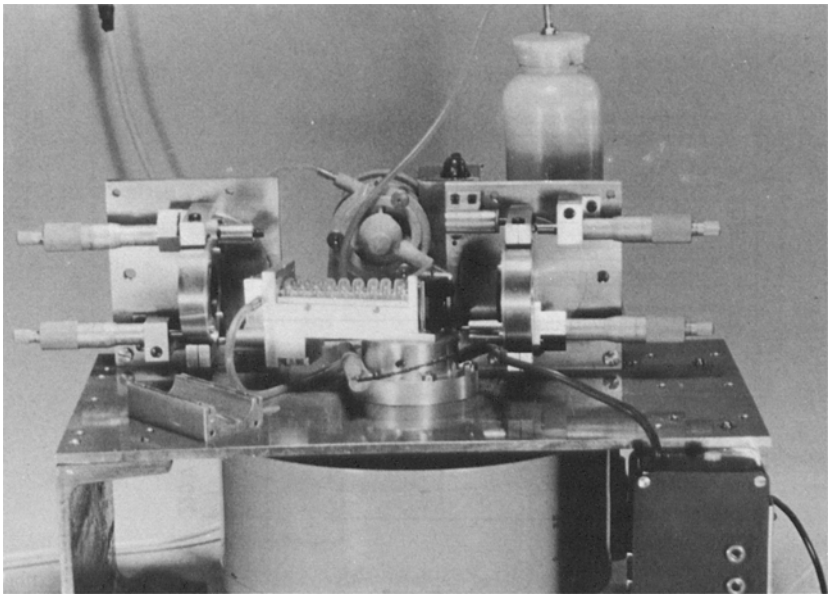

Fig. 1.40. Photograph of a dye laser with helical flashlamp

rangement with a linear, 8-cm-long xenon lamp of 5 mm bore diameter and a low-inductance 0.3 μF/20 kV capacitor, a risetime of 300 ns can be obtained. By comparison, a helical flashlamp of 8 cm helix length and 13 mm inner diameter of the helix gives a risetime of about 0.5 μs. For reasons connected with the accumulation of molecules in the triplet state, discussed in the last section, much effort has gone into the development of high-power lamps of short risetime. Very fast risetimes (70 ns) can be achieved by the use of small capillary air sparks fed by an energy storage capacitor in the form of a flat-plate transmission line (Aussenegg and Schubert 1969). Another type with a very fast risetime is a low-inductance coaxial lamp in which the cylindrical plasma sheet surrounds the cuvette. This type was first developed for flash photolysis work (Claesson and Lindquist 1958). Later it was used successfully for dye-laser pumping (Sorokin and Lankard 1967; W. Schmidt and Schäfer 1967). An improved version of this lamp was developed by Furumoto and Ceccon (1969a). With this lamp too a spark gap is used in series with the lamp, so that a voltage much higher than the breakdown voltage of the lamp can be used. At the same time the pressure can be adjusted so that the plasma fills the lamp uniformly. By comparison the original design shows constricted spark channels which move from shot to shot. The improved version offers nearly uniform illumination of the cuvette and the pulse height is reproducible from shot to shot. Risetimes of 150 ns using a 0.05 μF capacitor were achieved with this lamp. For smaller capacitors even shorter risetimes can be obtained.

This configuration is also amenable to up-scaling, and this has been done by Russian workers (Alekseev et al. 1972; Baltakov et al. 1973) who obtained

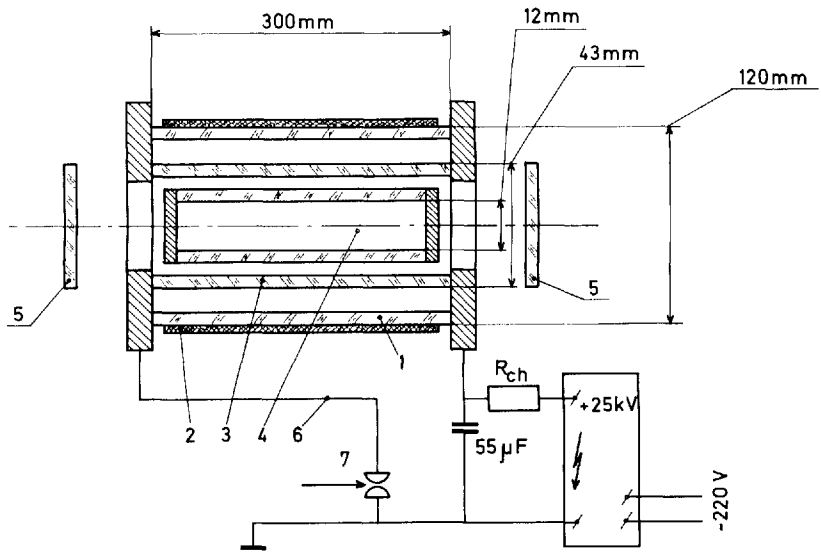

Fig. 1.41. Cross-section through a high energy dye laser with coaxial flashlamp. (*1*) external tube, (*2*) silicon dioxide coating, (*3*) internal tube, (*4*) dye cuvette, (*5*) mirrors, (*6*) external current lead, (*7*) triggered spark gap, R_{ch} = charging resistor. (From Alekseev et al. 1972)

dye-laser pulses of up to 150 J output energy. Figure 1.41 shows a cross-section through a dye laser using such a lamp. A great disadvantage of this arrangement, however, is the enormous increase in beam divergence during the laser pulse from 1.8–3 mrad at the start of the pulse to 36–91 mrad near the end of the pulse (Baltakov et al. 1974).

A significant improvement in reliability and flashlamp lifetime, in particular for high repetition rate lasers, was achieved by the introduction of a simmer mode of operation of the flashlamps (Stephens and Hug 1972) and by solid-state switches (Jethwa and Schäfer 1974). This development resulted in dye lasers of over 100 W average power at 50 Hz repetition frequency (Jethwa et al. 1978). Other reports on flashlamp-pumped dye lasers of 100 W and 90 W average power were published by Morey and Glenn (1976) and Mack et al. (1976).

1.5.3 Time Behavior and Spectra

The time behavior of flashlamp-pumped dye lasers is more complex than that of laser-pumped dye lasers because of time-dependent triplet losses and thermally or acoustically induced gradients of the refractive index. Several authors have derived solutions of the rate equations for flashlamp-pumped dye lasers under various approximations (Bass et al. 1968; M. J. Weber and Bass 1969; Sorokin et al. 1968). In view of the many quantitative uncertainties, a calculation of the time behavior of flashlamp-pumped dye lasers is of rather limited value. Instead, experimental results are given here.

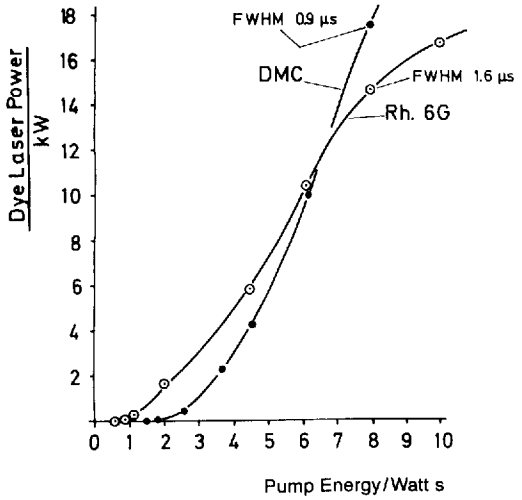

Fig. 1.42. Dye laser peak output power vs flashlamp pulse energy at 100 Hz pulse repetition frequency for rhodamine 6G (Rh. 6G) and 7-diethylamino-4-methylcoumarin (DMC). (From W. Schmidt 1970)

For small coaxial lamps having a fast risetime and short pulsewidths, the time behavior is similar to that of laser-pumped dye lasers. Thus, Furumoto and Ceccon (1970) obtained a pulse of 40 kW peak power and 100 ns duration in the ultraviolet from a solution of p-terphenyl in DMF using a lamp of 50 ns risetime and 20 J energy capacity. With similar lamps Hirth et al. (1972) and Maeda and Miyazoe (1972) were able to obtain laser emission from many cyanines in the visible and near-infrared.

Lasers equipped with commercial xenon flashlamps have slower risetimes. Consequently the number of dyes that will lase in these devices is restricted and triplet quenchers must be used if long pulse emission is wanted. Nevertheless, high average and peak powers and relatively high conversion efficiencies can be obtained in this way. Figure 1.42 shows a plot of dye-laser peak power versus flashlamp energy for the small laser head shown in Fig. 1.39 (W. Schmidt 1970). An optimized version allowed operation at 100 Hz pulse repetition frequency and an average dye-laser output power of 3.5 W (W. Schmidt and Wittekindt 1972). With linear flashlamps in an elliptical pump cavity powers of up to 1 MW were obtained (Bradley 1970). Figure 1.43 shows the average power vs the repetition frequency of a 100 W dye laser, and Fig. 1.44 gives the corresponding oscillograms of flashlamp current and laser power per pulse.

With a lumped constant transmission line in place of a single capacitor, a long, flat-top pump-light pulse can be formed. Figure 1.45 is an oscillogram of such a pump-light pulse from a helical flashlamp and the dye-laser pulse excited by it (Ringwelski and Schäfer 1970). A 400 µs long dye-laser pulse is obtained from an air-saturated methanol solution of rhodamine 6G. Here, proper filtering of the pump-light through a copper sulfate solution was required to reduce unnecessary heating. Also, an optimal concentration of the dye was chosen, so that heating due to pump-light absorption was reasonably uniform throughout the cuvette volume. With the same pumping arrangement Snavely

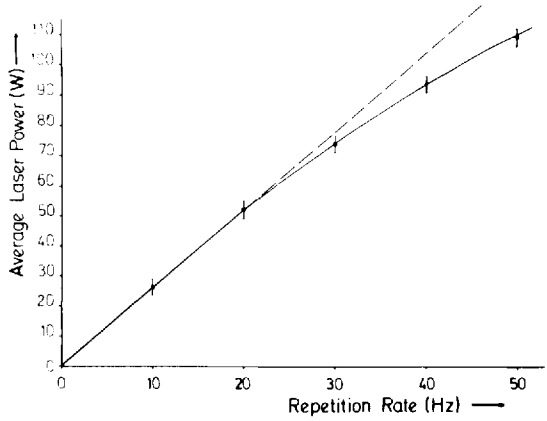

Fig. 1.43. Average power as a function of the repetition rate of a flashlamp-pumped dye laser. (From Jethwa et al. 1978)

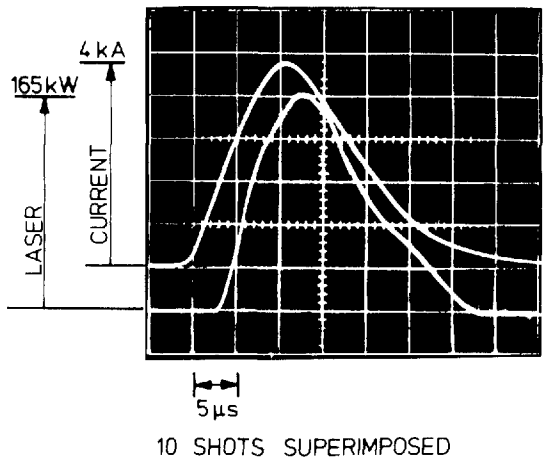

Fig. 1.44. Current and laser pulse forms for the laser of Fig. 1.43. (From Jethwa et al. 1978)

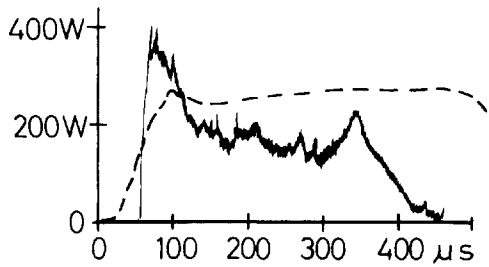

Fig. 1.45. Oscillogram of pump-light pulse (*broken line*) of a dye laser using a helical flashlamp and a lumped parameter transmission line and dye-laser pulse (*solid line*) from an air-saturated rhodamine 6G solution

and Schäfer (1969) had obtained 140 μs long pulses from rhodamine 6G and rhodamine B solutions; the duration clearly indicated that a steady state of the triplet population had been reached, provided the solution was saturated with oxygen or air. No laser emission was obtained, even at twice the original threshold, if nitrogen was bubbled through the solution for a time sufficient

to purge the oxygen. Pappalardo et al. (1970b) using a laser with a 600-μs pump pulse obtained a 500 μs dye laser pulse from a 5×10^{-5} molar rhodamine 6G solution containing 5×10^{-3} mole/l of cyclooctatetraene as triplet quencher. Such results with long pulses first proved that triplet absorption cannot prevent cw dye-laser emission if the necessary triplet quenchers are added. In fact, it was concluded from these experiments that an absorbed pump-light power of less than 4 kW/cm^3 for a 5×10^{-5} molar air-saturated methanol solution of rhodamine 6G should be sufficient to reach threshold with steady-state triplet population. The thermal problem, on the other hand, remains a serious one. To alleviate this problem one might employ a solvent with higher specific heat and use it at a temperature where the variation of the refractive index with temperature is at a minimum. In this respect water near freezing point or, even better, heavy water at 6°C would be an ideal solvent.

A miniature long-pulse dye laser with 60 s pulse duration, 100 Hz repetition frequency, and a very low threshold of only 6J was described by Hirth et al. (1977).

Extremely high dye-laser pulse energies have been obtained with large coaxial lamps. The laser shown in Fig. 1.41 gives an output energy of 32 J with an alcoholic rhodamine 6G solution at 17.3 kJ electrical energy input, i.e. 0.2% efficiency, and a specific output energy of 1 J/cm^3. The output power was reported as 10 MW, so that the half-width of the pulse must be about 3.2 μs. The lamp was filled with xenon at 1 Torr pressure in this case. The laser reported by Baltakov et al. (1973) generated 110 J in 20 μs, and 5.5 MW peak power.

The characteristics and limitations of coaxial and U-shaped flashlamps as pumping sources for dye lasers are described in (Anikiev et al. 1976; Marling et al. 1974; Hirth et al. 1973b; Drake and Morse 1974; Baltakov and Barikhin 1976; Strizhnev 1976; Ornstein and Derr 1974; Maeda et al. 1977). Guided sparks, discharges in a gas vortex, and laser-produced plasmas were tested in some investigations as pump sources: (Weysenfeld 1974; Brown 1975; Ferrar 1972; Silfvast and Wood II 1975a and 1975b; Ferrar 1973). Of the more exotic pumping sources the plasma focus (N.T. Kozlov and Protasov 1975/6), the high pressure mercury capillary lamp (Dal Pozzo et al. 1975), and semiconductor diodes (G. Wang and Webb 1974; G. Wang 1974) should be mentioned. Four papers discussed the prospects for dye lasers pumped by electrochemiluminescence: (Measures 1974; Keszthelyi 1975; Measures 1975; C.A. Heller and Jernigan 1977). Xenon-ion lasers proved useful because of their longer pulse width as replacements for nitrogen lasers in ultra-narrow bandwidth dye laser work (Hänsch et al. 1973; Schearer 1975; Levenson and Eesley 1976), while copper-vapor lasers as pump sources can improve the overall efficiencies of dye lasers (Decker et al. 1975; Pease and Pearson 1977), and excimer lasers can extend the short-wavelength limit of dye lasers (Sutton and Capelle 1976; Bücher and Chow 1977).

The spectral range of flashlamp-pumped dye lasers at present extends from 340 nm in p-terphenyl to 850 nm in DTTC (Maeda and Miyazoe 1972). Time-resolved spectra of flashlamp-pumped dye lasers show even greater variety than those of laser-pumped dye lasers (Ferrar 1969a). Some dyes show almost

no wavelength sweep during an emission of 300 ns, while others have either monotonic or reversing sweeps. In these experiments triplet–triplet absorption and thermal effects due to nonuniform illumination of the cuvette may have been of importance. If the triplet–triplet spectrum is known, the sweep can be predicted. Thus in rhodamine 6G a sweep towards shorter wavelengths should be observed in a uniformly illuminated laser cuvette (Snavely 1969).

In addition to these fast sweeps there is a long-term drift in wavelength associated with increasing loss due to products of photochemical decomposition of the dye. Thus, in a 100 Hz flashlamp-pumped rhodamine 6G laser, the laser wavelength was observed to drift from 570–600 nm in a 10 min period (W. Schmidt 1970). The absorption spectrum of the solution taken after this experiment gave clear evidence of a photodecomposition product with absorption increasing towards shorter wavelengths.

1.6 Wavelength-Selective Resonators for Dye Lasers

A coarse selection of the dye-laser emission wavelength is possible by judicious choice of the dye, the solvent, and the resonator Q, as described in Sect. 1.4.1. Fine tuning and simultaneous attainment of small linewidths can only be achieved by using a wavelength-selective resonator.

Up to now the following four classes of wavelength-selective resonators seem to have been employed:

1) resonators including devices for spatial wavelength separation,
2) resonators including devices for interferometric wavelength discrimination,
3) resonators including devices with rotational dispersion,
4) resonators with wavelength-selective distributed feedback.

The various implementations of these classes of wavelength-selective resonators and their relative merits will be discussed in the above order.

The first wavelength-selective resonator was constructed by Soffer and McFarland (1967). They replaced one of the broad-band dielectric mirrors by a plane optical grating in Littrow mounting. This arrangement is shown in Fig. 1.46 together with a diagram of laser output vs wavelength obtained with a grating of 610 lines per mm in the first and second order for a rhodamine 6G solution. Consider the grating equation $m\lambda = \delta(\sin\alpha + \sin\beta)$ which for autocollimation ($\alpha = \beta$) reduces to $m\lambda = 2d\sin\alpha$. Here m is the order, λ is the wavelength, β is the angle of incidence, α is the angle of diffraction from the normal to the grating, and d is the grating constant. Then the angular dispersion is $d\alpha/d\lambda = m/2d\cos\alpha$.

If the dye laser has a beam divergence angle $\Delta\alpha$, the passive spectral width of this arrangement would be

$$\Delta\lambda_\alpha = \frac{2d\cos\alpha}{m}\,\Delta\alpha \ . \tag{1.13}$$

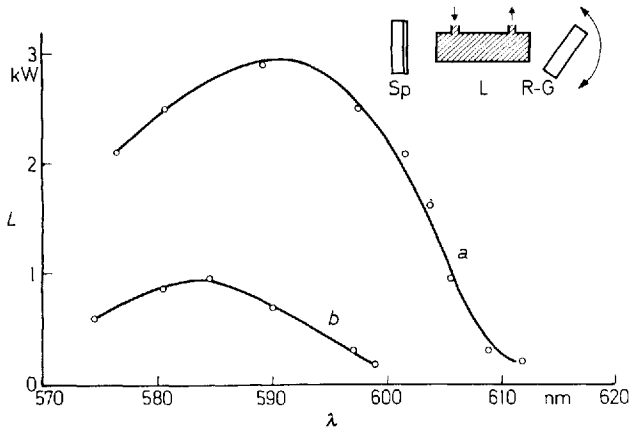

Fig. 1.46. Tuning of dye-laser wavelength with an optical grating. Output powers vs wavelength for a 10^{-4} M solution of rhodamine 6G in methanol, grating 610 lines/mm, a first order, b second order. (Insert: optical arrangement; Sp = 98% mirror, L = laser cuvette, R-G = optical grating in rotatable mount)

On the other hand, if the laser has diffraction-limited beam divergence, $\Delta\alpha = 1.22\lambda/D$, where D is the inner diameter of the cuvette, then the passive spectral width is

$$\Delta\lambda_D = 2.44 d\lambda \cos\alpha/mD \ . \tag{1.14}$$

For a typical case, $\Delta\alpha = 5$ mrad, $D = 2.5$ mm, $d = (1/1200)$ mm, $m = 1$, and $\lambda = 600$ nm, one obtains $\Delta\lambda_\alpha = 7.8$ nm, and $\Delta\lambda_D = 0.37$ nm. If beam expanding optics are used within the cavity to reduce the beam divergence by a factor of ten, this would give $\Delta\lambda_{\alpha r} = 0.78$ nm and $\Delta\lambda_{Dr} = 0.037$ nm. The active spectral width at threshold is smaller than the passive width depending on the available gain. Passive bandwidths are quoted here since these give an upper limit for the spectral bandwidth. The experimental value of the spectral width for a rhodamine 6G laser with 5 mrad beam divergence and a 2160 lines/mm grating was 0.06 nm, as compared with a passive width of 4.6 nm (Soffer and McFarland 1967).

For another laser with a 600 lines/mm grating the spectral width was 2 nm in the first and 0.4 nm in the second order, as compared with the passive width of 16 nm and 8 nm, respectively (Marth 1967). Thus the active bandwidth is smaller by a large factor (between 8 and 80 in these cases) than the passive bandwidth. The peak power is reduced by a factor of only two to five if the grating is blazed for this wavelength. In a laser with a Brewster angle cuvette and resultant polarized emission, this ratio can be even more favorable for the polarization which gives higher grating efficiency.

While high-quality gratings can have efficiencies of up to 95% at the blaze wavelength, most gratings have lower efficiencies, 65% being a realistic value. Thus, the insertion loss due to the grating is substantial.

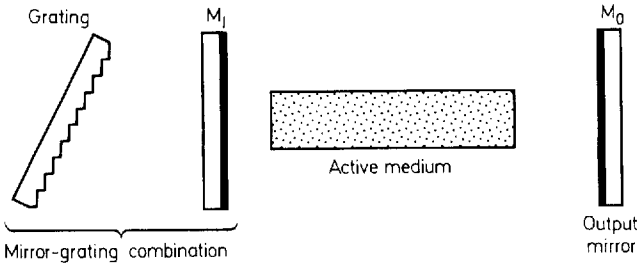

Fig. 1.47. Schematic diagram showing the use of a mirror-grating combination in a laser. M_1 is the intermediate mirror. (From Bjorkholm et al. 1971)

Another disadvantage of the grating is the reflecting metal film which may be damaged by high power and energy pulses. An improvement may be expected from holographically produced bleached transmission gratings (Kogelnik et al. 1970). This problem can also be circumvented by the use of a high-power beam-expanding telescope. The use of such a beam-expanding device is especially indicated in the case of laser-pumped dye lasers, as shown in Fig. 1.21. Most suitable for this purpose are prism beam expanders, of which many different designs have been described. Simple ones use a single prism (Myers 1971; Hanna et al. 1975; Wyatt 1978); more complicated designs, using several prisms in series, allow higher magnification (Klauminzer 1978; Duarte and Piper 1980, 1982). A comparison of the various designs can be found in (Rácz et al. 1981). An unexpanded beam of a fraction of one mm diameter would cover only a few lines on the grating and thus also seriously impair the spectral resolution. Another way to prevent the burning of a grating is by the use of an additional semitransparent mirror in front of the grating, as shown in Fig. 1.47 (Bjorkholm et al. 1971). This scheme not only reduces the power incident on the grating to a few percent of what it would have been without the mirror, but also significantly reduces the laser threshold, since the mirror-grating combination acts as a high-reflectivity resonant reflector for the tuned wavelength. The authors report a reduction in threshold by a factor of two and in bandwidth by a factor of 3.3 over the use of a grating only.

An important improvement was developed by several groups in 1977 when they used a grating in grazing incidence in combination with a maximum reflectivity mirror as shown in Fig. 1.48. As is immediately obvious, this arrangement obviates the need for intracavity beam expanders. Outcoupling is via the zeroth order (Shoshan et al. 1977; Littman 1978; Saikan 1978). A further improvement was the use of a second grating instead of the mirror, as shown in Fig. 1.49 (Littman and Metcalf 1978). Single-mode operation could easily be achieved in such an arrangement.

Alternatively, tuning and spectral narrowing may be achieved by one or more prisms in the laser cavity (Yamaguchi et al. 1968). The relatively small angular dispersion of a single prism is sufficient to isolate one of several sharp lines in gas lasers, for example, where this method has long been used. But it

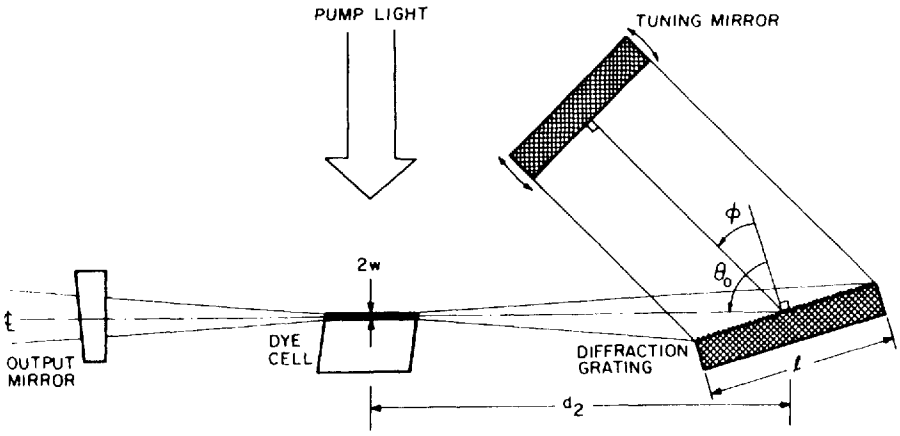

Fig. 1.48. Grazing incidence laser-pumped tunable dye laser. (From Littman and Metcalf 1978)

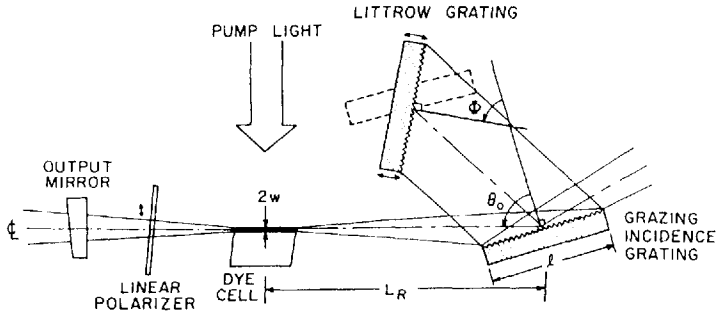

Fig. 1.49. Grazing incidence laser-pumped tunable dye laser with a second grating. (From Littman 1978)

gives hardly any reduction in spectral bandwidth of a flashlamp-pumped dye laser, so that multiple-prism arrangements have to be used. With the notation of Fig. 1.50 one has $\alpha = 2i - \beta$ and $r = \frac{1}{2}\beta$ so that

$$\frac{d\mu}{d\alpha} = \frac{\cos \frac{1}{2}(\alpha + \beta)}{2 \sin \frac{1}{2}\beta} \,. \tag{1.15}$$

Since it is better to work near the Brewster angle where $d\alpha/d\mu = 2$, the angular dispersion of a prism is

$$d\alpha/d\lambda = 2\, d\mu/d\lambda \,. \tag{1.16}$$

Using z prisms in autocollimation with a dye laser of beam divergence $\Delta\alpha$, the passive spectral width is

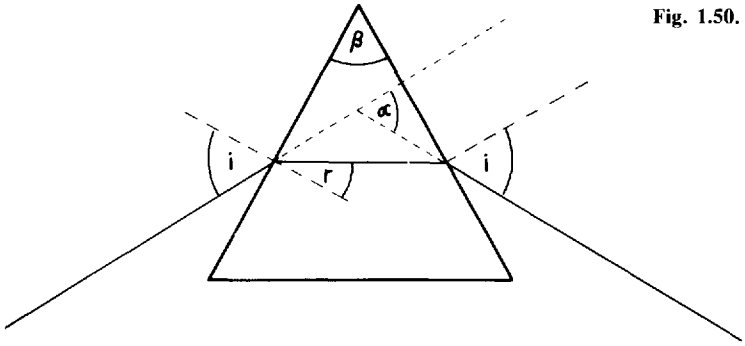

Fig. 1.50. Prism geometry

$$\Delta\lambda_\alpha = \frac{\Delta\alpha}{4z\,d\mu/d\lambda} \,. \tag{1.17}$$

If $\Delta\alpha = 1.22\lambda/D$, in the diffraction-limited case one has

$$\Delta\lambda_D = \frac{1.22\lambda/D}{4z\,d\mu/d\lambda} \,. \tag{1.18}$$

Consider 60°-prisms of Schott-glass SF10 for which $\mu_D = 1.72802$ and $d\mu/d\lambda = 1.35\times10^{-4}\,\mathrm{nm}^{-1}$. Then the following values are obtained for 1 or 6 prisms in autocollimation:

Values of $\Delta\lambda$ [nm] for a number of prisms

No. of prisms	$\Delta\lambda_\alpha$	$\Delta\lambda_{\alpha r}$	$\Delta\lambda_D$	$\Delta\lambda_{Dr}$
1	9.3	0.93	0.54	0.05
6	1.5	0.15	0.09	0.01
grating 1200 lines/mm	7.8	0.78	0.37	0.04

As above, it is assumed that $\Delta\alpha = 5$ mrad and $D = 2.5$ mm, with and without tenfold beam expanding optics.

A comparison of passive spectral widths, as given in the above table, shows that it should be better to use two or more prisms rather than one grating. In addition, the cumulative insertion loss of even 6 prisms near the Brewster angle is much smaller than that of one grating.

A five-prism arrangement has been reported by Strome and Webb (1971) and a six-prism arrangement by Schäfer and Müller (1971). Another method for obtaining increased angular dispersion uses a prism at angles of incidence of slightly less than 90 degrees. This results in a very high dispersion at only slightly reduced resolution, as in early spectrographs. The high reflection at the prism face that was detrimental in those spectrographs is an advantage here,

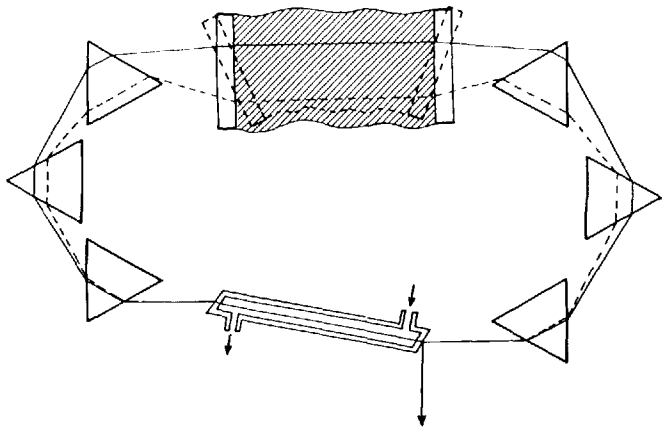

Fig. 1.51. 6-prism ring laser with variable wedge. (From Schäfer and Müller 1971)

since it serves as an outcoupling device, variable between 20% reflection at 80° incidence to 100% reflection at 90° (Myers 1971). In the prism there is a considerable increase in beam width and a concomitant reduction in beam divergence, which makes the additional insertion of a grating attractive, again particularly in nitrogen-laser-pumped dye lasers.

The prism method lends itself to use in ring lasers. Schäfer and Müller (1971) incorporated six 60°-prisms made of the Schott-glass SF 10 as dispersive elements in a ring laser whose optical path is completed by two glass plates connected by a rubber bellows which is filled with an index-matching fluid so that a variable wedge is formed. The laser wavelength is selected by the setting of the refracting angle of the wedge (Fig. 1.51). A linewidth of less than 0.05 nm was obtained with 40 J electrical input energy pumping a 10^{-4} molar rhodamine 6G solution flowing in a 7.5-cm-long dye cuvette of 2.5 mm inner diameter, placed in the center of a 2″ helical flashlamp. The Fresnel reflection of one of the dye cuvette windows, intentionally set a few degrees off the Brewster angle, generated the output beam. It is noteworthy that the spectrum showed none of the satellite lines that are usually found in linear lasers using prisms or gratings for spectral narrowing. These satellite lines near the selected wavelength are probably associated with rays passing through inhomogeneities in the dye solution. Hence they form an angle with the optical axis which may be greater than the beam divergence of the main part of the beam. Insertion of an aperture into the cavity for reducing the beam divergence eliminates these lines. In a ring laser the cuvette evidently acts in this way, resulting in much improved discrimination against satellites. Another ring laser using four Abbé or Pellin-Broca prisms was described by Marowsky et al. (1972). The four 90° constant-deviation prisms made of SF 10 glass are so arranged at the corners of a square that a closed path exists for the selected wavelength. The wavelength tuning was achieved by simultaneous counter rotation of the four mechanically coupled prisms. The spectral range covered reached from 430 nm

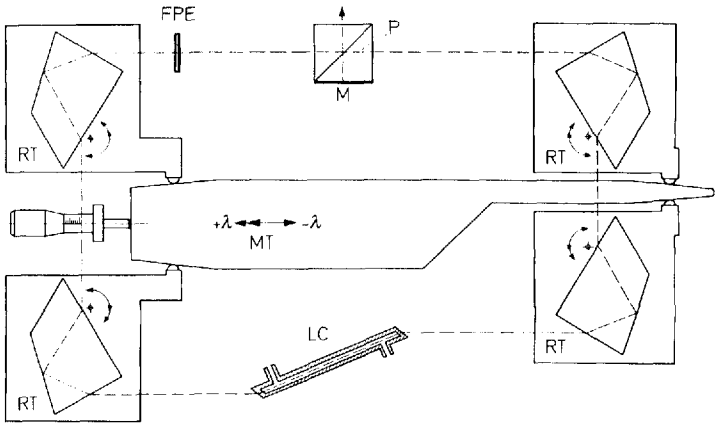

Fig. 1.52. Ring laser. (LC: laser cuvette, RT: rotating prism tables with Abbé prisms, axis and sense of rotation indicated, MT: movable table, FPE: Fabry-Perot etalon, P: beam-splitting output prism with high reflectivity mirror M). (From Marowsky et al. 1972)

to beyond 700 nm and the spectral width was 0.8 nm at 600 nm and decreased towards shorter wavelengths (Marowsky 1973a). This type of ring laser is shown in Fig. 1.52.

A noteworthy advantage of these multiprism ring lasers is that they obviate the need for mirrors with broadband dielectric reflective coatings. Additional aspects of prism tuning are discussed in (Marowsky 1973a, c, 1975; Marowsky et al. 1975; Yamagishi and Inaba 1976).

If only fixed wavelengths are needed, the simplest way of utilizing interference effects is to have narrowband reflective coatings on the resonator mirrors. Often supposedly broadband reflectors show a certain selectivity. At wavelengths where the reflectivity drops slightly, e.g. a quarter of one percent, holes are produced in the broadband spectrum of the dye laser at this wavelength; these holes have sometimes been misinterpreted as due to some property of the dye molecules. Resonant reflectors and reflectors of the Fox-Smith type are useful only in conjunction with suitable preselectors because of their narrow free spectral range.

In a method which is especially well suited for achieving a small spectral bandwidth, one or more Fabry-Perot etalons or interference filters are inserted into the cavity (Bradley et al. 1968a, b). The wavelength λ of maximum transmission in kth order for a Fabry-Perot of thickness d, refractive index μ, and with an angle α between its normal and the optical axis, is given by $k\lambda = 2\mu d \cos\alpha'$. Here α' is the refracted angle $\mu \sin\alpha' = \sin\alpha$. Thus, for air ($\mu = 1$) the angular dispersion is

$$d\lambda/d\alpha = \lambda \tan\alpha \ . \tag{1.19}$$

Hence the spectral bandwidth for beam divergence $\Delta\alpha$ is (independent of the finesse)

$$\Delta\lambda_\alpha = \lambda\,\Delta\alpha\,\tan\alpha \ . \tag{1.20}$$

The wavelength shift $\Delta\lambda_s$ for turning the Fabry-Perot from a position normal to the optical axis ($\alpha = 0$, corresponding to a wavelength λ_0) through an angle α is

$$\Delta\lambda_s = (1-\cos\alpha)\lambda_0 \ . \tag{1.21}$$

The free spectral range $\Delta\lambda_F$ between adjacent orders is

$$\Delta\lambda_F = \lambda/k \ . \tag{1.22}$$

The spectral width near λ_0 is determined by the reflection coefficient R of the Fabry-Perot mirrors,

$$\delta\lambda = \Delta\lambda_F/F \ , \tag{1.23}$$

where

$$F = \frac{\pi\sqrt{R}}{1-R} \tag{1.24}$$

is the so-called finesse factor.

From these relations it is easy to determine the required properties of the laser and the Fabry-Perot for narrow band emission and wide band tunability. The attainable minimum bandwidth is determined by the minimum angle which avoids reflection from the first mirror of the Fabry-Perot back into the cuvette. If q is the ratio of the diameter of the cuvette to the distance between the Fabry-Perot and the nearest cuvette window, the minimum bandwidth is

$$\Delta\lambda_{\alpha\min} = \lambda\,\Delta\alpha\,\tan\tfrac{1}{2}q \ . \tag{1.25}$$

Assume a prism preselector in the cavity which gives $\Delta\lambda_\alpha = 3$ nm for $\Delta\alpha = 5$ mrad at 600 nm. Then the optimum free spectral range of the Fabry-Perot should be $\Delta\lambda_F = \lambda/k = 3$ nm so that $k = 200$ and $d = 60\,\mu$m. With a typical value of $q = 0.05$ this yields a beam-divergence-limited bandwidth of $\Delta\lambda_{\alpha\min} = 0.075$ nm. As the angle is increased to tune over the free spectral range, the bandwidth increases according to (1.20) to $\Delta\lambda_{\alpha\min} = 0.3$ nm. Thus, a large tuning range is possible only at the expense of a relatively large increase in bandwidth. In addition to an increasing bandwidth, the use of Fabry-Perot etalons at high angles also introduces serious walk-off losses, which become more serious the larger the ratio of etalon thickness to beam diameter and the higher the angle. In order to realize a specified narrow bandwidth, one would have to reduce the tuning range and/or the beam divergence of the laser. Wavelength selection and simultaneous spectral narrowing were achieved in this way with laser-pumped and flashlamp-pumped lasers. An emission bandwidth of less than 50 pm was first achieved in practice (Bowman et al. 1969a), later less than 1 pm (W. Schmidt 1970). Hänsch (1972) reported that the inser-

tion of a Fabry-Perot etalon into the dye laser cavity shown in Fig. 1.21c reduced the bandwidth from 3 pm, obtained with the grating only, to 0.4 pm. At the same time the output dropped from 20 kW to about 3 kW, thought to be primarily due to high losses in the available broadband coatings. Probably at least some of these losses are due to other sources, like the walk-off in the etalon. This is substantiated by the small reduction of output powers after the successive insertion of an interference filter (low-order Fabry-Perot etalon) and two Fabry-Perot etalons used near the minimum useful angle. In his rhodamine 6G laser at 600 nm wavelength and 20 J pump energy Marowsky (1973b) obtained 2.4 kW at 50 pm bandwidth with only an interference filter in the cavity. The insertion of the first Fabry-Perot decreased the peak power to 2.2 kW and the bandwidth to 7 pm. The insertion of the second etalon decreased the peak power to 2.0 kW and the bandwidth to 0.1 pm.

As Fabry-Perot etalons one usually uses either plane-parallel quartz plates coated with dielectric multilayer broadband reflective coatings, or optically contacted air Fabry-Perots (Bates et al. 1968).

For high resolution spectroscopy a very convenient method is the pressure scanning of a Fabry-Perot etalon in the resonator of a dye laser, as described by J.M. Green et al. (1973a); Flach et al. (1974) and Wallenstein and Hänsch (1975).

If the length of the dye laser resonator is very small, only a few well-separated longitudinal modes can oscillate, of which one can easily be singled out by some simple filter. When the length is decreased to only a few meters, only one longitudinal mode lies within the fluorescence band, and small changes in resonator length allow an easy scanning of the laser wavelength. Figure 1.53 gives an example of this (Schäfer 1970). Later, this tuning method for short cavity dye lasers was further refined by Cox and Scott (1979) and Cox et al. (1982).

Several methods of wavelength selection make use of the rotation of polarization. One method utilizes birefringent filters in the cavity (Soep 1970). A simple arrangement consists of a quartz plate cut parallel to the optic axis, which has a retardation of several half-wavelengths at the center of the tuning range, and a set of Brewster plate polarizers as shown in Fig. 1.54. In this case there are transmission maxima for retardations of multiple half-wavelengths,

$$k\lambda/2 = \Delta\mu x_0 \cos\alpha \ . \tag{1.26}$$

Here k is the order number, $\Delta\mu$ the birefringence and x_0 the crystal thickness, both for normal incidence. Thus the wavelength spread for beam divergence $\Delta\alpha$ is

$$\Delta\lambda = -\lambda \tan\alpha \Delta\alpha = -\lambda \frac{\cos\alpha \sin\alpha}{\mu^2 - \sin^2\alpha} \Delta\alpha \ . \tag{1.27}$$

This expression is very small near $\alpha = 0$.

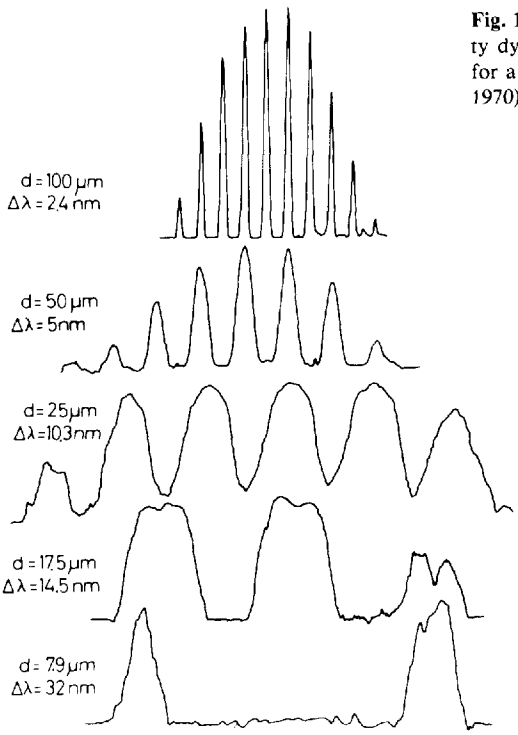

Fig. 1.53. Spectra of the output of a short-cavity dye laser with resolved longitudinal modes for a series of cavity lengths d. (From Schäfer 1970)

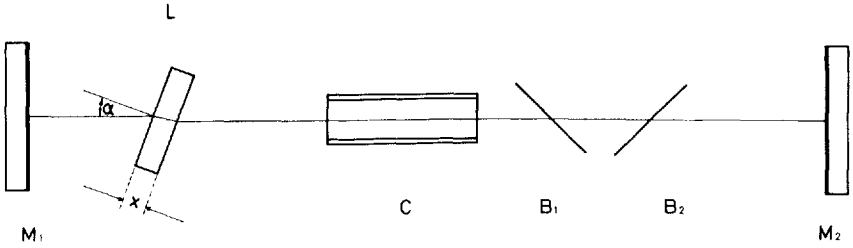

Fig. 1.54. Dye laser with birefringent filter. ($M_{1,2}$ mirrors, C dye cuvette, L quartz plate of thickness x, $B_{1,2}$ Brewster angle polarizers). (From Soep 1970)

Now, however, the bandwidth is not determined by the beam divergence of the laser, as in the methods discussed above, but rather by the transmission T of the birefringent filter,

$$T = \cos^2(\pi \Delta\mu d/\lambda) \ . \tag{1.28}$$

If a reduction of 10% in transmission compared to maximum transmission brings the laser below threshold, one would expect an active bandwidth of

$$\Delta\lambda_a = \tfrac{1}{6}\lambda^2/\Delta\mu d \ . \tag{1.29}$$

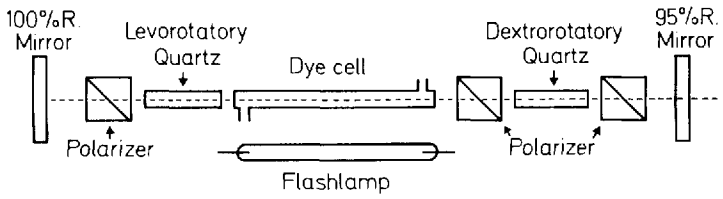

Fig. 1.55. Dye laser with double-state rotatory dispersive filter. (From D. Kato and Sato 1972)

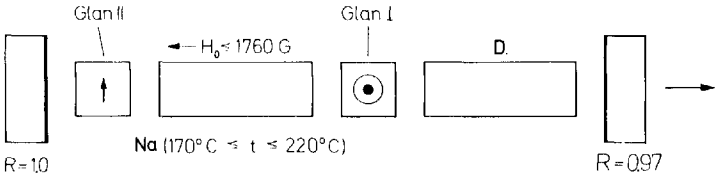

Fig. 1.56. Experimental arrangement to lock the dye laser wavelength to a spectral line. (D dye cuvette, Na sodium vapor cell, H_0 indicating magnetic field of solenoid surrounding cell). (From Sorokin et al. 1969)

This spectral width can be reduced further by the introduction of one or more additional quartz plates of greater thickness, as in Lyot or similar birefringent filters. Using KDP crystals of suitable orientation instead of the quartz plates, one can vary the transmission wavelength by applying a voltage (Walther and Hall 1970). The actual tuning range in a flashlamp-pumped rhodamine 6G laser with a quartz plate of 0.36 nm thickness and an angle of incidence between 35° and 50° was from 570–600 nm with a spectral bandwidth of 1 nm (Soep 1970). Walther and Hall (1970) obtained a spectral bandwidth of less than 1 pm and an electrical tuning range of 0.4 mm. The birefringent Fabry-Perot etalon is treated in (Holtom and Teschke 1974; Okada et al. 1975, 1976).

Another method makes use of the rotatory dispersion of z-cut quartz crystals. D. Kato and Sato (1972) used one dextro- and one levorotatory quartz crystal of 45 mm length each between 3 polarizers (Fig. 1.55). The tuning rate of this arrangement is 0.24 nm/degree if the central polarizer is rotated. The spectral half-width was rather wide, about 2 nm, since the rotatory dispersion of quartz is rather weak.

In an ingenious method, the large Faraday rotation in the vicinity of an atomic absorption line is used to lock the laser wavelength to the line (Sorokin et al. 1969). In the experimental arrangement of Fig. 1.56, the dye laser emission obtained consisted of two doublets locked to the sodium D lines. The components of both doublets are displaced symmetrically above and below the atomic line and each has a spectral width of less than 0.1 cm^{-1}. The splitting of the laser doublets may be adjusted by varying sodium vapor pressure and magnetic field.

Another important aspect of dye laser tuning methods is dual-wavelength operation. Many different designs have been devised, most of which make use

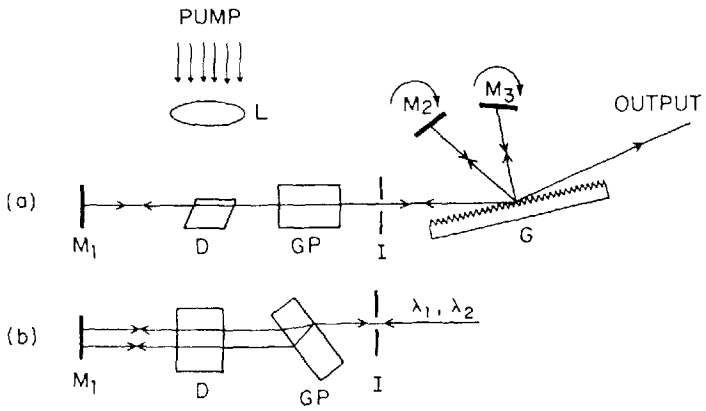

Fig. 1.57. Dual-wavelength grazing incidence dye laser, (a) top view, (b) side view. Dye cell D, glass plate GP, iris I, grating G, mirrors $M_{1,2,3}$, cylindrical lens L. (From Prior 1979)

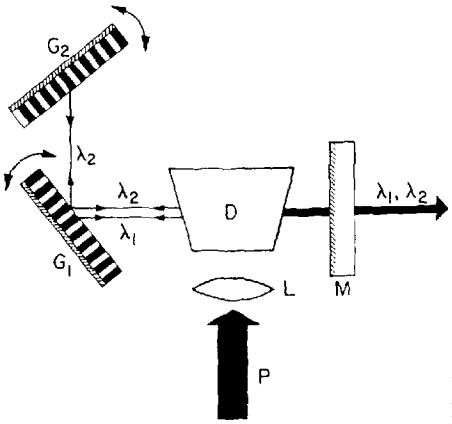

Fig. 1.58. Dual-wavelength dye laser. (From Friesem et al. 1973a)

of a grating in combination with two mirrors for feedback of the desired wavelengths, as shown in the example of Fig. 1.57, taken from (Prior 1979). Other papers describing similar designs are (Dinev et al. 1980; Inomata and Carswell 1977; Kittrell and Bernheim 1976; Dorsinville 1978).

Some other designs make use of two gratings, as shown in the example of Fig. 1.58 taken from (Friesem et al. 1973a). Further papers on this type of dual-wavelength dye lasers are (Pilloff 1972; Wu and Lombardi 1973; Dorsinville and Denariez-Roberge 1978; Nair 1979; Nair and Dasgupta 1980; Kong and Lee 1981). Still other variants can be found in (A. J. Schmidt 1975b; Lotem and Lynch 1975; Matsuzawa et al. 1976; Winter et al. 1978; Chou and Aartsma 1986).

Rapid tuning is possible with electro-optic elements in the resonator as described above (p. 76) or using an acousto-optic deflector in combination with

a grating (Streifer and Saltz 1973; Hutcheson and Hughes 1974a, b; Telle and Tang 1974a, 1974b, 1975; K. Kopainsky 1975; Turner et al. 1975).

1.6.1 Distributed-Feedback Dye Lasers

Dye lasers with distributed feedback might become very important active elements for integrated optics. Their time behavior, which makes them very suitable for the production of single picosecond pulses, is described in Chap. 4. The first distributed-feedback dye laser was described by Kogelnik and Shank (1971). They produced a distributed-feedback structure by inducing a periodic spatial variation of the refractive index μ according to $\mu(z) = \mu + \mu_1 \cos Kz$, where z is measured along the optic axis and $K = 2\pi/\Lambda$, Λ being the period or fringe spacing of the spatial modulation and μ_1 its amplitude. They calculated that a threshold could be reached in a dye laser with a gain of 100 and a length of 10 mm, if $\mu \geqq 10^{-5}$. This was easily obtained by exposing a dichromated gelatin film to the interference pattern of two coherent uv beams from a He-Cd laser. After exposure the gelatin film was developed in the usual manner and soaked in a solution of rhodamine 6G to make the dye penetrate into the porous gelatin layer. After drying, the film was transversely pumped with the uv radiation from a nitrogen laser. Threshold was reached at pump densities of 1 MW/cm^2 and dye-laser emission less than 0.05 nm wide was observed at about 630 nm. In uniform gelatin under the same pumping conditions the emission was 5 nm wide and centered at about 590 nm.

Shank et al. (1971) showed that a distributed-feedback amplifier can also be operated with the feedback produced by a periodic spatial variation of the gain of the dye solution. They used the experimental arrangement shown in Fig. 1.59, pumping a rhodamine 6G solution with the fringes of two coherent beams from a frequency-doubled ruby laser, meeting at an angle 2θ. Then the wavelength of the dye laser is given by $\lambda_L = \mu_s \lambda_p / \sin\theta$, where μ_s is the index of refraction of the dye solution at the lasing wavelength λ_L, and λ_p is the pump wavelength. Thus, tuning is possible by varying either θ or μ_s. The result of angle tuning is given in Fig. 1.60, while the results of tuning by variations of the refractive index of a solvent mixture of methanol and benzyl alcohol are given in Fig. 1.61. At about 180 kW peak pump power, the peak output power of the distributed-feedback dye laser was 36 kW. The spectral width with reduced pump power was less than 1 pm and apparently due to a single mode.

Narrowband laser oscillation from such a system was also observed when the period of the distributed-feedback structure was two or three times larger than the oscillation wavelength (Bjorkholm and Shank 1972b), probably due to harmonic frequencies in the spatial gain modulation.

The pumping arrangement described above needs as pump light source a laser of sufficiently small spectral bandwidth and good spatial coherence over the beam cross-section in order to create an interference pattern of high visibility. A nitrogen laser for example would not give satisfactory results.

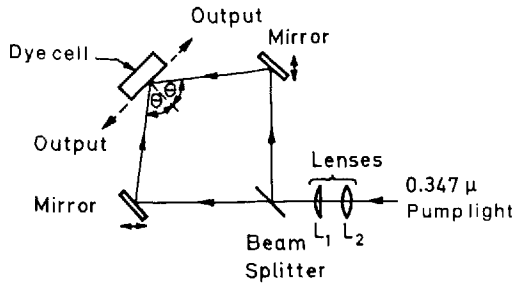

Fig. 1.59. Experimental arrangement of distributed feedback dye laser. (From Shank et al. 1971)

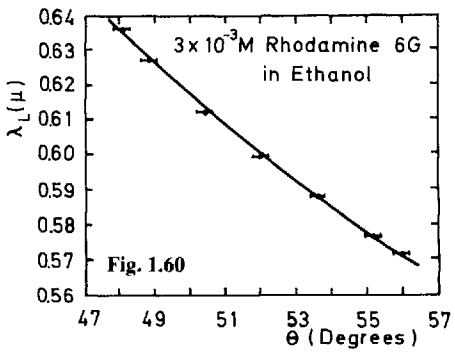

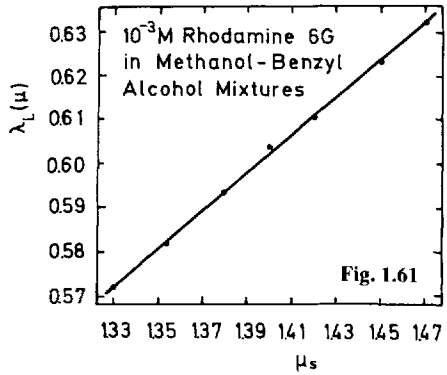

Fig. 1.60. Lasing wavelength λ_L as a function of the angle θ for 3×10^{-3} M rhodamine 6G in ethanol. The points are experimental, the curve is theoretical. (From Shank et al. 1971)

Fig. 1.61. Lasing wavelength λ_L as a function of the solvent index of refraction μ_s for $\theta = 53.8°$. The dye solution was 10^{-3} M rhodamine 6G in a methanol-benzyl alcohol mixture. The points are experimental and the curve is theoretical. (From Shank et al. 1971)

A greatly improved pumping arrangement avoiding these restrictions was described by Bor (1979). It is shown in Fig. 1.62. The use of a holographic grating as a beamsplitter and a judicious choice of the geometry results in a high visibility interference pattern even with broadband lasers of low spatial coherence as pump lasers, e.g. nitrogen, excimer, and dye lasers.

Another very recent version of a distributed-feedback laser that allows broadband pumping is shown in Fig. 1.63. It uses a coarse grating of about 50 lines/mm that is imaged by a microscope objective into a dye cell in contact with the objective. A beam stop blocks the zeroth order. This arrangement is widely tunable by changing the distance between grating and microscope objective (Szatmári and Schäfer 1988).

Another possibility for distributed feedback was described by Kaminow et al. (1971). They used a sample of polymethylmethacrylate with the dimensions $4\times10\times38$ mm, doped with 8×10^{-6} mole/l of rhodamine 6G. In this sample they produced two three-dimensional phase gratings of about $2\times2\times2$ mm by a 2-minute exposure of two intersecting uv beams of 0.7 mW each from a He-Cd laser as shown in Fig. 1.64. The sample was pumped by the second har-

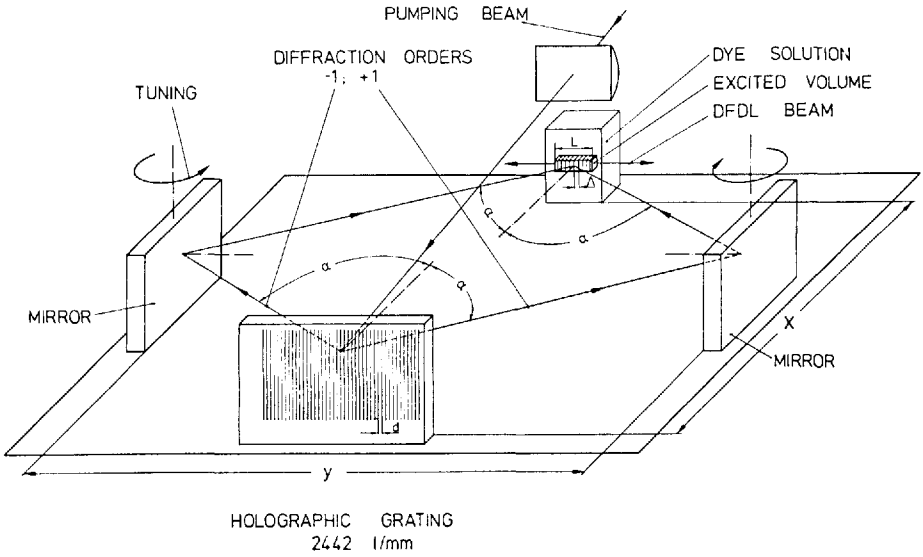

Fig. 1.62. Experimental arrangement of an achromatic distributed-feedback dye laser. (From Bor 1979)

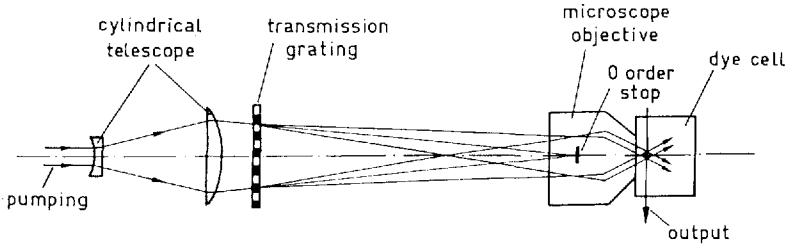

Fig. 1.63. Achromatic, tunable distributed-feedback dye laser using a microscope objective and a coarse grating. (From Szatmári and Schäfer 1988)

monic from a Nd laser. Again, the dye-laser wavelength was determined by the Bragg condition $\lambda_L = 2\mu_s \Lambda$ that must be fulfilled with $2\Lambda = \lambda_{uv}/\sin\theta$. The output consisted of one strong line of 0.5 pm near threshold. At higher pumping power, several modes separated by $c_0/2\mu_s L$ were observed, where $L = 20$ mm is the distance between the two gratings. The application of mechanical stress to the region of the gratings allowed a tuning of 1.1 nm.

Yet another possibility of producing a phase grating in polymethylmethacrylate was reported by Fork et al. (1971). They dissolved 2 mmole/l rhodamine 6G tosylate and 0.1 mole/l acridizinium ethylhexanesulfonate photodimers in methylmethacrylate and acrylic acid and polymerized the resulting solution to form a hard, transparent plastic. The sample was then cut and polished into 1 cm × 1 cm × 1 mm chips. The photodimers were first broken

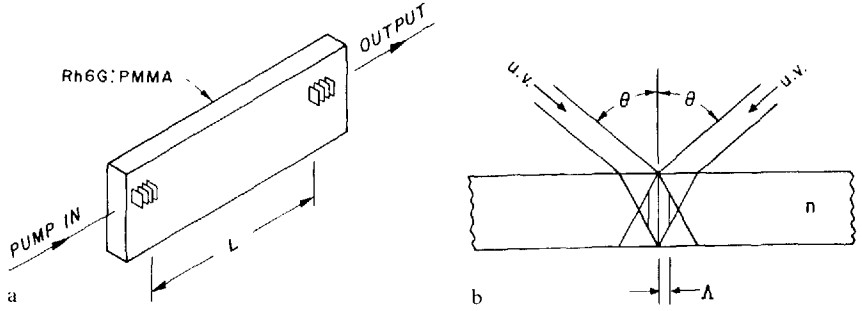

Fig. 1.64. (**a**) Dye-doped polymethylmethacrylate laser with internal grating resonator. (Dimensions: $4\times10\times38$ mm; grating spacing $L = 20$ mm). (**b**) Preparation of gratings by intersecting uv beams through the broad face of the plastic sample. (From Kaminow et al. 1971)

to a depth of 80 μm by illumination with an erase beam of 313 nm light from a mercury arc and then selectively remade in a grating pattern by two intersecting writing beams from an argon laser, in the manner described above for the other examples. The sample was then pumped by the 10-kW pulse from a neon laser focused on the sample by a cylindrical lens. The output showed a few narrow lines with a spacing determined by the $c_0/2L$ separation for the length $L = 1$ cm of the laser.

Fork and Kaplan (1972) rpeorted on a distributed-feedback dye laser with a variable phase grating which can be optically written into photodimer optical memory material with the interference fringes of a 364 nm Ar^+ laser, or erased with the 313 nm light of a Hg arc lamp. The laser material is a solid PMMA host, doped with rhodamine 6G and photodimers of acridizinium ethylhexanesulfonate. The photodimer can be broken with the erasing light and remade with the writing laser light of longer wavelength. Writing times as short as 3 ns appear possible with high-power pulsed lasers. A gain of $8\,cm^{-1}$, twice above threshold, was obtained, when the small active volume ($1\,cm\times80\,\mu m\times10\,\mu m$) was pumped with a pulsed neon laser at 540 nm with 10 kW peak power. The narrowband dye-laser output consists of several peaks, some less than 1.2 GHz wide.

Instead of having the distributed feedback within the laser beam, one can also provide feedback for the evanescent wave and gain within the main laser beam in the dye solution adjacent to the distributed-feedback structure (Hill and Watanabe 1972). A schematic cross-section of such a laser is shown in Fig. 1.65. In the experimental implementation of the device the cover plate was a quartz optical flat, the organic dye solution a 3×10^{-2} molar solution of rhodamine 6G in benzyl alcohol, or a mixture of benzyl and enthyl alcohols, and the feedback structure was a gelatin film grating on a glass substrate. The dichromated gelatin film had been exposed to two coherent intersecting laser beams and developed as described above. By varying the relative refractive indices of dye solution and gelatin film one could either have normal-wave gain and evanescent-wave feedback, or evanescent-wave gain and normal-wave feed-

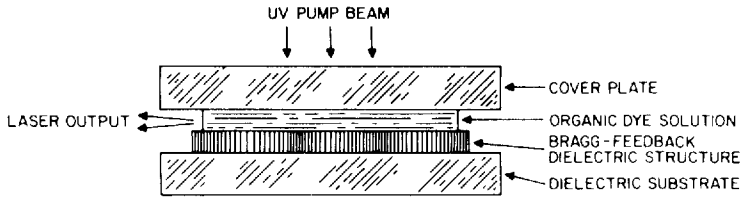

Fig. 1.65. Cross-section of the distributed feedback side-coupled laser. (From Hill and Watanabe 1972)

back, or gelatin film and dye solution acting together as a waveguide for higher-order modes for the case of nearly equal refractive indices.

Distributed feedback in a thin film dye laser can also be produced by providing a periodic perturbation of the film thickness, which can be achieved using photoresist and ion-milling techniques (Schinke et al. 1972; Kotani et al. 1976; Deryugin et al. 1976b; Kolbin et al. 1976).

Distributed feedback dye laser action in an optical fiber by evanescent field coupling was described by Periasamy and Bor (1981).

1.6.2 Thin-Film and Waveguide Dye Lasers

It is easy to prepare a dye laser structure having transverse dimensions of a few micrometers which supports only a small number of low-order waveguide modes. Modes of low losses are known in straight dielectric waveguides, even if the embedding medium has a higher index of refraction than the guiding core, as in hollow waveguide gas lasers. Burlamacchi and Pratesi (1973a) have utilized this phenomenon in a flashlamp-pumped superradiant dye laser, contained in a small-bore glass capillary. In general, it is more desirable to use a surrounding dielectric medium of lower refractive index to permit waveguiding by total internal reflection, and the wide choice of available liquid and solid dye-laser host materials makes it easy to meet this condition. Such waveguiding liquid dye lasers have been constructed by using benzyl alcohol ($n = 1.538$) as a solvent and filling the liquid dye solution into thin glass capillaries (Ippen et al. 1971; Zeidler 1971) or sandwiching a liquid dye film between flat glass substrates (Zeidler 1971).

H.P. Weber and Ulrich (1971) have reported the successful operation of a solid thin-film dye laser. They produced the active waveguiding structure by coating glass substrates with a thin film of polyurethane ($n = 1.55$) doped with 8×10^{-3} M/l rhodamine 6G. At a typical thickness of 0.8 μm, such a film can support only the fundamental TE_0 and TM_0 modes. A gain as high as 100 dB/cm was obtained when the film was pumped by a pulsed N_2 laser. In order to provide feedback for laser oscillation, the doped light-guiding film was applied on the surface of a cylindrical glass rod of 5 mm diameter, as shown in Fig. 1.66. In this way a closed optical path is established along any circumference of the rod. A narrow circumferential strip of the beam is il-

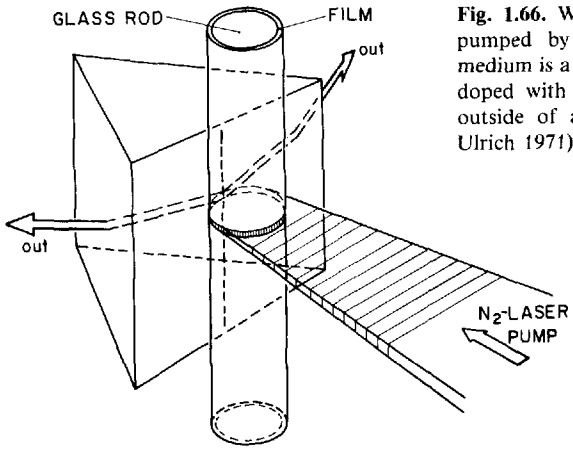

Fig. 1.66. Waveguiding thin-film ring laser, pumped by a nitrogen laser. The active medium is a 0.8 μm thick polyurethane film, doped with rhodamine 6G, coated on the outside of a glass rod. (H. P. Weber and Ulrich 1971)

luminated by a sheetlike beam of the N_2 laser. The dye-laser light is coupled out via its evanescent wave by a closely spaced prism. Two beams are obtained, corresponding to the two opposite directions of rotation. A peak power of 100 W was measured in each beam when the film absorbed about 1 kW of the incident pump light. The laser operated near 620 nm with a bandwidth of 11 nm. Individual axial modes of the ring resonator could be resolved with a Fabry-Perot interferometer, confirming the feedback around the rod. A similar arrangement was described by Deryugin et al. (1976a).

An entirely different approach to waveguiding dye lasers is realized in the evanescent-field-pumped dye laser, as reported by Ippen and Shank (1972a). Here the dye molecules are not incorporated in the waveguide, but are located in the surrounding (liquid) medium. They are pumped by the evanescent wave of the pump-laser light travelling through the waveguide, and they radiate by stimulated emission into a waveguide mode. In the experiment the pump light of a frequency-doubled Nd:glass laser was coupled via a prism into a thin waveguiding glass film, covered by a solution of rhodamine 6G in a benzyl alcohol glycerol mixture. The superradiant dye laser output was measured for different liquid refractive indices and different pump powers. The reported scheme appears particularly attractive because it is easy to replenish photobleached dye molecules. A theoretical estimate indicates that it should be possible to construct a rhodamine 6G dye laser with a waveguide cross-section of $1 \times 3\ \mu m^2$, which could exhibit a threshold of only 5 mW at a round-trip loss of 10%.

In a similar way a rhodamine-B-doped thin polyurethane film was pumped by a nitrogen laser and light of a He-Ne laser coupled in and out through two prisms. A gain of $13\ cm^{-1}$ was observed (Chang et al. 1972).

A special class of waveguide dye lasers is the one using thermally produced waveguiding structures, as mainly developed by Burlamacchi and coworkers (Burlamacchi and Pratesi 1973b, c; Burlamacchi et al. 1974, 1975a, b; Burlamacchi and Salimbeni 1976; Burlamacchi et al. 1976; Fowler and Glenn 1976).

1.7 Dye-Laser Amplifiers

The dye-laser oscillators discussed above are broadband amplifiers with selective or non-selective regenerative feedback. Because of its high inherent gain, a dye laser needs very little feedback to reach the threshold of oscillation. Thus, it is usually somewhat difficult to build a dye-laser amplifier, carefully avoiding all possibilities of regenerative feedback.

The first report on broadband light amplification in organic dyes pumped by a ruby laser was by Bass and Deutsch (1967). They set a Raman cell containing toluene in the ruby-laser beam and behind it a dye cell containing DTTC dissolved in DMSO. The ruby beam and the first stimulated Raman line pumped the dye solution, and broadband laser emission was obtained with the four-percent Fresnel reflection from the cuvette windows. However, when the concentration of the dye was set to a value such that the dye would lase near or at the wavelength of the second Stokes line at 806.75 nm, the broadband oscillation of the dye was quenched and the sharp Stokes line strongly amplified instead. The Raman signal being present from the beginning of the pump process used up all available inversion in the dye so that no free oscillation could start. This, too, is an experimental proof of the homogeneous broadening of the fluorescence band of the dye, at least on a nanosecond scale. Since there was four-percent feedback here, the amplification process was a multipass amplification. Similar results were obtained with CS_2 as Raman liquid and with cryptocyanine as amplifying dye. These results were confirmed by a similar investigation by Derkacheva and Sokolovskaya (1968).

In the ingenious experimental arrangement shown in Fig. 1.67 Hänsch et al. (1971 b) obtained broadband, wide-angle light amplification in several dye solutions pumped by a nitrogen laser. The amplifier calls with an active length of 1.3 mm were made from 10-mm-diameter Pyrex tube sections. The antireflection-coated windows were sealed to the ends under a wedge angle of about 10° to avoid multiple reflections. In a typical experiment two cells were used, one acting as an amplifier and the other as an oscillator. Both were filled with the same dye solution and excited simultaneously by the same nitrogen laser. Part of the dim fluorescent light of the oscillator cell, showing a noticeable preference for near-axial propagation (superradiance), was collected by a field lens and focused by an additional multielement photographic lens into the active volume of the amplifier cell. Here it was amplified and emerged as a bright light cone at the other end, illuminating a circular area on a projection screen. If now any object, such as a photographic transparency, was put into the object plane of the photographic lens, it gave rise to a bright projected image on the screen despite its own faint illumination. The gain was determined by comparing the output with and without excitation of the amplifier, absorption in the amplifier cell and background, i.e. stimulated emission of the amplifier alone, being taken into account as corrections. For small signals (input energies of up to 8 μJ), a single-pass gain of 1000 or 23 dB/mm was obtained when a rhodamine 6G solution was excited by 100-μJ pulses of the nitrogen laser. At input signals of 25 μJ the gain dropped to 14 dB/mm, indi-

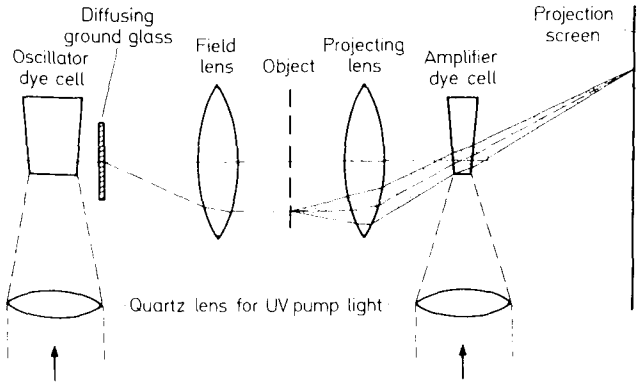

Fig. 1.67. Test setup for image amplification using a dye laser. (From Hänsch et al. 1971b)

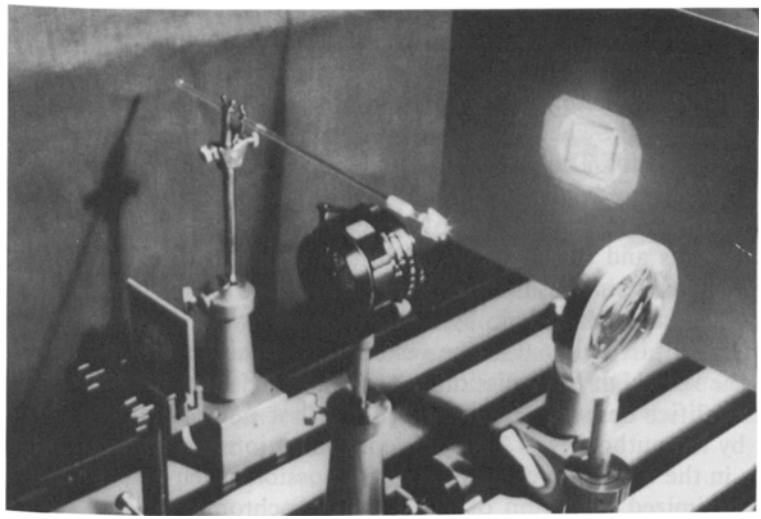

Fig. 1.68. Prototype of dye-laser image amplifier. (Hänsch et al. 1971b)

cating saturation. With rhodamine B and fluorescein, the gain coefficients were about 4 dB/mm lower. Figure 1.68 shows a photograph of the experimental setup.

Erickson and Szabo (1971) also used a dye cell pumped by a nitrogen laser as an amplifier. The 1-cm cell was placed in a resonator consisting of a 99% and a 40% reflectivity mirror spaced 4.2 cm apart. When the acid form of 4-methylumbelliferone was pumped 20% above threshold, the spectral width of the dye-laser emission was 40 nm. Injecting the 514.5 nm line of an argon laser into the resonator caused practically the same energy to be emitted in the region around 514.5 nm in a bandwidth of only 0.16 pm, or about 4 times the width of the injected argon line. This is equivalent to a multi-pass amplifica-

tion in the dye cell of 10^5 or a single-pass gain of 100. A similar regenerative amplifier experiment was described by Vrehen and Breimer (1972). They longitudinally pumped a dye cell filled with a mixture of cresyl violet and rhodamine B with a frequency-doubled Nd laser. The cell was placed in a resonator consisting of two mirrors, one of which had 10% reflectivity at 530 nm to pass the pumping laser beam and 95% reflectivity at 632.8 nm, while the other had 20% transmission at this wavelength for the injection of 1 mW from a He-Ne laser. Here, too, the total output energy from the dye laser with and without injection was found to be constant, the effective total gain for the injected radiation being 10^6. The output of the regenerative amplifier consisted of one or several longitudinal modes centered around the injected line, the number and linewidth depending on the length of the cavity that could be tuned piezoelectrically.

The gain obtainable in flashlamp-pumped dye-laser amplifiers is much smaller than that in laser-pumped amplifiers because of the high triplet losses. Huth (1970) measured the wavelength and time dependence of a flashlamp-pumped amplifier. The amplifier cell had a 5.3 mm inner diameter and was 3.8 cm long. It had antireflection-coated windows with 30-minute wedges. Pumping was by a flashlamp of 3-μs half-width in an elliptical cylinder and with typically 20 J energy. The dye solution was a 2×10^{-4} molar solution of rhodamine 6G in ethanol. The signal to be amplified was derived from a dye-laser oscillator, had a bandwidth of 0.1 nm tunable by a grating over the range from 570–630 nm, and a peak power of typically 20 W/cm^2. It had a duration of about 400 ns and could be shifted in time over the flashlamp pulse length. The maximum gain thus found was 2.3, or 95 dB/m. Even less gain was found in a six-stage amplifier chain by Flamant and Meyer (1971) who measured an energy gain of only 6.0 in the whole chain. This low value was attributable to the very high transmission losses, indicated by the fact that the ratio of the amplifier outputs when pumped and not pumped, termed "apparent gain" by the authors, was 700. These investigations suggest that great improvements in the operation of amplifiers are possible when all parameters are carefully optimized. Injection of a strong monochromatic signal into a regenerative dye-laser amplifier (termed "forced oscillator" in this work) was used by Magyar and Schneider-Muntau (1972). The amplifier cell had an inner diameter of 9 mm and a length of 160 mm and was pumped in a close-coupled configuration by six linear air-filled flashlamps, enclosed by a cylindrical reflector of aluminum foil. The energy of the pump pulse was 4.2 kJ, its risetime 2 μs and its half-width 15 μs. The dye was rhodamine 6G in water of somewhat less than 7×10^{-5} molar concentration, with the addition of 1.5% Ammonyx and 0.2% cyclooctatetraene. One resonator mirror was 99% reflecting, the outcoupling mirror 50%. The output without injection was 1.6 J in a 12 nm wide spectral band. A cell could be placed into the cavity under the Brewster angle that had the twofold purpose of containing an absorbing dye solution and injecting the signal by reflection from its front window. The injected signal was derived from a dye laser oscillator that was spectrally narrowed and tuned by two tilted Fabry-Perot interferometers and had a maxi-

mum output of 55 mJ in 400 ns and a bandwidth of less than 10 pm. Careful timing of the signal resulted in most of the energy of the amplifier appearing in the amplified injected line. Complete frequency locking, however, could only be achieved by adding a few drops of a solution of a suitable absorbing dye, e.g. 1,1′-diethyl-4,4′-cyanine iodide, to the absorber cell which previously contained only solvent. The output then contained only the injected line and had a total energy of 600 mJ. This frequency locking by an absorbing dye was first demonstrated with ruby lasers (Opower and Kaiser 1966). Since the injected signal had a duration of only 400 ns while the amplified signal was 5 μs long, only the front part was true amplification and the forced oscillator continued its emission at the same frequency in the later part of the pulse. Because of the complexity of the operation of this device, it is difficult to make a meaningful statement concerning power or energy gain. Nevertheless, the practical interest of this type of regenerative amplifier or forced oscillator is considerable.

The maximum useful single-pass gain is also determined by the amplified spontaneous emission, because a high noise level at the output reduces the gain by saturation. Typical saturation parameters are on the order of 100 kW/cm^2 to 1 MW/cm^2. The intensity of the amplified spontaneous emission must be kept well below this saturation intensity if "superradiant" emission is to be avoided. Amplification factors of up to 1000 have been realized in practice without violating this condition. Much higher gains should be possible if the dye-laser amplifier is subdivided into several stages and the number of modes of the transmitted noise radiation reduced by spatially limiting apertures and spectral filters.

Unlike solid-state lasers, dye lasers cannot store pump energy for longer than a few nanoseconds, i.e. the lifetime of the excited state. Hence dye-laser amplifiers are only suitable for the amplification of relatively short pulses to extremely high powers. An example of this type of multistage amplifier for the amplification of picosecond or femtosecond pulses to the gigawatt level is to be found at the end of Chap. 4.

1.8 Outlook

To end this chapter, the reader might be interested in a few speculative remarks about possible trends for future developments of dye lasers. Regarding the chemical aspects, the reader is referred to the concluding remarks in Chap. 5. The most important topics with regard to the physical aspects of dye lasers are new pumping methods and pump-light sources, followed closely by the physical dimensions of dye lasers. Some properties can be extrapolated to foreseeable physical limits.

The usual pumping methods using lasers and flashlamps will certainly be improved with respect to efficiency, power, control over pulse shape, and several other parameters. The long-standing problem of an incoherently pumped cw dye laser has just been resolved by Drexhage and coworkers (Thiel

et al. 1987) using a specially constructed arc lamp and dye jet technology. Further developments of this first realization might scale it to very high output powers at reasonable efficiencies.

For very small pulsed or continuous dye lasers direct electrical pumping might be feasible. Some dyes are reported to form relatively stable anions and cations in certain aprotic solvents, e.g. the ions of diphenylanthracene (DPA) in dimethylformamide, which can be formed electrochemically and which, at recombination, leave one molecule in the excited state so that the fluorescence of the neutral molecule is emitted (Chandross and Visco 1964; Hercules 1964; Measures 1974, 1975; Keszthelyi 1975):

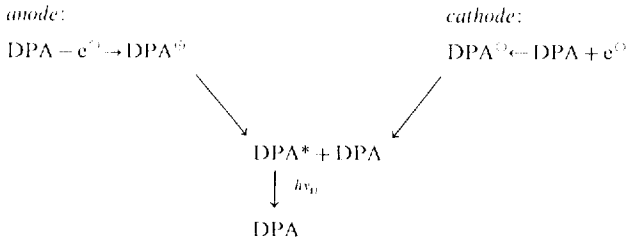

This method would have definite advantages for applications with integrated optics.

For very large volumes of dye solution, flashlamp-pumping would be very cumbersome and expensive; in this case chemical energy storage is more economical, one kilogram of explosive storing about 5 MJ of mechanical energy. This high energy content can be used to excite a shock wave in a gas (so-called argon bombs) (Held 1968) which thus becomes brightly luminescent. A cross-section through a possible structure utilizing such an argon bomb is shown in Fig. 1.69 (Schäfer 1969). The cylindrical mantle of explosive is ignited simultaneously at many lines of the circumference and excites a compressive shock wave in the argon layer that is traveling towards the symmetry axis of the structure. The dye solution is excited by the luminescent output from the shock wave and the concomitant superradiant output can be focused, e.g. by a parabolic ring mirror to the center point of the axis. One can expect outputs of several kJ focused on this spot, which would be useful for plasma experiments.

An extrapolation of present dye-laser properties into the next few years would give an estimate of extended wavelength coverage of 300 to 2000 nm for pulsed lasers and 380 to 950 nm for cw lasers. Together with frequency mixing and multiplication and stimulated Raman emission, this would in effect give complete coverage from the vacuum ultraviolet to the far-infrared.

The maximum power output of a laser is reached when a pulse containing the saturation energy (in photons per square cm) $E_s = 1/\sigma_{fl}$ is being amplified. For a dye $\sigma_{fl} \approx 10^{16}\,\mathrm{cm}^2$, and thus $E_s = 10^{16}$ photons/cm^2, equivalent (at 600 nm) to a power of 3.3 GW/cm^2 for a pulse of 1 ps duration. Since the cross-section of a dye solution is practically unlimited, pulses of terawatt peak power could be generated with dye lasers.

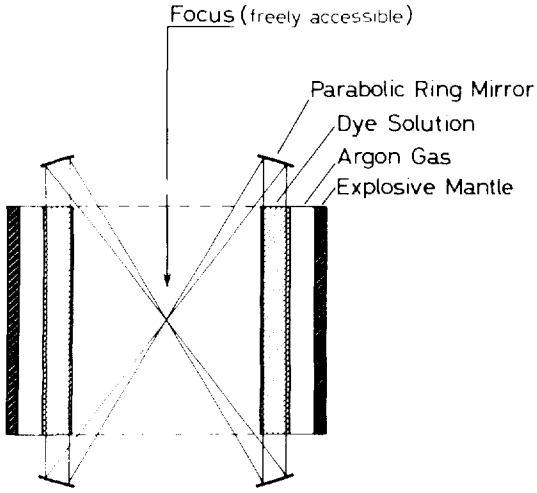

Fig. 1.69. Cross-section of a dye laser pumped by an argon bomb. (From Schäfer 1969)

The pulse energies of more than 1 J/cm^3 of dye solution that have been reported are higher than the stored energy and can only be obtained by multiple pumping of the dye molecules by a strong pump-light pulse. The stored energy at 10% inversion, 600 nm laser wavelength and a concentration of 10^{-3} mole/l is only 20 mJ/cm^3. Since this energy is stored for typically a few ns, the molecules can be pumped many times during a pulse of some μs duration. Thus, multikilojoule pulses from a few liters of dye solution appear feasible provided the problem of sufficiently strong pumping of such large volumes is resolved.

For a discussion of ultimate frequency stability of cw dye lasers, the reader is referred to the review by Salomon et al. (1988) while the question of the shortest possible pulses is discussed in Chap. 4.